Study of Factors Affecting an HF/VHF Direct Broadcasting Satellite Service

C. Rush
J. Aarons
F. Stewart
J. Klobuchar
P. Doherty
M. PoKempner
R. Reasoner

TABLE OF CONTENTS

LIST OF FIGURES

Page

LIST OF FIGURES

LIST OF FIGURES

LIST OF FIGURES

LIST OF FIGURES

LIST OF TABLES

LIST OF TABLES

STUDY OF FACTORS AFFECTING
AN HF/VHF DIRECT BROADCASTING SATELLITE SERVICE

C. Rush*, J. Aarons** F. Stewart*, J. Klobuchar***, P. Doherty†,
M. PoKempner††, R. Reasoner*

The Institute for Telecommunication Sciences has undertaken an assessment of the link margin required for the satisfactory performance of a direct broadcasting satellite service operating in the high frequency (HF) and in the very high frequency (VHF) bands. The assessment involved the determination of a number of issues relating to performance of HF and VHF satellite-based transmission systems. These issues included determining under what conditions a frequency allocated to the broadcasting service can be expected to reach the surface of the Earth from a satellite, the loss of signal strength due to passage through the ionosphere, the impact of sporadic E and ionospheric ducting, the effect of scintillation on broadcast performance, the impact of Faraday rotation on system design, and the possibility of a satellite-based broadcasting service interfering with existing ground-based services. In this report, the results of this study are presented.

Key words: direct broadcasting satellite; Faraday rotation; HF broadcasting satellite; HF propagation; ionospheric loss; ionospheric penetration frequency

1.   INTRODUCTION

In recent years, attention has been focused on the possibility of using space-borne platforms to provide high frequency (HF) international broadcast services. Studies reported by Phillips and Knight (1978) and more recently by Haydon et al. (1982) indicate that the use of earth satellites to effect broadcasting objectives is technically feasible for the scenarios that were investigated. These studies concentrated on the use of the 26 MHz band for satellite broadcasting purposes. The HF spectrum allocated to broadcasting spans the frequency range from 5 MHz to almost 26 MHz. While concentration on the 26 MHz band may tend to minimize the impact of the ionosphere on the overall performance of an HF broadcasting satellite system, it may yield results that have a narrow

application for actual operations. In this study, the entire HF and VHF spectrum was considered as being potentially useful for satellite broadcasting purposes. In actual fact, because of the shielding effect of the ionosphere, only those frequencies that are greater than about 9 MHz need to be given serious consideration for broadcasting applications.

In order to assess the degree to which the HF and VHF spectrum lends itself to satellite-based operations, a number of items must be considered. Obviously, a signal that is emitted from the satellite must reach the intended area of the globe for which the service is to be provided. At frequencies corresponding to VHF (greater than 30 MHz) and above, the signal emitted from the satellite can be assumed to a first approximation, at least, to travel on a more or less straight line between transmitter and receiver. At HF, the ionosphere will refract and, perhaps, reflect signals that are incident upon it. Thus, it is necessary to first determine if a given frequency that is allocated to the HF broadcasting service can penetrate the ionosphere and be received in the intended service area. This will depend upon the structure of the ionosphere (which in turn depends upon the local time, season, solar cycle condition, and geographical location) and upon the relative location of the satellite with respect to the service area. Having obtained an estimate of the percentage of time that a frequency will reach the target area, it is then necessary to determine the losses that the signal will suffer as it travels through the ionosphere between the satellite and the surface of the earth. In the case of a satellite-based broadcasting service, this loss will include ionospheric absorption loss and any loss due to polarization mismatch and defocusing.

Once it is known that a particular frequency will penetrate the ionosphere, and knowing the associated losses, the ground coverage area can be determined. In determining the extent to which a satellite signal will cover the earth's surface, account must be taken of the ionospheric structure. It is possible that gradients and anomalous ionization such as sporadic E can trap or guide radio signals to regions of the world that are not intended for a satellite broadcasting service. These signals could interfere with the existing broadcasting service that is provided to the region(s) using conventional ground-based broadcasting operations.

In addition to the items discussed above, it is necessary to consider the effects of ionospheric irregularities on the signals that are received at the ground. These irregularities can give rise to rapid fading and fluctuations of signal amplitude and phase. This phenomenon, known as scintillation, can render

a signal useless as far as imparting information to an intended audience if procedures are not adopted to avoid the situation. Also, the plane of polarization of a linearly polarized radio wave will be rotated as the wave propagates through the ionosphere to the surface of the earth. This, too, must be taken into account in determining the overall link margin of a satellite broadcasting service.

An effort has been undertaken at the Institute for Telecommunication Sciences in response to a request from the National Aeronautics and Space Administration's Lewis Research Center to study the following aspects of the link margin assessment for a direct broadcasting satellite (DBS) service operating in the HF and VHF bands:

(a) determining the percentage of time that a given frequency assigned to the HF broadcasting service will penetrate the ionosphere to a given target area,

(b) estimating the ground coverage provided by signals transmitted from a satellite,

(c) estimating the ionospheric losses for those signals transmitted from a satellite that reach the ground,

(d) determining the percentage of time that frequencies between the lowest penetration frequency, f_1, and about 100 MHz will be impacted by sporadic E, ionospheric gradients, and other anomalous ionospheric structures,

(e) identifying potential interference problems to the HF broadcasting service resulting from a DBS system,

(f) determining the range of Faraday rotation expected for signals in the range from f_1, to about 100 MHz that propagate through the ionosphere,

(g) assessing the likelihood that fading or scintillation exceeding a given level will occur for the frequencies in the range f_1 to 26 MHz and 60 MHz to 100 MHz, and

(h) determining overall link margins.

Satellites in geostationary orbits with high and low elevation angles and in Molniya or hovering type orbits that would be candidates for an operational DBS were considered. In addition, it was assumed that the transmitter was aimed at the center of the area to be covered.

In the next section, the procedures that have been developed to determine the percentage of time a signal penetrates the ionosphere and the area on the surface of the earth covered by the signal are described. Also, the methods used to determine the ionospheric losses associated with the penetration frequencies

are given. In Section 3, the results of calculations performed to address these aspects of DBS operations are presented. Section 4 provides for a discussion of the effect of sporadic E on DBS performance. In Section 5, interference and ducting effects are considered. Faraday rotation of the plane of polarization of a transionospheric signal is described in Section 6, along with results that are applicable to the DBS scenario. In Section 7, the impact of ionospheric scintillation is discussed in detail. Finally, in Section 8, the results are summarized and areas where further work needs to be undertaken are pointed out.

2. IONOSPHERIC IMPACT ON SATELLITE-TO-GROUND HF SIGNALS

2.1 Ionospheric Penetration Frequencies and Area Coverage

It is useful to first consider the properties of an HF radio signal that originates on the earth's surface and is received on a satellite. In the ensuing discussion, we confine our attention to frequencies greater than $2f_H F2$ where $f_H F2$ is the electron gyrofrequency at the F2-peak. For the sake of simplicity, it is assumed that a curved ionosphere surrounds a curved earth and that the only variation in the electron density distribution is with altitude; this variation can be adequately represented by a single parabolic profile. Under these conditions, Snell's law can be cast into the form:

$$\mu\rho \sin \phi = R_E \cos \kappa \tag{1}$$

where μ = the index of refraction at height h,

$\rho = R_E + h$,

R_E = radius of the earth,

ϕ = the angle of incidence of the radio wave at ρ, and

κ = the take-off angle of the radio wave at the surface of the earth.

It can be shown (Maliphant, 1967) that if the effects of the earth's magnetic field and collisions between particle constituents are unimportant in the determination of the refractive index, an HF wave that first penetrates the ionosphere will be governed by

$$\cos \kappa = \frac{\rho_m}{R_E} \left[1 - \left(\frac{f_c}{f} \right)^2 \right]^{1/2} \tag{2}$$

where $\rho_m = R_E + hmF2$,

hmF2 = the height of the F2 region peak,

f_c = the critical frequency of the F2 region, and

f = the frequency of the radio wave.

4

From equation (2), it follows that if f_c/f is greater than unity, the radio wave is reflected from the ionosphere and is returned to the earth's surface. As f_c/f goes from 1 to 0, the radio wave will penetrate the ionosphere at lower and lower take-off angles, assuming f_c is constant over the entire ionosphere.

When viewed from the satellite, radio energy penetrating through a homogeneous ionosphere near the critical frequency will reach a region on the earth's surface only in the immediate vicinity of satellite nadir; e.g., the satellite "iris" would be small. Frequencies greater than the critical frequency will penetrate through the ionosphere at lower take-off angles, which implies penetrating through the ionosphere at distances farther removed from the subsatellite point; e.g., the satellite "iris" would be large.

While equations (1) and (2) are useful in considering the physical mechanisms involved in the penetration of an HF signal through the ionosphere, they do not lend themselves to the numerical simulations that are required for this study. Rather, it is more appropriate to determine the deviation angle from a straight-line propagation path that is taken by a given frequency propagated from a satellite toward the earth's surface. The procedure adopted follows that given by Maliphant (1962).

Referring to Figure 1, it can be seen that the deviation angle (α) is given by

$$\alpha = \theta_T - \theta_1 \dots\dots\dots\dots\dots \tag{3}$$

where θ_T is the angle subtended at the center of the earth by the limits of the true ray path in the ionosphere, and θ_1 is the angle subtended from the same height limits by the apparent or straight-line ray path.

The application of Snell's law yields

$$\rho\mu \sin i = \rho \sin \phi = \text{constant} \dots\dots\dots \tag{4}$$

where i is the angle of incidence of the true ray path at height ρ at which the index of refraction is μ, and ϕ is the angle of incidence at ρ.

It can be shown (Maliphant, 1962) that the angle subtended at the center of the earth may be deduced from the relation

$$d\theta = \frac{\tan i}{\rho} d\rho \dots\dots\dots\dots \tag{5}$$

which, combined with (4), gives

$$d\theta = \frac{\sin \phi}{\rho\sqrt{\mu^2 - \sin^2 \phi}} d\rho \dots\dots\dots \quad . \tag{6}$$
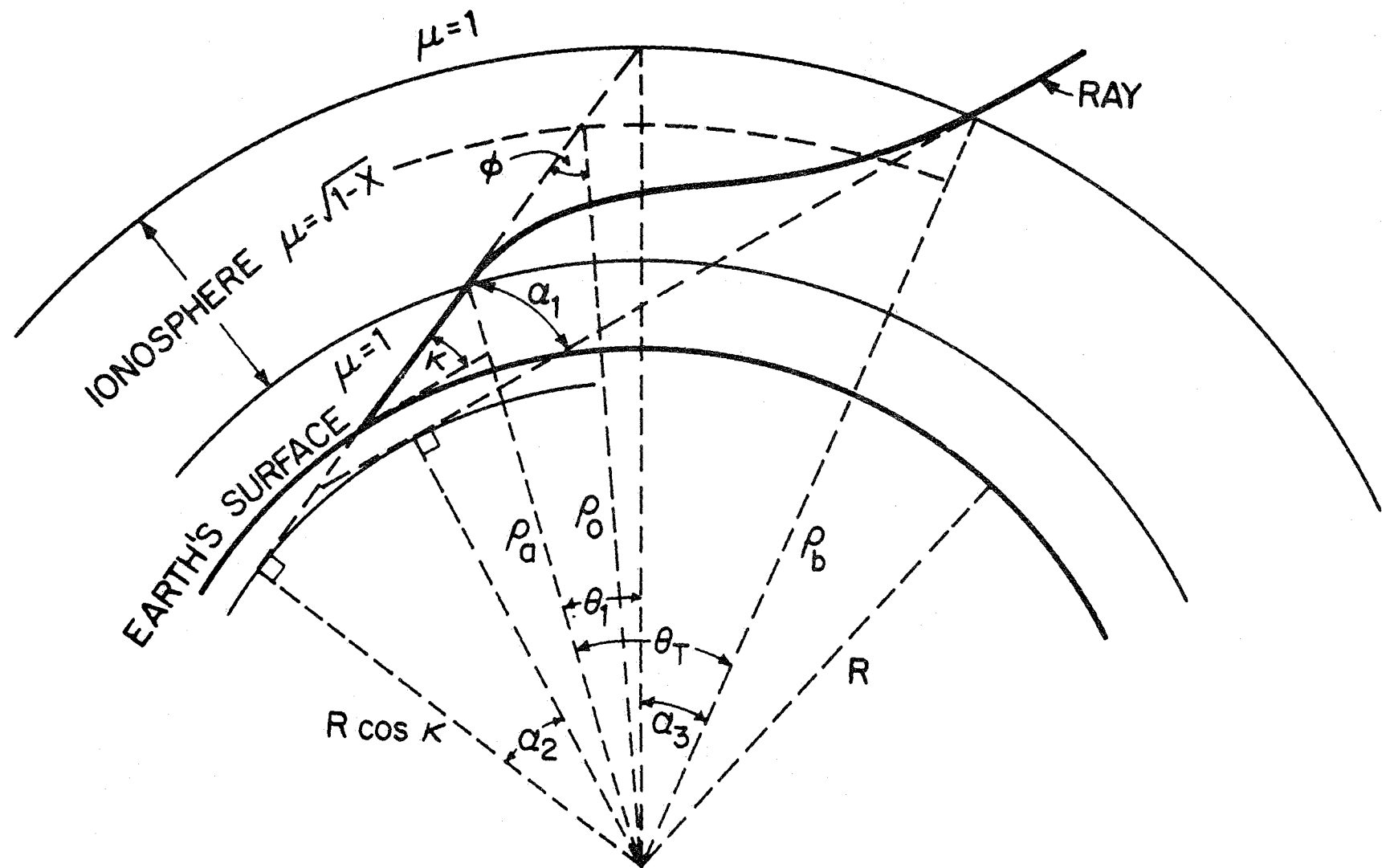
Figure 1. Geometry for transionospheric HF propagation (after Maliphant, 1962).

When collision effects and the magnetic field can be neglected, the Appleton-Hartree equation for the index of refraction can be written (Ratcliffe, 1959)

$$\mu^2 = 1 - \left(\frac{f_c}{f}\right)^2 \cdot \frac{N}{N_m} \quad \ldots\ldots\ldots\ldots\ldots \quad (7)$$

where N is the electron density corresponding to the frequency, f, and N_m is the maximum electron density.

Defining a function, x, such that equation (7) is written as

$$\mu^2 = 1 - x \quad \ldots\ldots\ldots\ldots\ldots \quad (8)$$

then, by combining (6) and (8), the total angle (θ_T) subtended at the center of the earth by the limits of the ray path in the ionosphere is given by

$$\theta_T = \int_a^b \frac{\sin \phi}{\rho \sqrt{\cos^2 \phi - x}} \, d\rho \quad \ldots\ldots\ldots\ldots \quad (9)$$

where a and b represent the lower and upper height limits of the ionosphere.

If the index of refraction were held constant at unity over the height range of the ionosphere, the ray would travel in a straight line. The angle θ_1 may, therefore, be found from (9) by setting

$$x = 0$$

to obtain

$$\theta_1 = \int_a^b \frac{\tan \phi}{\rho} \, d\rho \quad \ldots\ldots\ldots\ldots\ldots\ldots \quad . \quad (10)$$

Thus, from (3), (9), and (10) the deviation angle is given by

$$\alpha_3 = \int_a^b \frac{\tan \phi}{\rho} [(1 - u)^{-1/2} - 1] \, d\rho \quad \ldots\ldots \quad (11)$$

where

$$u \equiv x \sec^2 \phi \quad \ldots\ldots\ldots\ldots\ldots \quad . \quad (12)$$

It may be seen from (2), (7), and (8) that at the height of reflection of a ray,

$$u = 1 \quad \ldots\ldots\ldots\ldots\ldots \quad (13)$$

when the magnetic field is neglected. At the height of maximum electron density, u is simply the square of the deviation factor. In the case where the magnetic

field is included, equation (13) is a very good approximation for frequencies well above the gyrofrequency (Maliphant, 1962).

At all other heights along the ray path

$$u < 1 \ldots\ldots\ldots\ldots\ldots \quad . \tag{14}$$

Hence, (14) may be expanded by the binomial theorem for all rays that penetrate the ionosphere, to give

$$\alpha_3 = \frac{1}{2} \int_a^b x \frac{\tan \phi \sec^2 \phi}{\rho} [1 + \frac{3}{4} u + \frac{5}{8} u^2 + \frac{35}{64} u^3 + \ldots] \, d\rho \ldots \tag{15}$$

which, by application of the second law of the mean for integrals, may be written in the form

$$\alpha_3 = \frac{1}{2} \xi \int_a^b x \frac{\tan \phi \sec^2 \phi}{\rho} \, d\rho \ldots\ldots\ldots \tag{16}$$

where ξ is a number between the greatest and least values of the series over the interval (a, b).

For a ray that penetrates the ionosphere, u is zero at the limits (a, b) and has a maximum value, less than unity, near the height of maximum electron density. The limiting condition for penetration occurs just before u becomes unity at the height of maximum electron density. The value of u, therefore, lies between unity and the value of the series at the height of maximum electron density.

Application of the same law of the mean to (16) yields the deviation angle

$$\alpha_3 = \frac{1}{2} \xi \frac{\tan \phi_0 \sec^2 \phi_0}{\rho_0} \int_a^b x \, d\rho \ldots\ldots\ldots \tag{17}$$

where ρ_0 is some radius between the limits (a, b) and ϕ_0 is the value of ϕ at this radius.

Substituting for x in equation (17), the deviation angle is given by

$$\alpha_3 = \frac{1}{2} (\frac{f_c}{f})^2 \xi \frac{\tan \phi_0 \sec^2 \phi_0}{\rho_0} \cdot \frac{n_T}{N_m} \ldots \tag{18}$$

where n_T, the total electron content of a vertical column of unit cross section of the ionosphere, is given by

$$n_T = \int_a^b N \, d\rho \ldots \ldots \ldots \ldots \ldots \quad . \qquad (19)$$

Following Maliphant (1962), ρ_0 was assumed to be adequately represented by the following expression

$$\rho_0 = \rho_m \left[1 + 0.5333 \frac{Y_m}{\rho_m} \right] \qquad (20)$$

where Y_m is the semithickness of a parabolic layer with a maximum electron density occurring at ρ_m. Rather than determining the total electron content from (19) directly, the total electron content was determined [again following Maliphant (1962)] using the expression

$$n_T = \frac{8}{3} Y_m N_m \quad . \qquad (21)$$

The determination of the deviation angle involves calculating appropriate values of N_m, Y_m, and ρ_m. These parameters will vary with latitude and longitude, local time, season, and solar cycle. In this study, the values N_m, Y_m, and ρ_m were determined from numerical coefficients that represent the global variation of these parameters as given in the HF propagation prediction program described by Barghausen et al. (1969). These parameters are given as hourly median values that vary over the solar cycle.

For a given period of time, the median values of N_m, Y_m, ρ_m can be determined for any location on the surface of the earth. In this study, these parameters were evaluated at specific latitude and longitude points within a given area. The grid thus determined varied in size according to the region of the globe where calculations were to be performed. The magnitude of the gradients in foF2 was the controlling factor in setting the grid size for a specific region of the globe. The formation of the grid for each of the parameters was accomplished in the manner given by Stewart et al. (1983).

To determine if a given frequency penetrates the ionosphere, it is necessary to know N_m, Y_m, ρ_m at the point of penetration. The point of penetration will depend upon the structure of the ionosphere and the location of the satellite with respect to the penetration point. An iterative procedure must be adopted in order to determine if, when, and where a given frequency will penetrate the ionosphere. The procedure used in this study was to first determine those ranges of frequencies and take-off angles at the earth's surface that would penetrate a given ionospheric structure using the method of HF propagation simulation

developed by Stewart et al. (1983). It was assumed that if a given frequency was not reflected from the ionosphere then it penetrated the ionosphere. In addition to the median values of N_m, Y_m, ρ_m, the temporal distribution of the variations of these parameters about the median are available from Stewart et al. (1983). These distributions enable the percentage of time that a given frequency will penetrate through a given median ionosphere to be determined.

Having determined the frequency and angles that penetrate the ionosphere, it was then possible to use these values for the coverage determination. Because the height of the satellite is known and the deviation angle of the radio path between it and a location on the ground has been calculated, it is possible to determine the area covered by a given frequency.

The angle subtended at the center of the earth by the apparent ray path between the earth's surface and the height of the satellite is given by substitution of these height limits in equation (10) to obtain

$$\theta' = \int_{R}^{\rho_s} \frac{\tan \phi}{\rho} \, d\rho \quad \ldots\ldots\ldots\ldots\ldots \tag{22}$$

where

$$\sin \phi = \frac{R}{\rho} \cos k \quad \ldots\ldots\ldots\ldots\ldots \tag{23}$$

Thus

$$\theta' = R \cos k \int_{R}^{\rho_s} \frac{d\rho}{\rho \sqrt{\rho^2 - R^2 \cos^2 k}} \quad \ldots\ldots\ldots\ldots \tag{24}$$

$$= \arccos \left(\frac{R}{\rho_s} \cos k \right) - k \quad \ldots\ldots\ldots\ldots\ldots \tag{25}$$

The total angle subtended at the center of the earth by the ground station and the satellite is then given by

$$\theta = \theta' + \alpha \quad \ldots\ldots\ldots\ldots\ldots \tag{26}$$

The distance between the ground station and the location on the earth's surface directly below the satellite is given by

$$D = R\theta \quad \ldots\ldots\ldots\ldots\ldots \tag{27}$$

An example of the penetration frequencies and the corresponding area covered by those frequencies on the surface of the earth is shown in Figure 2. This figure gives the median penetration frequency for 1800 hrs UT in June for a relatively high part of the solar cycle--a sunspot number of 100. The area shown

10
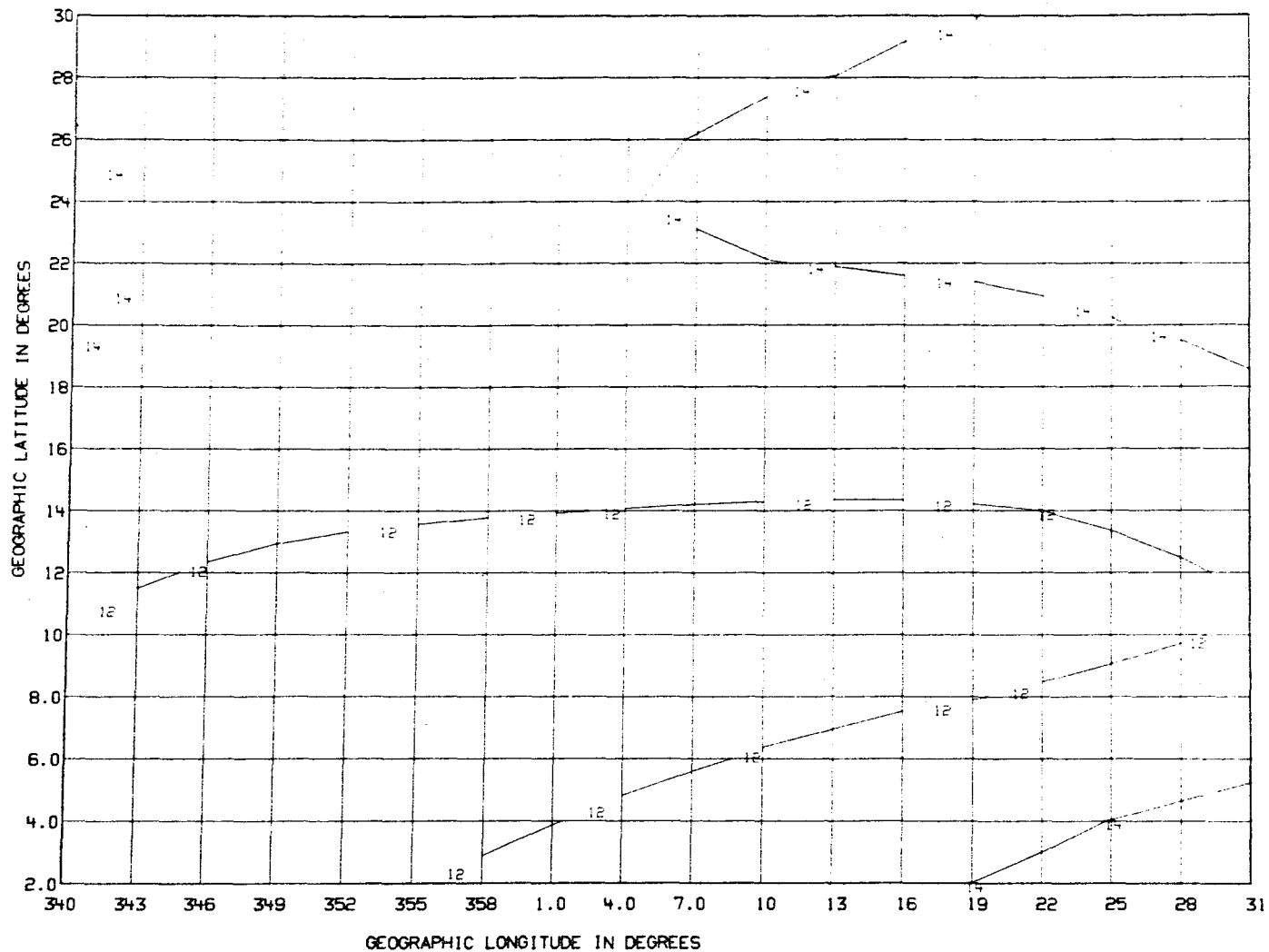
Figure 2. Median penetration frequencies (in MHz) for June, 1800 hrs UT, sunspot number 100 (SSN=100) for a satellite in geostationary orbit on the Greenwich meridian.

extends from 20°W to 30°E and from 2°N to 30°N. In determining the penetration frequency and area coverage, the satellite was assumed to be in geostationary orbit at 35860 km on the Greenwich meridian (0°). The contours show the location of the median penetration points of the 12 and 14 MHz frequencies. Everywhere within the area bounded by a given contour, higher frequencies than those marked on the contour will penetrate for the same geometry. Frequencies of 14 MHz or greater will penetrate to the surface of the earth at least 50 percent of the time for this particular geometry, time, and sunspot number.

2.2 Ionospheric Losses

In determining the required link margin for an operational DBS system, the amount of signal loss that is suffered by the frequencies that are intended to provide the service must be calculated. For the operational scenarios envisioned for a DBS system, the largest loss in signal strength is that associated with the free-space loss. In this study, the free-space loss L_{fs}, was determined using the expression

$$L_{fs} = 32.44 + 20 \log_{10} f + 20 \log_{10} P \tag{28}$$

where f is the wave frequency in megahertz and P is the path length in kilometers.

The ionospheric loss is assumed to result from absorption of signal amplitude as the radio wave passes through the D, E, and F regions of the ionosphere. The D- and E-region absorption L_D, in dB, is assumed to be nondeviative and is explicitly calculated according to the formulas used to determine the D- and E-region losses for a ground-based HF radio circuit in Stewart et al. (1983).

$$L_D = \frac{143(1 + 0.0087x_n) (1 + 0.005S) \cdot \cos^m(\psi_{12})}{\nu^2/4\pi^2 + (f + f_H)^2} \tag{29}$$

$$\cdot \left[\frac{\cos(0.893\psi)}{\cos(0.893\psi_{12})}\right] \cdot \sec\phi_{100} , \quad (dB) ,$$

where

$$m = 2.25 - 0.32x_n , \tag{30}$$

where x_n is the geographic latitude in degrees measured positive from the equator, S is the monthly average sunspot number, ψ is the solar zenith angle in degrees, ψ_{12} is the solar zenith angle at local noon, ϕ_{100} is the angle of incidence of the radio ray at 100 km, ν is the collision number, and f_H is the gyrofrequency, in megahertz, at 100 km.

At night, the factor

$$(1 + 0.005S) \cos^m(\psi_{12}) \frac{\cos(0.893\psi)}{\cos(0.893\psi_{12})} \qquad (31)$$

of equation (29) is set equal to 0.01 to give results that agree with observations on ground-based circuits.

The only difference between the D- and E-region loss equations used in this study and that used by Stewart et al. (1983) is in the coefficient, 143, in equation (29). In Stewart et al. (1983), the coefficient is twice this value to account for the two penetrations of a radio wave through the absorbing lower ionosphere on a single ground-based mode reflected from the ionosphere. For purposes of this study, the radio wave passes through the lower ionosphere only once--hence, the value of 143.

The F-region absorption used in the determination of the ionospheric loss was deduced from the work of Rush and Elkins (1975). The F-region absorption is assumed to be deviative in nature and depends upon the ratio of the wave frequency to the frequency, f_p, that penetrates through the ionosphere for a given location. When the wave frequency is far removed from the penetration frequency, the deviative F-region absorption reduces to very small values. The F-region absorption, L_F, was determined from the expressions derived from Rush and Elkins (1975):

f/f_p ratio	F-Region Absorption
$1.0 < f/f_p \leq 1.1$	$10 - 80 \ (f/f_p - 1.0)$
$1.1 < f/f_p \leq 1.5$	$2 - 5 \ (f/f_p - 1.1)$
$f/f_p > 1.5$	0

where f is the wave frequency and f_p is the penetration frequency.

No other processes (polarization mismatch between transmitter and receiver antenna, or loss due to defocusing of the signal as it passes through ionospheric irregularities, for example) are expressly taken into account in the estimation of the ionospheric loss.

Figure 3 shows an example of the total system loss in decibels for the same conditions and frequencies given in Figure 2. Figure 4 shows the ionospheric loss (D-, E-, and F-region absorption) for the same conditions. The ionospheric absorption in Figure 4 is due primarily to F-region deviative absorption that

13
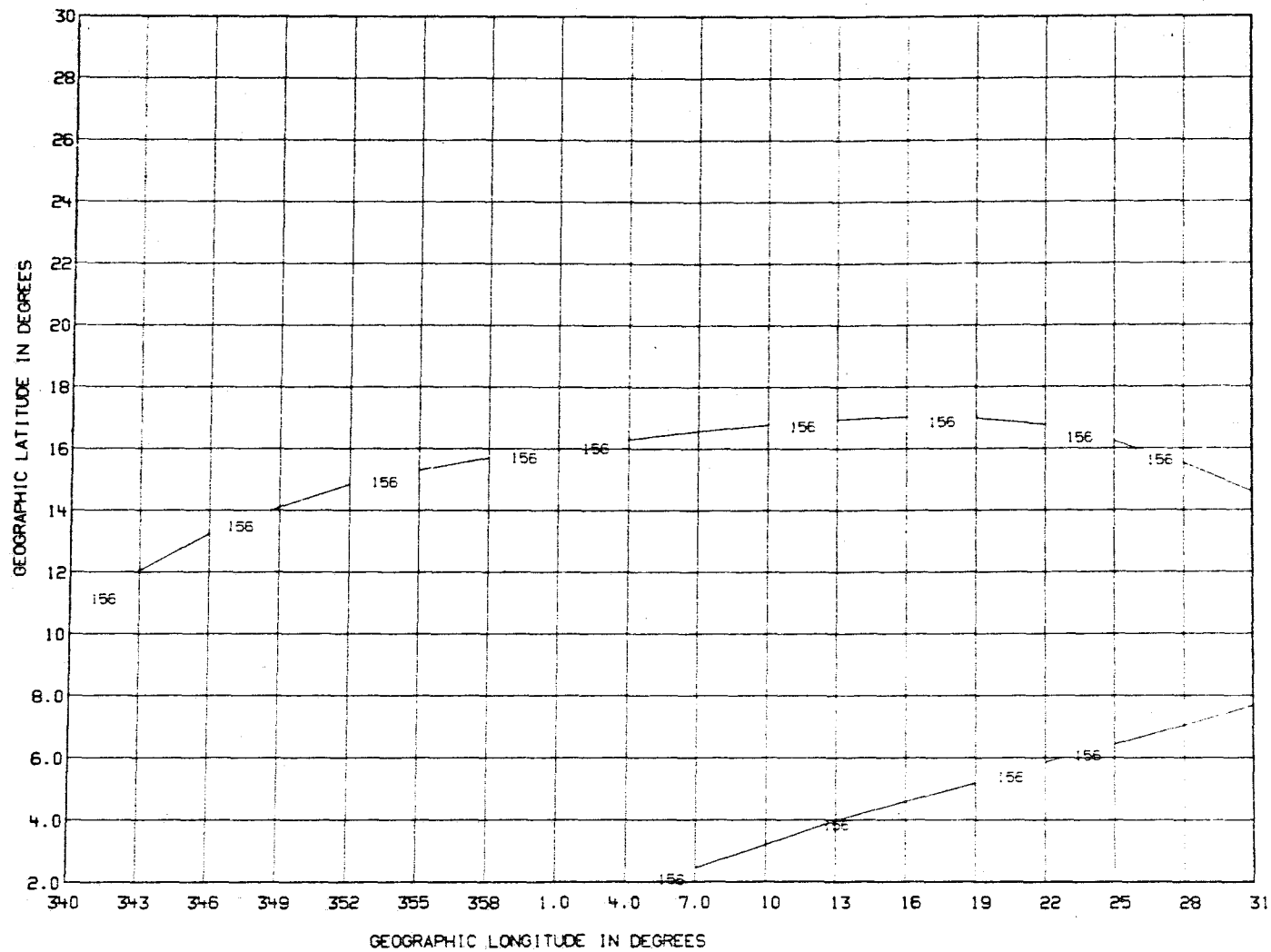
Figure 3.   Median value of the total loss (free space and ionospheric) in dB for June, 1800 hrs UT, SSN=100 for a satellite in geostationary orbit on the Greenwich meridian.

14
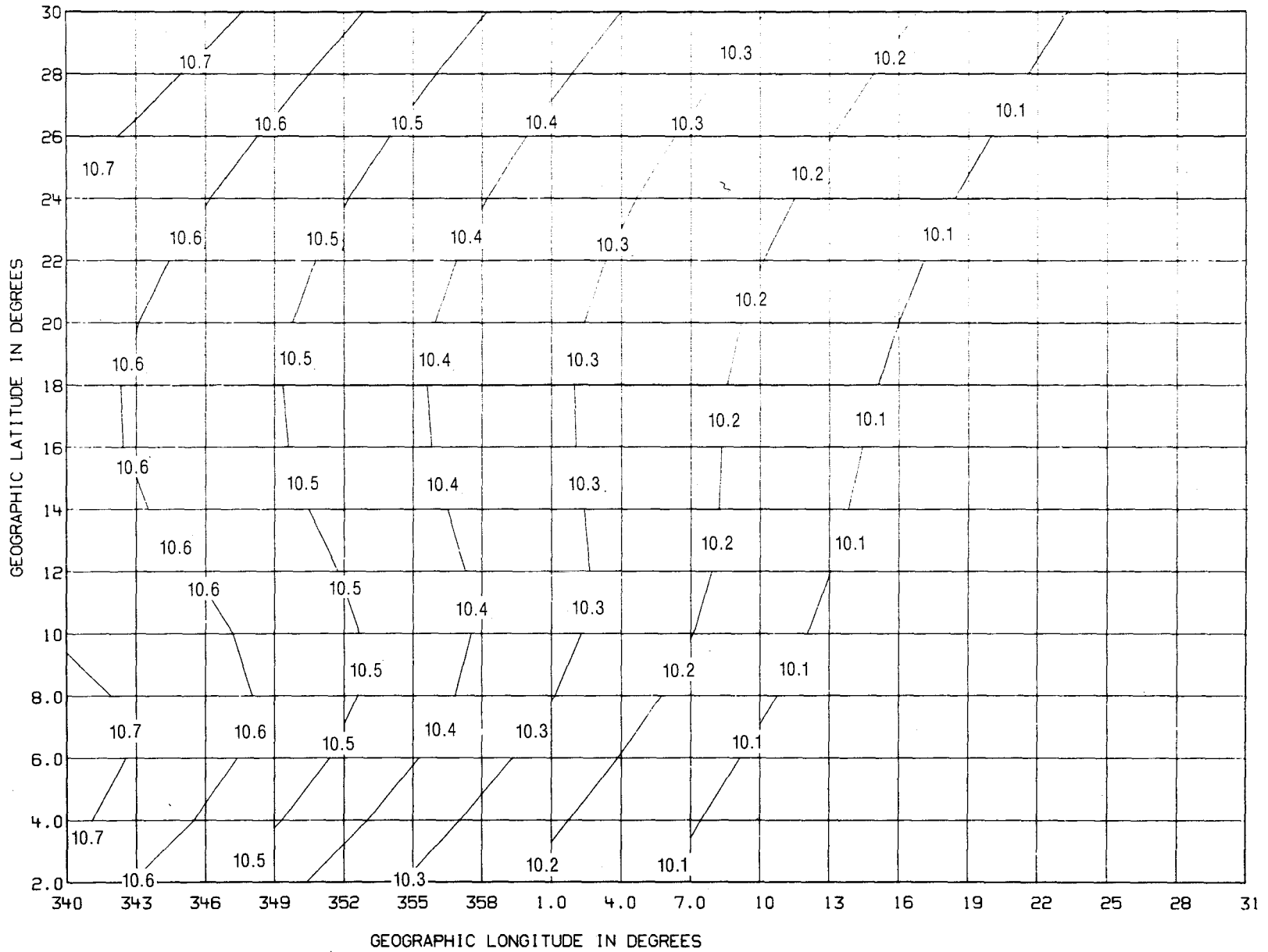
Figure 4.   Median value of the ionospheric loss in dB for June, 1800 hrs UT, SSN=100 for a satellite in geostationary orbit on the Greenwich meridian.

results when the radio wave just penetrates the ionosphere. The slight variations seen are the result of changes in D- and E-region absorption.

In the next section, results of studies to determine appropriate penetration frequencies, ground coverage areas, and loss of signal due to ionospheric absorption are provided for different regions of the globe where a DBS service may be considered for operation.

3. PENETRATION FREQUENCIES, AREA COVERAGE, AND IONOSPHERIC LOSS

3.1 Background

The procedures described in the previous section have been employed to determine characteristics of the performance of a DBS in differing orbital configurations and at different locations of the world. Figure 5 shows the areas of the world that are target areas for a DBS system operating at HF or VHF. These areas, indicated as eight distinct zones, span a wide range of the globe. In three of the zones (1, 2, and 4), the ionospheric structure that is encountered is characteristic of both the middle-latitude ionosphere and the low-latitude ionosphere. Zones 3, 5, and 7 encompass middle-latitude regions, while Zones 6 and 8 are more or less confined to the low-latitude regions of the ionosphere. As is evident from the discussion presented in the previous section, the DBS parameters (penetration frequency, coverage area, and ionospheric loss) will vary in accord with the ionospheric structure. This structure varies as a function of solar cycle, season, and local time. Also, the DBS parameters will be a function of the location of the satellite with respect to the target area.

In order to obtain a realistic estimate of the parameters required from this study, it is necessary that the results be typical of the periods of time that span the major variations in the ionosphere. The International Radio Consultative Committee (CCIR) has suggested that two levels of solar conditions, corresponding to solar minimum and solar maximum, respectively, can be used for HF broadcasting planning purposes (CCIR, 1983). For the solar minimum period, a sunspot number (SSN) of 5 is considered appropriate and, at solar maximum, a sunspot number of 120 is appropriate. It has also been suggested by the CCIR (CCIR, 1983) that results of HF predictions applicable for the months of January, April, July, and October are adequate to specify the seasonal variations within a year. For broadcasting planning purposes, it is necessary to consider system performance characteristics during those local times that correspond to the
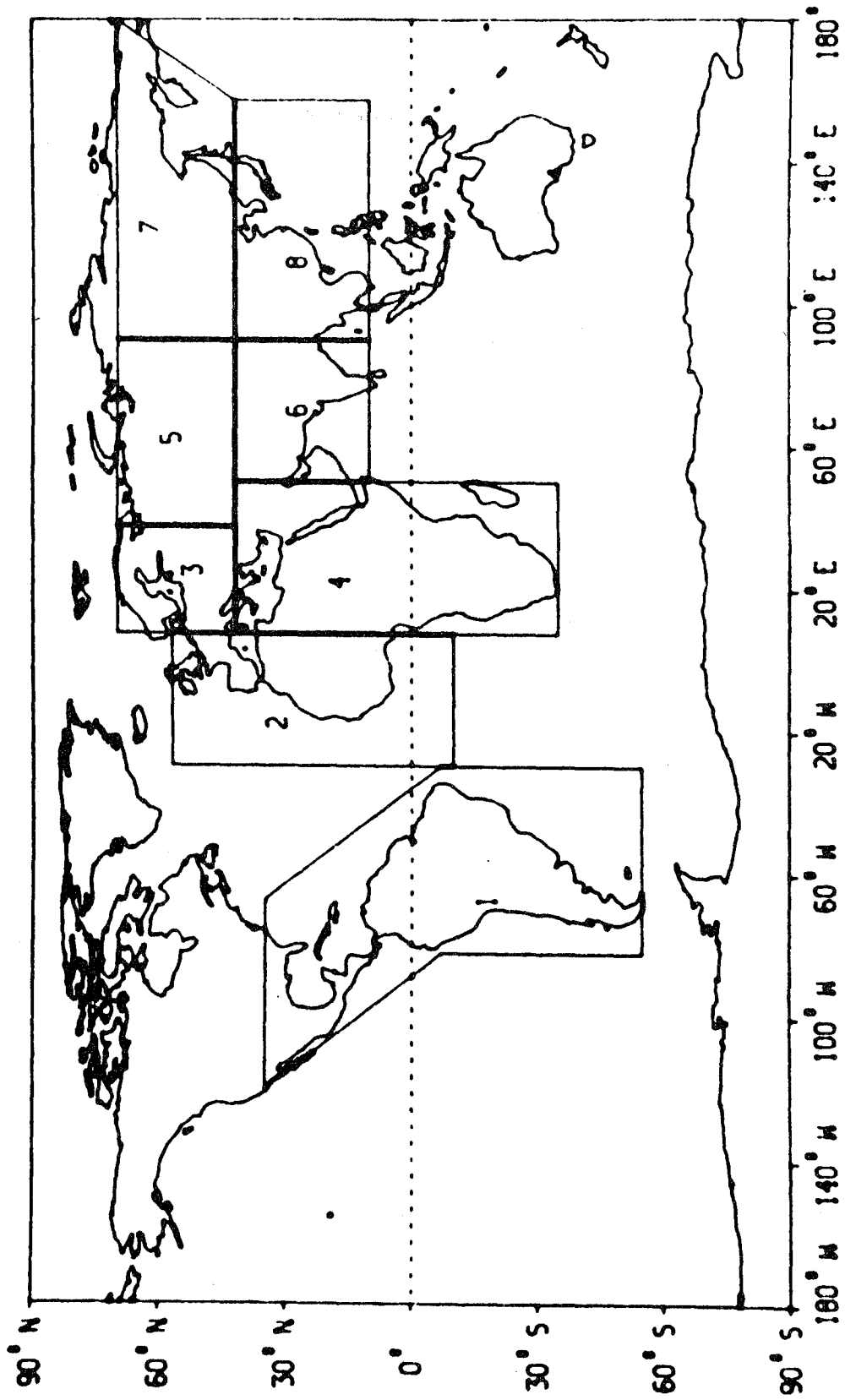
Figure 5.   HF direct broadcasting satellite reception zones.

primary listening hours. In this study, these hours are assumed to be 0530 to
0900 local time and 1800 to midnight local time.

3.2 Results for a Low-latitude Zone

Figure 6 shows the frequency that will penetrate the ionosphere in Zone 1
90 percent of the time at 0000 hrs universal time (UT) during January solar min-
imum (SSN=5). This figure was deduced assuming a DBS located in geostationary
orbit 35860 km above the equator at 70°W longitude (at 290°E longitude in the
figure). The area between 270° and 330° spans the local times between 1800 and
2200 hours. The results shown in Figure 6 are consistent with our understanding
of the morphological behavior of the ionosphere for this period of time. The
critical frequency of the F2 region at low and middle latitudes is higher during
the night and evening hours in the summer hemisphere than in the winter hemi-
sphere. The highest penetration frequencies in Figure 6 are seen to occur in the
summer hemisphere. For a satellite located above Zone 1, frequencies greater
than 14 MHz will penetrate the ionosphere 90 percent of the time or more during
January solar minimum and will provide coverage throughout the entire local time
period 1800 to midnight. Results for other seasons and universal times of 0000
hrs and 0200 hrs have been presented in NTIA Technical Memorandum 84-105 (NTIA-
TM-84-105), limited distribution, entitled "Some considerations on the operation
of an HF/VHF direct broadcasting satellite service." These results show that
frequencies in the range 14-16 MHz penetrate to the surface of the earth more
than 90 percent of the year at these times.

Figure 7 shows the penetration frequencies for 1200 hrs UT during January
solar minimum conditions. The local time span between 255° and 330° is 0500 to
1000 hours. It can be seen again that frequencies greater than 14 MHz will pene-
trate the ionosphere into Zone 1 more than 90 percent of the time, which in this
case corresponds to the entire early morning primary listening period.

Figures 8 and 9 show the results of the calculations of the ionospheric loss
for January at 0000 hrs and 1200 hrs UT for the frequencies that penetrate the
ionosphere 90 percent of the time. The ionospheric loss does not exceed 2 dB for
the evening period or 3 dB for the morning period. Results of similar calcula-
tions presented in NTIA-TM-84-105 corroborate the observation that the iono-
spheric loss does not exceed 3 dB during solar minimum.

Table 1 provides a summary of the results obtained for the morning and even-
ing hours for the solar minimum period above Zone 1. It is apparent from the
table that at the 90 percent level there is little variation with season for the
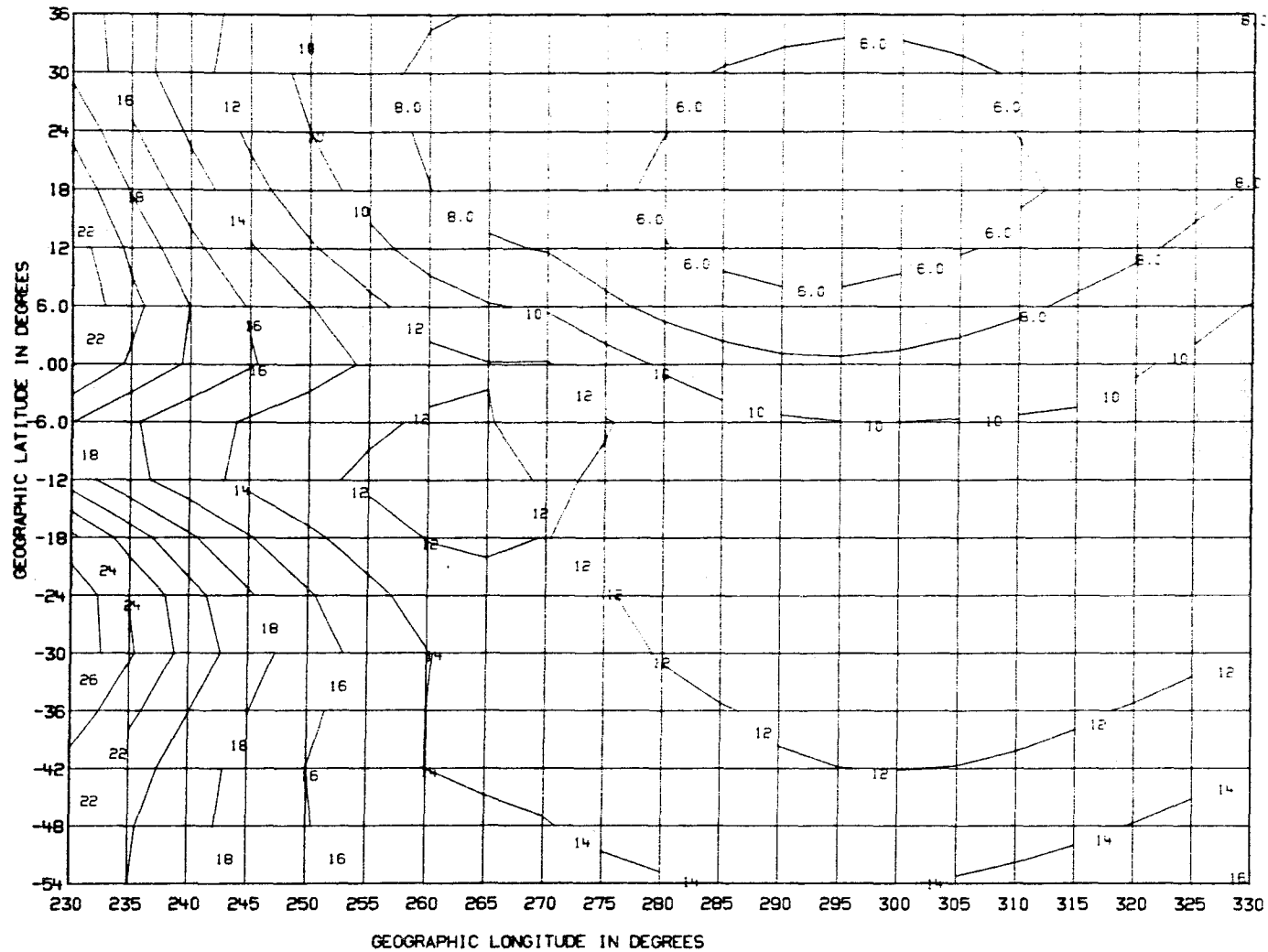
Figure 6.   Frequencies (in MHz) that will penetrate the ionosphere above Zone 1, 90 percent of the time during January, 0000 hrs UT, SSN=5 from a geo-stationary satellite at 290°E longitude.
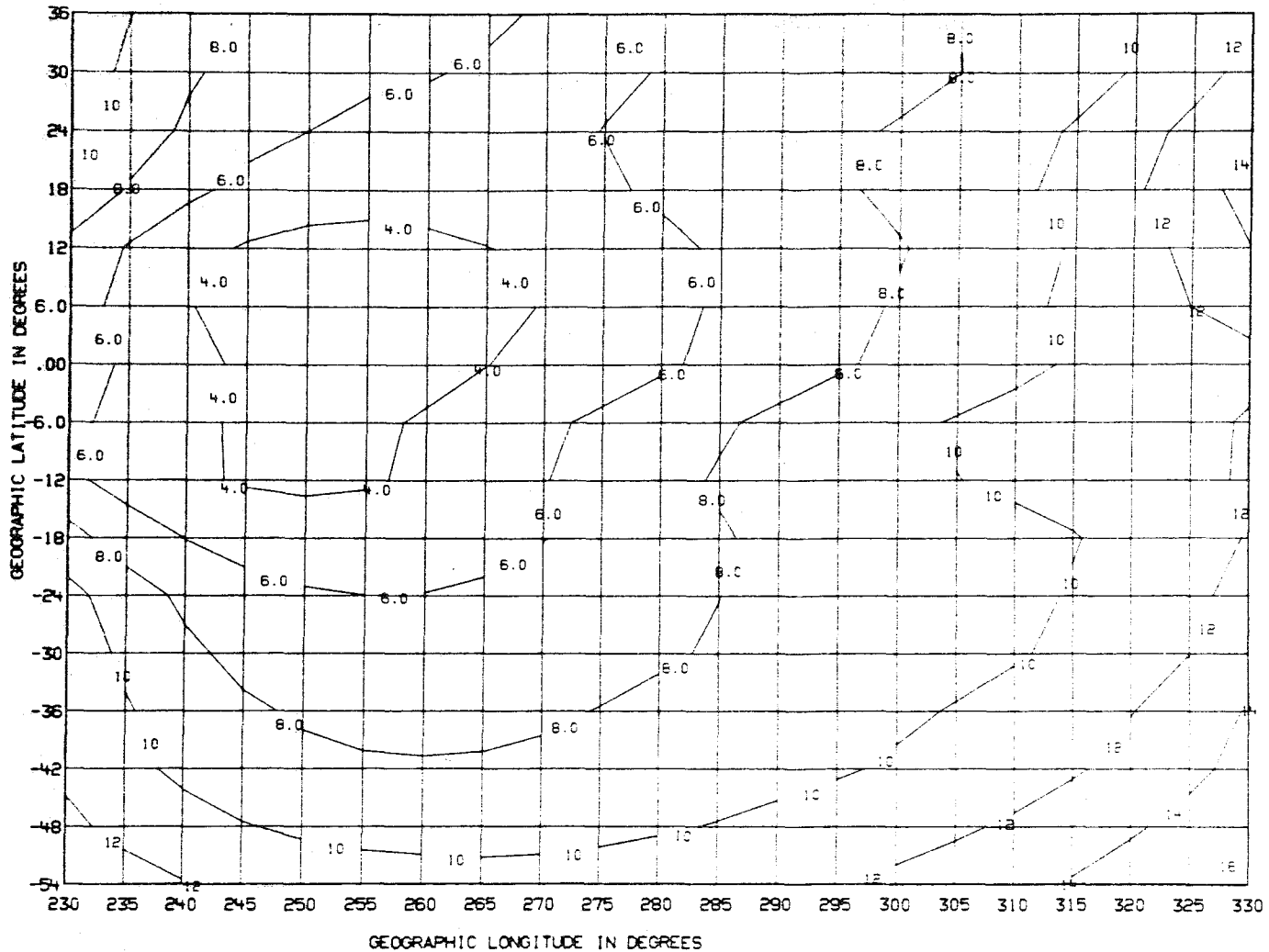
Figure 7. Frequencies (in MHz) that will penetrate the ionosphere above Zone 1, 90 percent of the time during January, 1200 hrs UT, SSN=5 from a geo-stationary satellite at 290°E longitude.
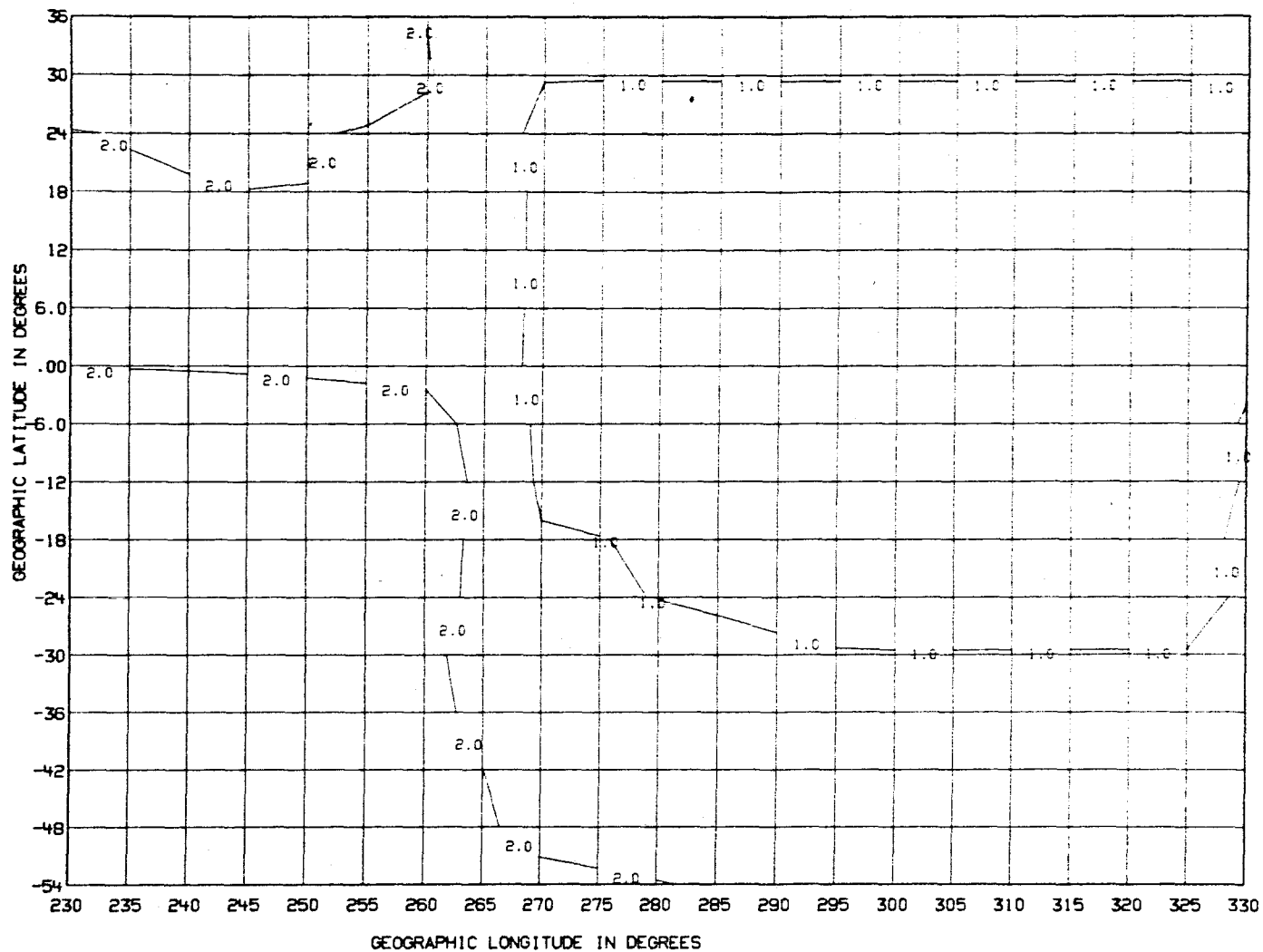
Figure 8. Ionospheric loss in dB for frequencies that penetrate the ionosphere above Zone 1, 90 percent of the time during January, 0000 hrs UT, SSN=5 from a geostationary satellite at 290°E longitude.
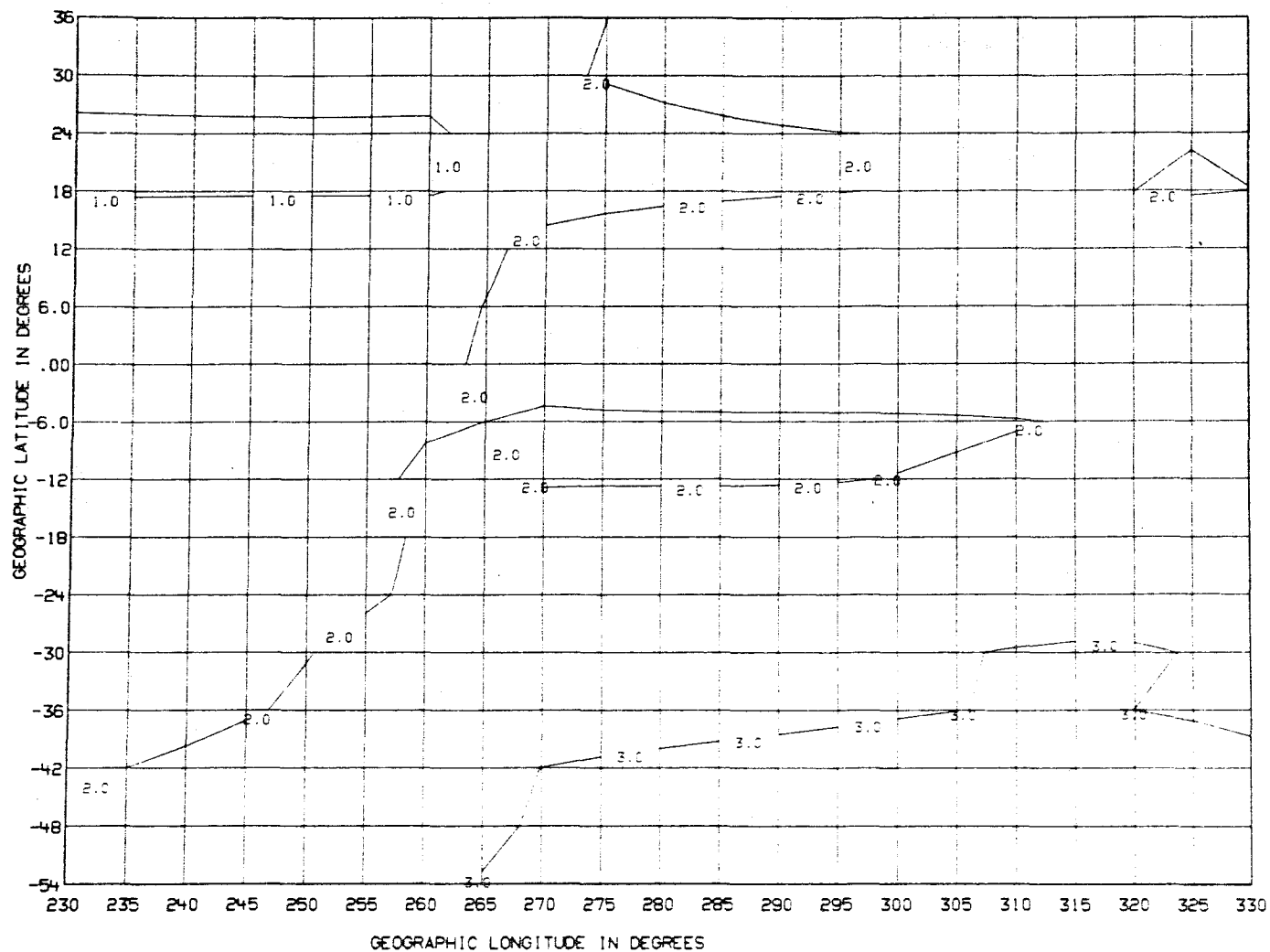
Figure 9.   Ionospheric loss in dB for frequencies that penetrate the ionosphere
above Zone 1, 90 percent of the time during January, 1200 hrs UT, SSN=5
from a geostationary satellite at 290°E longitude.

penetration frequency, area coverage, or ionospheric loss. Also, the variation between morning and evening hours is small.

Figures 10 and 11 show the 90 percent penetration frequencies and coverage areas for January solar maximum (SSN=120) for 0000 hrs UT and 1200 hrs UT. It can be seen from these figures that frequencies greater than about 20 MHz are needed to assure penetration over 90 percent of the time and provide the coverage to the entire Zone 1. As was the case for the solar minimum results, the satellite was assumed to be located in geostationary orbit on the 290° meridian. The results of calculations for each of the seasonal months in solar maximum (presented in NTIA-TM-84-105) show a rather obvious seasonal dependence with the equinox months of April and October requiring the highest frequencies for penetration and the month of July requiring the lowest. Frequencies as high as 26 MHz are needed to assure complete coverage in Zone 1 over 90 percent of the time unless the target area can be limited to the region immediately below the satellite or some small section of the zone. The high values that are required for penetration in the evening hours between 2000 and 2200 hrs local time, are the result of the location of the equatorial anomaly and the magnitude of the electron density at the crests of the anomaly during solar maximum conditions. The anomaly structure maximizes in the evening hours during solar maximum with vertical-incident critical frequencies (foF2) as high as 18 to 20 MHz. Unless a DBS system is operating close to the longitude of the intended target area, frequencies allocated to the HF broadcasting service may be of limited use in supplying information to audiences in the low latitudes during the evening hours at the higher parts of the solar cycle.

Figures 12 and 13 provide the results of the calculations of ionospheric loss for July, 0000 hrs UT and 1200 hrs UT. As was the case for solar minimum, the 90 percent loss does not exceed 3 dB.

Table 2 provides a summary of the results for Zone 1 for solar maximum conditions. A DBS system designed to overcome a 3 dB ionospheric loss at frequencies greater than that required to provide coverage to the zone would be expected to operate over the entire solar cycle neglecting for the moment losses due to other processes such as defocusing, polarization mismatch, and scintillation.

3.3 Results for a Mid-latitude Zone

Figure 14 shows the 90 percent penetration frequency and the average coverage for April solar minimum (SSN=5) at 1600 hrs UT for Zone 5. This zone is

Table 1. Summary of Results for Zone 1 for Solar Minimum

		JAN	APR	JUL	OCT
PENETRATION FREQUENCY (MHZ) NEEDED TO COVER ZONE 90 PERCENT OF TIME	MORNING (0530-0900)	14	14	12	14
	EVENING (1800-0000)	14	16	12	16
IONOSPHERIC LOSS (DB) FOR 90 PERCENT PENETRATION FREQUENCIES	MORNING (0530-0900)	3	3	3	3
	EVENING (1800-0000)	2	2	2	2

Table 2. Summary of Results for Zone 1 for Solar Maximum

		JAN	APR	JUL	OCT
PENETRATION FREQUENCY (MHZ) NEEDED TO COVER ZONE 90 PERCENT OF TIME	MORNING (0530-0900)	22	24	18	24
	EVENING (1800-0000)	22	26	18	26
IONOSPHERIC LOSS (DB) FOR 90 PERCENT PENETRATION FREQUENCIES	MORNING (0530-0900)	3	2	3	2
	EVENING (1800-0000)	2	3	3	3
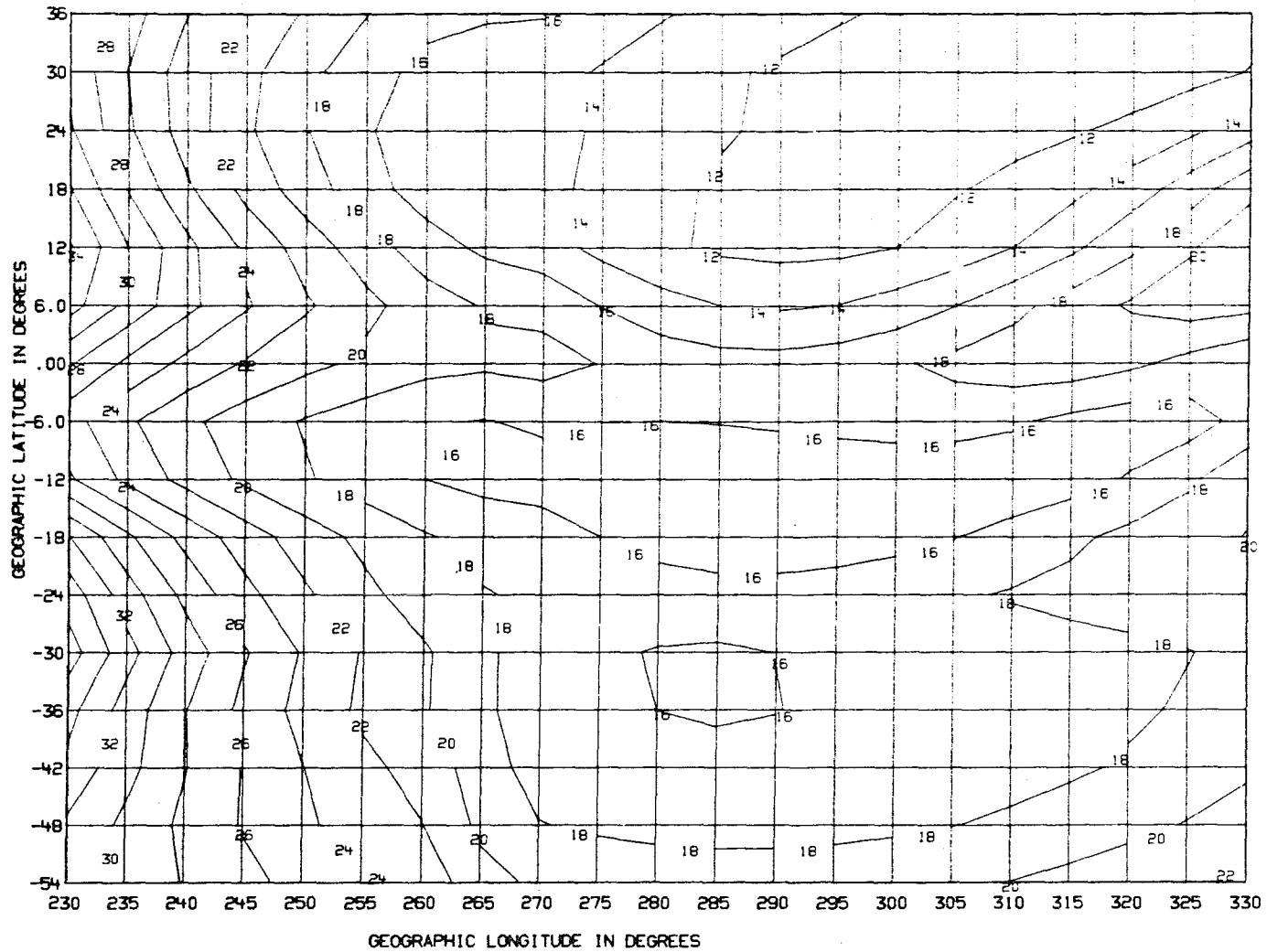
Figure 10. Frequencies (in MHz) that will penetrate the ionosphere above Zone 1, 90 percent of the time during January, 0000 hrs UT, SSN=120 from a geostationary satellite at 290°E longitude.
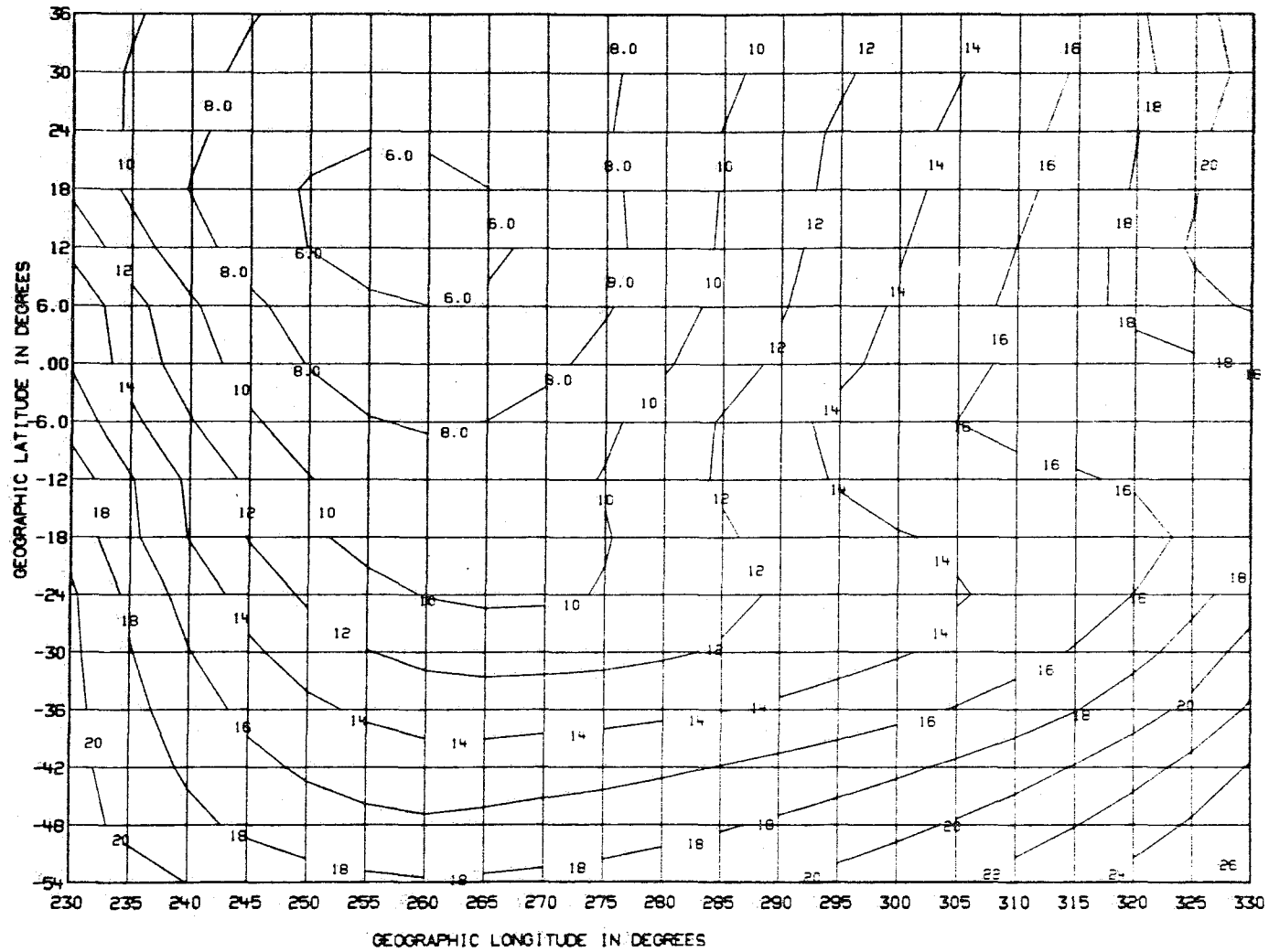
Figure 11. Frequencies (in MHz) that will penetrate the ionosphere above Zone 1, 90 percent of the time during January, 1200 hrs UT, SSN=120 from a geostationary satellite at 290°E longitude.
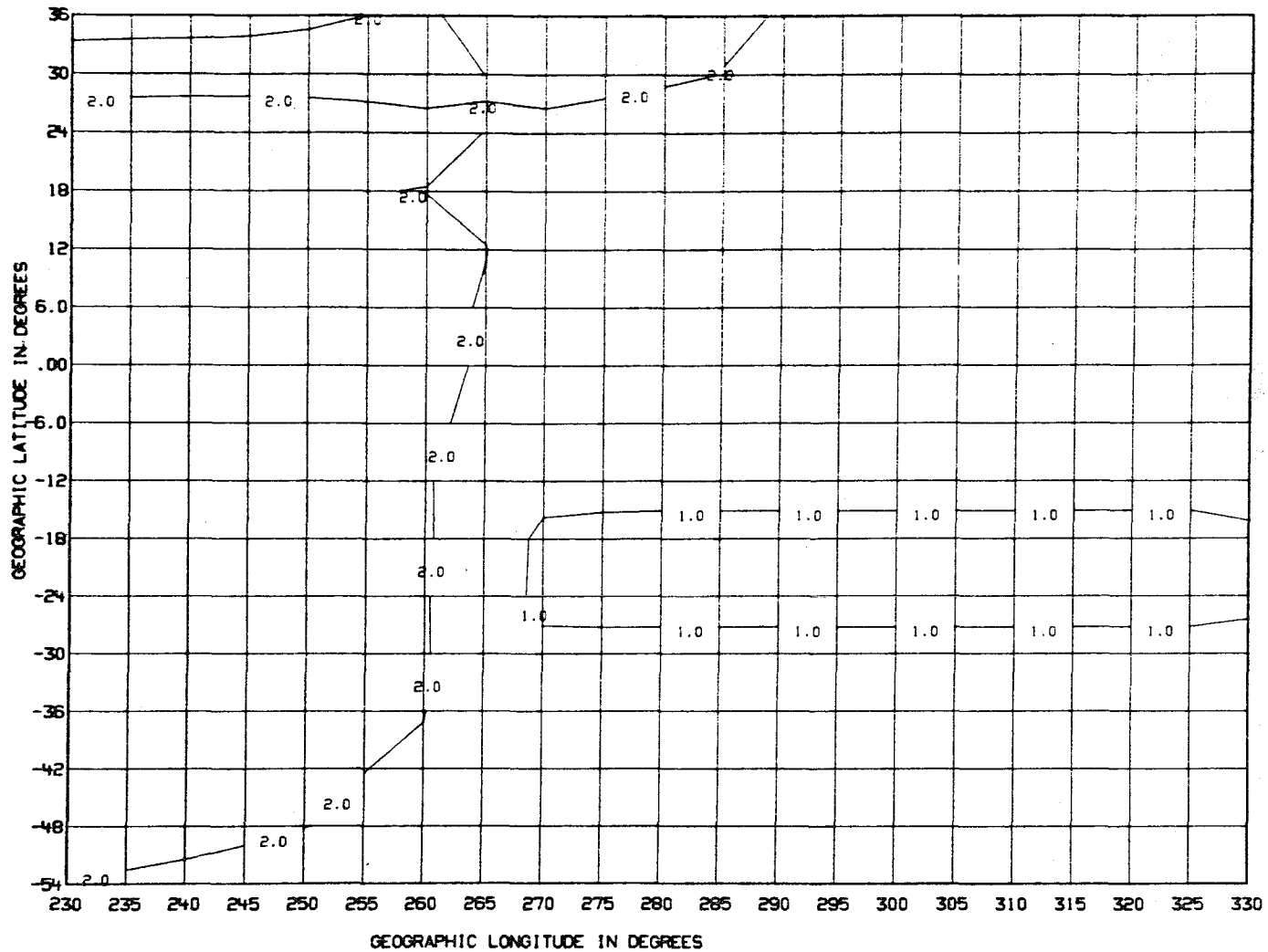
Figure 12.   Ionospheric loss in dB for frequencies that penetrate the ionosphere
above Zone 1, 90 percent of the time during July, 0000 hrs UT, SSN=120
from a geostationary satellite at 290°E longitude.

27
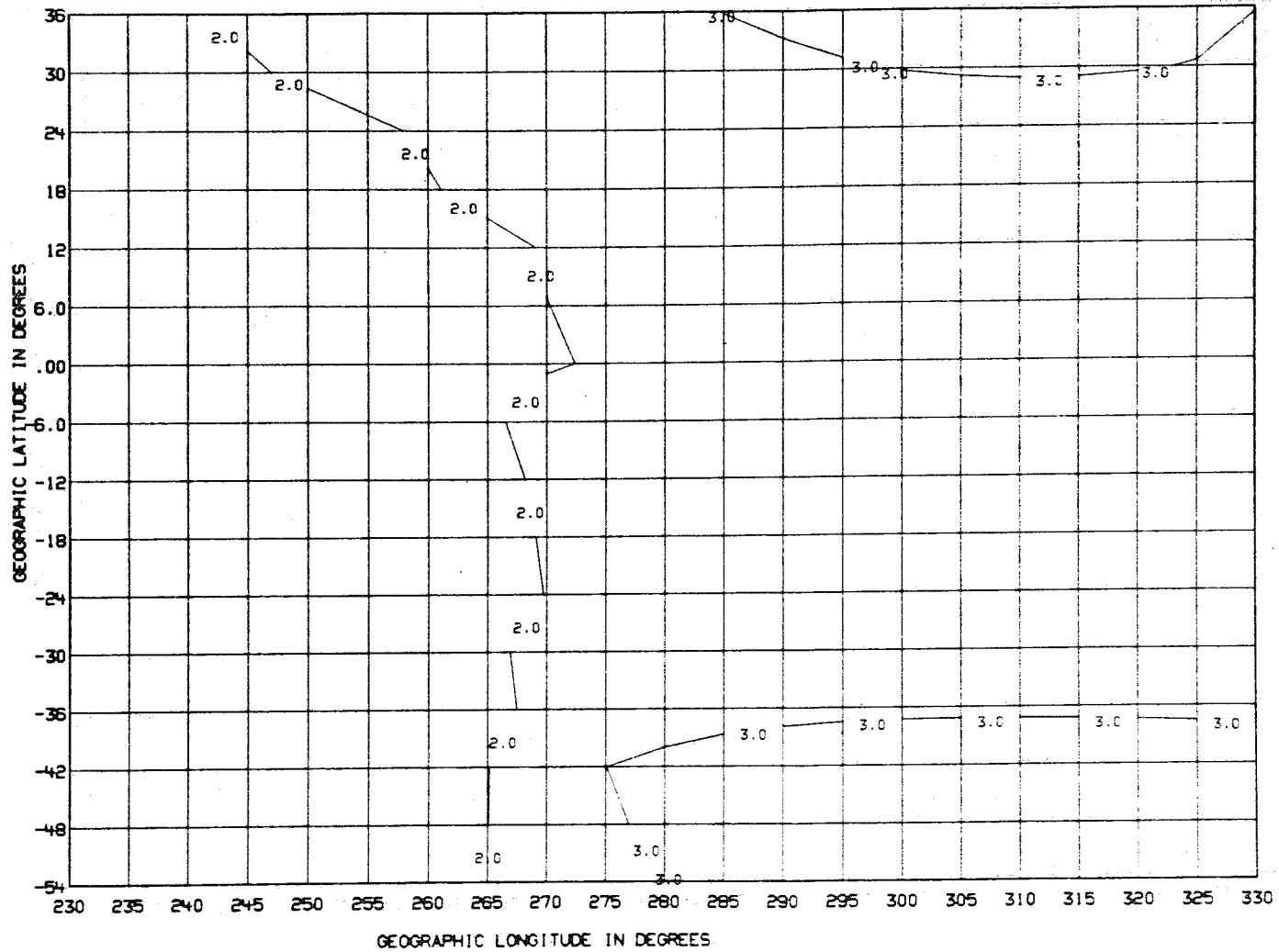
Figure 13.   Ionospheric loss in dB for frequencies that penetrate the ionosphere above Zone 1, 90 percent of the time during July, 1200 hrs UT, SSN=120 from a geostationary satellite at 290°E longitude.
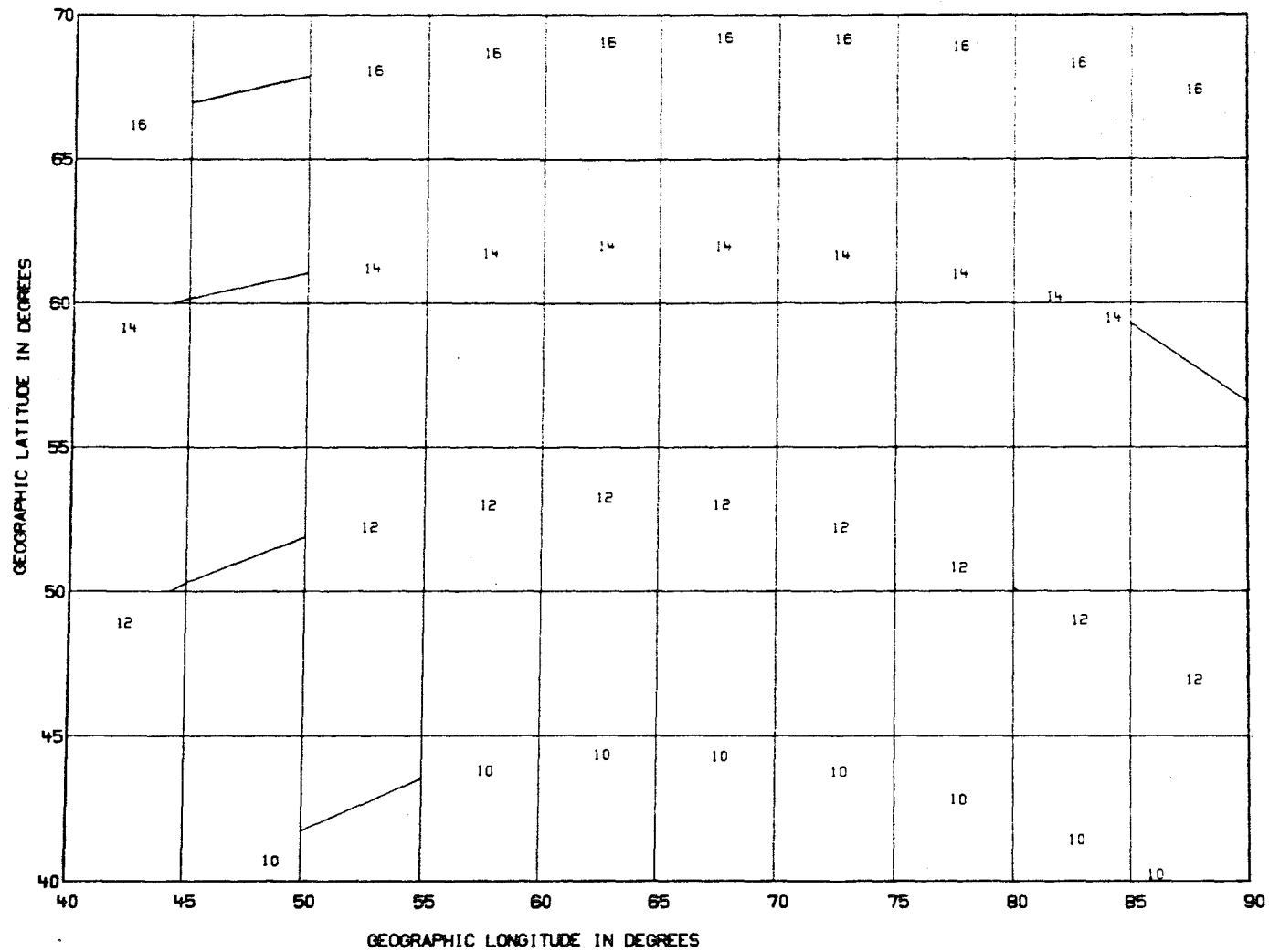
Figure 14.   Frequencies (in MHz) that will penetrate the ionosphere above Zone 5, 90 percent of the time during April, 1600 hrs UT, SSN=5 from a geostationary satellite at 55°E longitude.

typical of a mid-latitude broadcast reception area. The local time spanned by
this zone at 1600 hrs UT is about 1900 to 2200 hours. For the purpose of this
set of calculations, the satellite was assumed to be in geostationary orbit at
the 55° east meridian. The relatively high frequencies needed to penetrate the
northern part of the zone are the result of shallow incidence angles from the
satellite in order for the radio wave to reach all parts of this zone. It can be
seen that frequencies greater than 16 MHz are needed to cover Zone 5 over 90
percent of the month. Results of calculations for each of the seasonal months at
1600 hrs UT for SSN=5 (presented in NTIA-TM-84-105) show that the highest pene-
tration frequencies are required for the months of April and July. This is due
to a combination of shallow incidence angles and critical frequencies that must
be exceeded in order to effect penetration.

Figure 15 shows the results of calculations for April, SSN=5, at 0400 hrs
UT. This case corresponds to the morning hours in Zone 5. (At 0400 hrs UT, the
span of local time in Zone 5 is from about 0630 to 1000 hrs.) Frequencies
greater than 20 MHz are required to provide broadcasting service to this zone 90
percent of the time in the morning hours in April solar minimum. Results of
other calculations for each of the seasonal months at 0400 hrs UT for SSN=5 show
that the highest penetration frequencies are required during the equinoctial
months.

Table 3 provides a summary of the results of calculations for the morning
and evening hours for the entire year of solar minimum. The penetration fre-
quency required to provide coverage to Zone 5 90 percent of the time for each
season and the ionospheric loss associated with the penetration frequencies are
given in the table. Frequencies greater than 20 MHz will provide the coverage
for the entire year with ionospheric losses on the order of 2-3 dB.

Figures 16 and 17 show the 90 percent penetration frequency and area cover-
age maps for Zone 5 during July solar maximum (SSN=120) at 1600 hrs and 0400 hrs
UT. Table 4 provides the summary of the results of the calculations for solar
maximum in Zone 5. The required penetration frequencies tend to be smaller dur-
ing the evening hours than during the morning hours. The highest penetration
frequencies are needed during the equinoxes and the lowest during winter. In
order to cover the entire Zone 5 from a geostationary orbit throughout the solar
maximum period, frequencies greater than those allocated to the HF broadcasting
service must be used during equinox. This implies that frequencies in the VHF
band (60-100 MHz) would have to be employed if coverage to the entire zone is
necessary. If coverage could be confined to the region south of about 55°N, then

30

GEOGRAPHIC LATITUDE IN DEGREES

70

16

18

20

22

18

18

16

65

16

20

16

18

14

16

16

20

60

18

14

16

14

18

16

18

12

14

18

55

14

16

16

14

15

12

12

16

50

12

16

12

14

16

12

18

14

14

45

10

12

10

10

12

14

40
40   45   50   55   60   65   70   75   80   85   90

GEOGRAPHIC LONGITUDE IN DEGREES
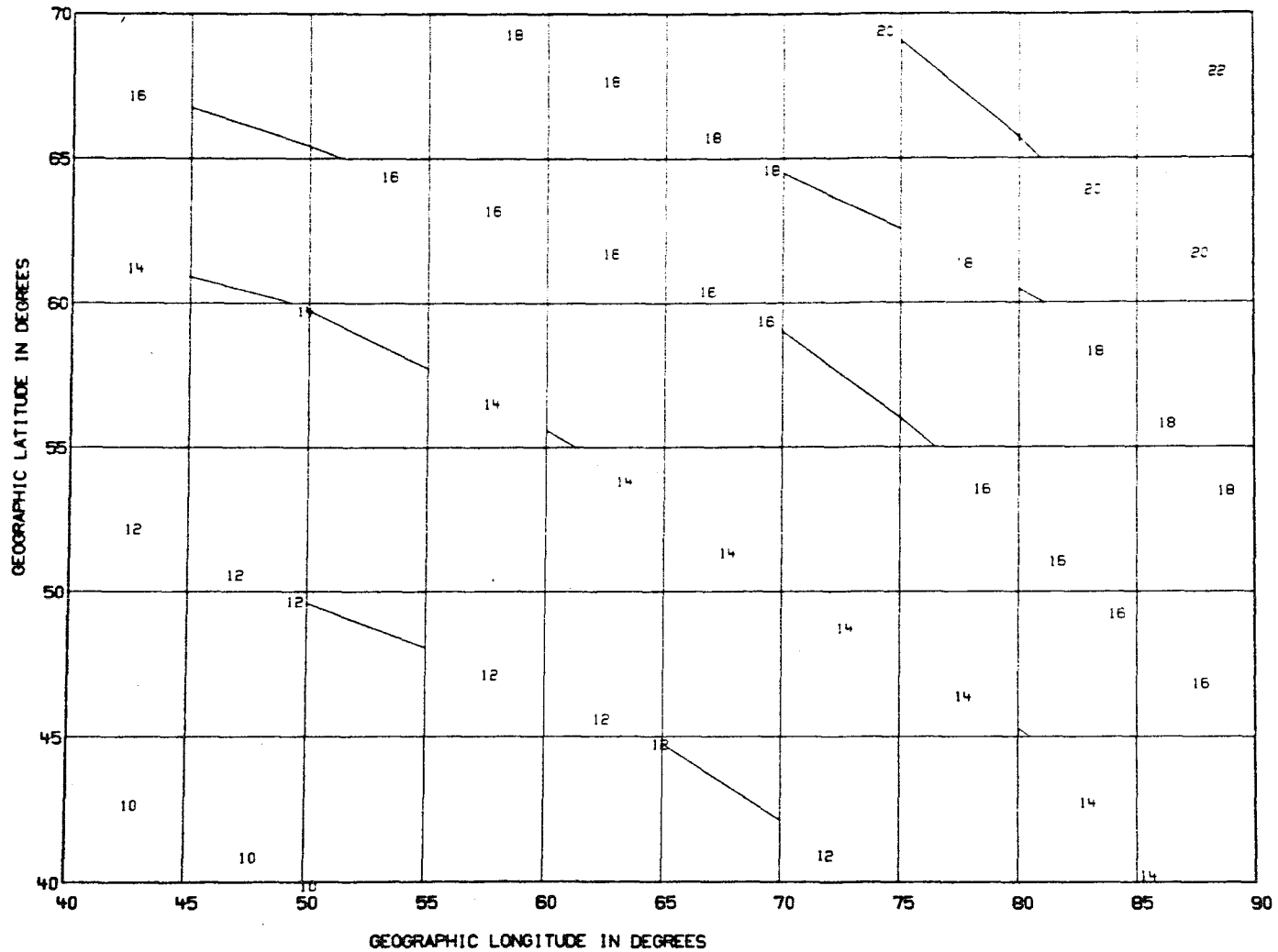
Figure 15.   Frequencies (in MHz) that will penetrate the ionosphere above Zone 5,
90 percent of the time during April, 0400 hrs UT, SSN=5 from a geo-
stationary satellite at 55°E longitude.
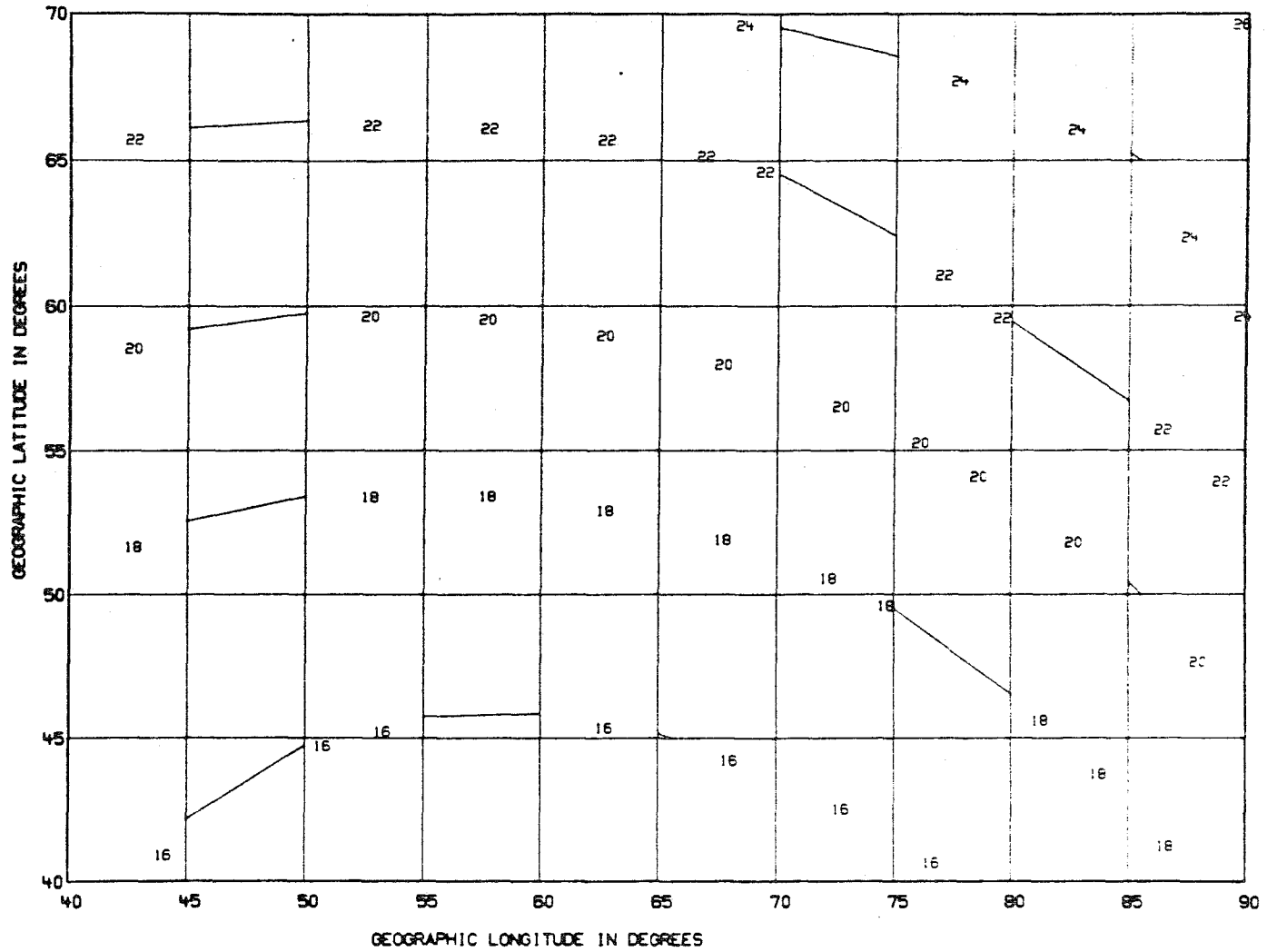
Figure 16. Frequencies (in MHz) that will penetrate the ionosphere above Zone 5, 90 percent of the time during July, 1600 hrs UT, SSN=120 from a geostationary satellite at 55°E longitude.

GEOGRAPHIC LATITUDE IN DEGREES

70

22

22

22

65

20

20

20

22

20

18

22

60

18

20

18

18

18

20

55

18

18

18

20

16

18

50

16

20

16

16

18

45

16

18

16

16

18

40

14

16

40   45   50   55   60   65   70   75   80   85   90

GEOGRAPHIC LONGITUDE IN DEGREES
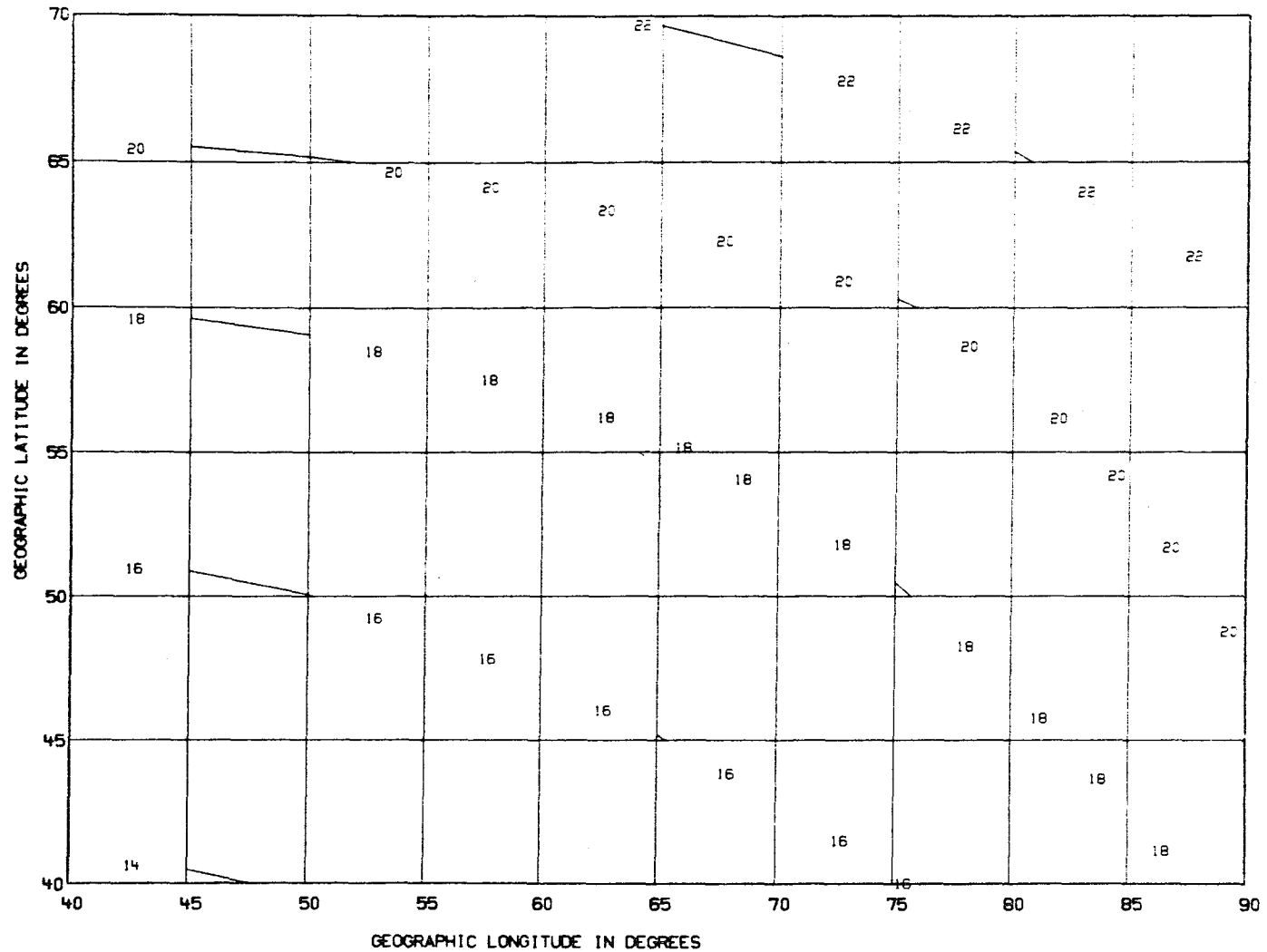
Figure 17.   Frequencies (in MHz) that will penetrate the ionosphere above Zone 5, 90 percent of the time during July, 0400 hrs UT, SSN=120 from a geostationary satellite at 55°E longitude.

Table 3. Summary of Results for Zone 5 for Solar Minimum

		JAN	APR	JUL	OCT
PENETRATION FREQUENCY (MHZ) NEEDED TO COVER ZONE 90 PERCENT OF TIME	MORNING (0530-0900)	16	20	18	20
	EVENING (1800-0000)	12	18	18	14
IONOSPHERIC LOSS (DB) FOR 90 PERCENT PENETRATION FREQUENCIES	MORNING (0530-0900)	2	2	3	2
	EVENING (1800-0000)	2	2	3	2

Table 4. Summary of Results for Zone 5 for Solar Maximum

		JAN	APR	JUL	OCT
PENETRATION FREQUENCY (MHZ) NEEDED TO COVER ZONE 90 PERCENT OF TIME	MORNING (0530-0900)	24	32	22	34
	EVENING (1800-0000)	20	32	24	20
IONOSPHERIC LOSS (DB) FOR 90 PERCENT PENETRATION FREQUENCIES	MORNING (0530-0900)	2	2	3	2
	EVENING (1800-0000)	3	2	2	1

the 26 MHz band could be used to provide coverage 90 percent of the time. Of course, limiting the target area to regions close to the subsatellite longitude would help to reduce the required penetration frequency. The ionospheric loss that is associated with the 90 percent penetration frequency is 2-3 dB irrespective of solar cycle, season, or local time.

3.4 Results for All Zones

The results presented in Sections 3.2 and 3.3 illustrate the solar cycle, seasonal, and local time variations of the DBS parameters obtained in this study for a typical low-latitude area (part of Zone 1) and a typical middle-latitude area (Zone 5). (Parts of Zone 1, particularly in the southern hemisphere, are more characteristic of the middle latitudes than the low latitudes.) Results of calculations made for the other zones could be presented in the same manner. However, because of the amount of information that must be digested, it is more practical to present results that are in the form of overall summaries rather than individual cases.

It is appropriate for broadcast planning purposes (using either HF or VHF) to design a service that will operate into a given area with a given confidence level over the entire projected lifetime of the service. This design information, which, for the purposes here, is the penetration frequency and ionospheric loss, can be obtained by calculating the DBS parameters under conditions that will give the highest penetration frequencies. According to the results presented thus far, equinoctial and summer months solar maximum (SSN=120) will yield these conditions.

Tables 5 and 6 provide the summary information for July and October, respectively, for all eight zones that were investigated in this study. The tables list the zone, the position of the geostationary satellite assumed to be broadcasting to that zone, the universal time, the local time span in the zone, the 90 percent penetration frequency required to cover the entire zone, and the ionospheric loss. Also shown is the closest frequency band above the penetration frequency that is allocated to the HF broadcasting service. It is seen from the tables that a 3 dB margin is sufficient to ensure a signal strength that will overcome the ionospheric absorption for almost all times. The penetration frequencies are highest for the northern-most zones primarily because of the shallow incidence angles at the satellite needed to reach these areas. Generally, the frequencies needed to provide service during the equinoxes are higher than those needed in local summer.

35

Table 5. Summary of Results for All Zones
for July Solar Maximum

Zone	Satellite Position	UT (hrs)	LT Span (hrs)	90 Percent[*] Penetration Frequency (MHz)	90 Percent Ionospheric Loss (dB)	Broadcast[*] Frequency Band (MHz)
1	0°, 70°W	0000	1800-2200	18	3	21
2	0°, 15°W	2000	1800-2100	18	2	21
3	0°, 15°E	1800	1800-2100	22 (18)	2	26 (21)
4	0°, 30°E	1600	1600-1930	18	2	21
5	0°, 55°E	1600	1830-2200	24 (20)	2	26 (21)
6	0°, 70°E	1600	1900-2200	18	2	21
7	0°,120°E	1400	2000-0200	24 (22)	1	26 (26)
8	0°,120°E	1400	2000-0200	16	1	17

[*]Values in parentheses in this column relate to frequencies appropriate for coverage in the zone indicated up to 55°N latitude.

Table 6. Summary of Results for All Zones
for October Solar Maximum

Zone	Satellite Position	UT (hrs)	LT Span (hrs)	90 Percent[*] Penetration Frequency (MHz)	90 Percent Ionospheric Loss (dB)	Broadcast[*] Frequency Band (MHz)
1	0°, 70°W	0000	1800-2200	26	3	26
2	0°, 15°W	2000	1800-2100	20	1	21
3	0°, 15°E	1800	1800-2100	26 (18)	2	26 (21)
4	0°, 30°E	1600	1600-1930	20	2	21
5	0°, 55°E	1600	1830-2200	24 (16)	1	26 (17)
6	0°, 70°E	1600	1900-2200	18	2	21
7	0°,120°E	1400	2000-0200	20 (18)	1	21 (21)
8	0°,120°E	1400	2000-0200	20	2	21

[*]Values in parentheses in this column relate to frequencies appropriate for coverage in the zone indicated up to 55°N latitude.

Use of frequencies below those given in Table 5 would provide coverage to selected areas within each of the eight zones. With the use of lower frequencies, however, the area covered within a given zone could be limited, and the ionospheric loss associated with these frequencies may be increased.

There are times (particularly during the equinoxes) that frequencies greater than those allocated to HF broadcasting must be used to cover an entire zone at least 90 percent of all time from a geostationary satellite. To provide total coverage, frequencies in the VHF band between 60-100 MHz must be used. If, however, services at latitudes greater than about 55° do not have to be provided from a geostationary satellite, the 26 MHz band could be utilized with a fair degree of confidence to provide service over the entire solar cycle. A better alternative, perhaps, is to employ a satellite in an orbit other than geostationary. A satellite in a hovering orbit or an orbiting spacecraft (for example, one in an 8-hour orbit) could provide service at frequencies below 26 MHz. This aspect of DBS service is discussed in the next section.

3.5 Dependence of Results on Satellite Position

The results presented thus far were obtained with the assumed DBS positioned in geostationary orbit on a longitude that was near the midpoint of the target area. This type of inclination for a geostationary orbit provides an almost optimum configuration for service to each zone. It is likely, however, that a DBS system may be configured in such a manner that satellites would be used to provide broadcast services to more than one of the eight zones illustrated in Figure 5. This would have the effect of utilizing a satellite in geostationary orbit that has low elevation angles to provide broadcast service to certain areas. It is also possible that orbits other than geostationary would be used to place satellites in a DBS operation. An orbit in which the spacecraft appears to hover above a given region of the globe could be employed to provide optimum service to that region. One such orbit is a Molniya orbit, in which the satellite can be configured to dwell for a number of hours above a specific region of the globe at altitudes near 35860 km. The advantage of such an orbit is that the penetration frequency needed to cover the middle-latitude regions would be smaller than that from a satellite in geostationary orbit.

Other types of orbits could be employed for DBS operation. A satellite in an 8-hour orbit, such as discussed by Phillips and Knight (1978), could provide broadcast services for selected regions of the earth if operational considerations were such that coverage does not have to be provided throughout the entire

37

primary listening hours. This type of orbit, being lower in altitude, enables the use of smaller spacecraft antenna and thereby reduces the spacecraft complexity. The position of the spacecraft could be adjusted so that the satellite passes near the target area. This, too, could give rise to lower penetration frequencies for selected orbits.

The effect of using satellites in geostationary orbits with low elevation angles and other orbits such as a hovering orbit and an 8-hour orbit are addressed separately.

3.5.1 Effect of nonoptimum geostationary orbit (offset from mid-zone longitude)

The most obvious effect of using an offset geostationary orbit is the lower elevation angle of the satellite as seen from each zone. With this lower elevation angle, the radio wave will have to be incident on the ionosphere at a take-off angle that is further from the zenith direction than if the satellite were at a mid-zone longitude. According to equation (2), the penetration frequency will be increased as the take-off angle departs more and more from the zenith. Thus, higher frequencies will be required to provide broadcast service than if mid-zone geostationary orbits were employed. This effect can be seen from the coverage maps given in the appropriate figures in the text.

To better quantify the effect of longitude-offset on the penetration frequency and area coverage, a number of calculations were performed for the same zone and universal time with the satellite in geostationary orbit placed on successive 15° longitude increments. Figures 18 to 22 show results for October solar maximum for Zone 4 at 1600 hrs UT. The satellite was initially assumed to be located at 30°E (assumed as optimum) and then moved to 15°E, 0°, ..., 30°W. Figures 23 to 26 show comparable results for Zone 3 also for October, 1600 hrs UT, solar maximum. For this zone, the satellite was initially placed on the 0° meridian and then moved to 15°W ... 45°W. These figures demonstrate quite vividly the increase in the minimum frequency required to cover the entire zone as the satellite is placed further and further away from a longitude near the middle of the zone.

Tables 7 and 8 provide a summary of the results presented in Figures 18 through 26 as well as a compilation of the ionospheric losses associated with the 90 percent penetration frequencies. When the satellite is moved 30 to 45 degrees from the center of the zone, frequencies on the order of 40 MHz are needed to provide coverage at the antisatellite edge of the zone. Lower frequencies could be used at solar minimum, particularly for the winter nighttime hours. However,

GEOGRAPHIC LATITUDE IN DEGREES

GEOGRAPHIC LONGITUDE IN DEGREES
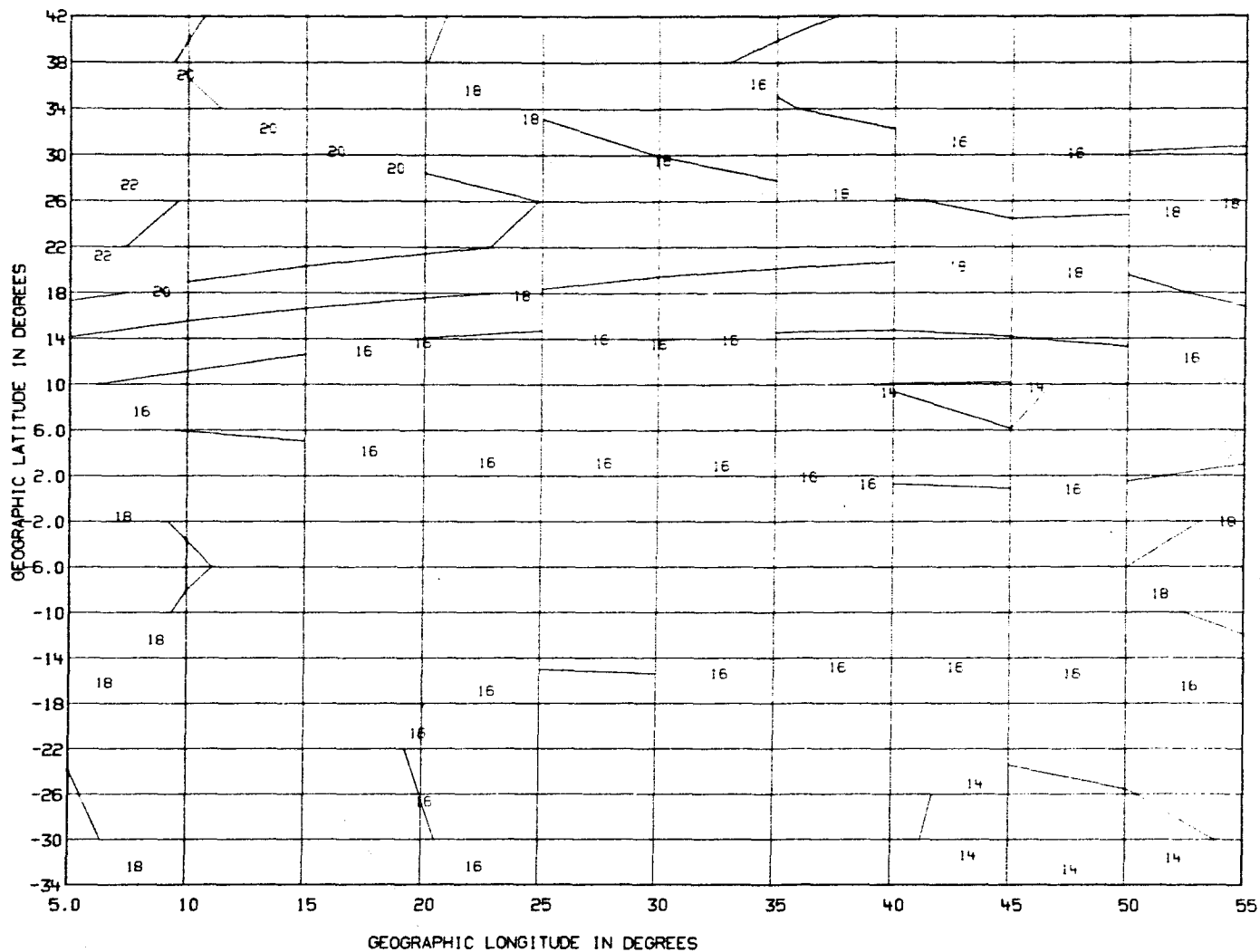
Figure 18.   Frequencies (in MHz) that will penetrate the ionosphere above Zone 4, 90 percent of the time during October, 1600 hrs UT, SSN=120 from a geo-stationary satellite at 30°E longitude.
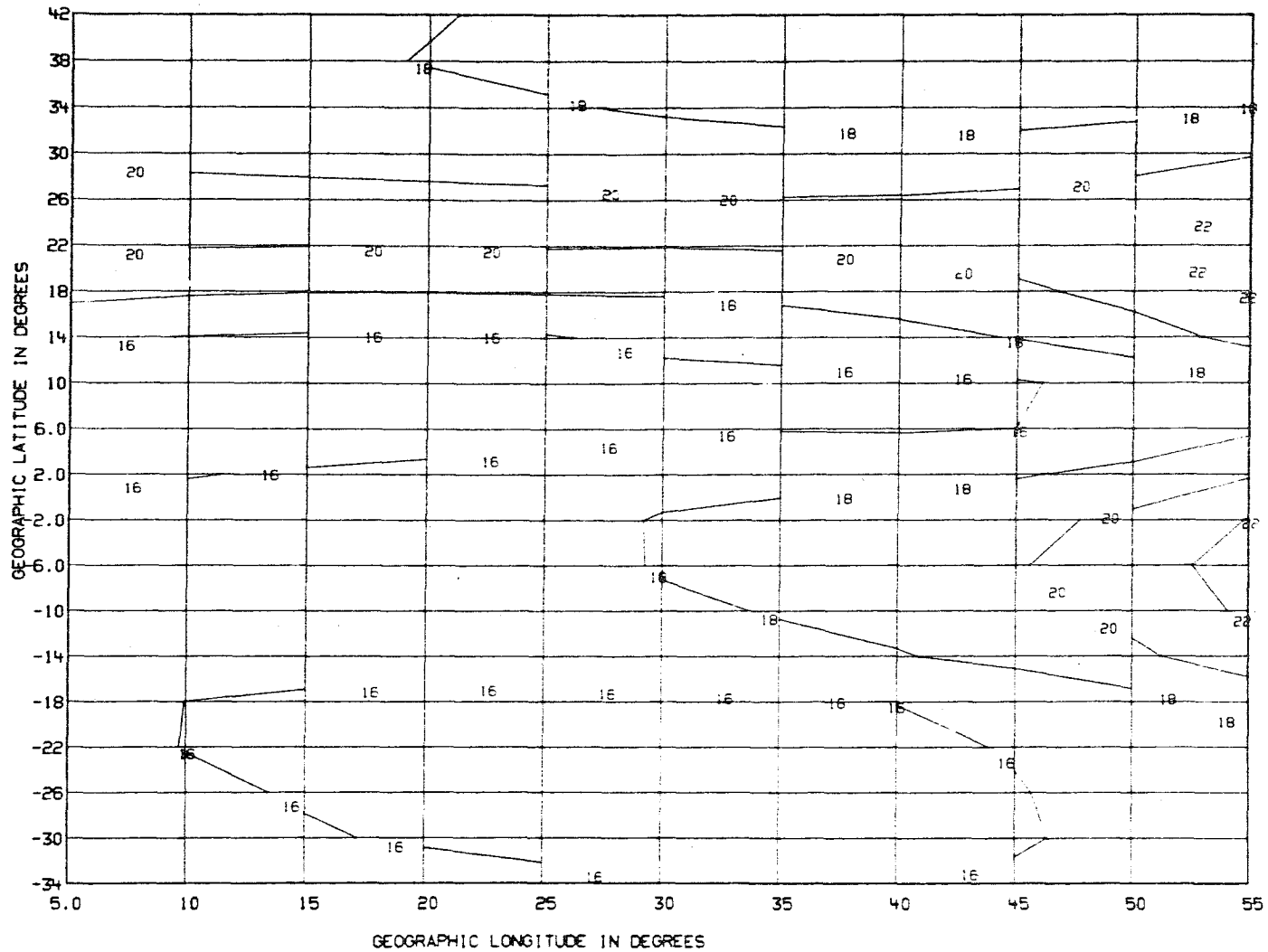
Figure 19. Frequencies (in MHz) that will penetrate the ionosphere above Zone 4, 90 percent of the time during October, 1600 hrs UT, SSN=120 from a geostationary satellite at 15°E longitude.
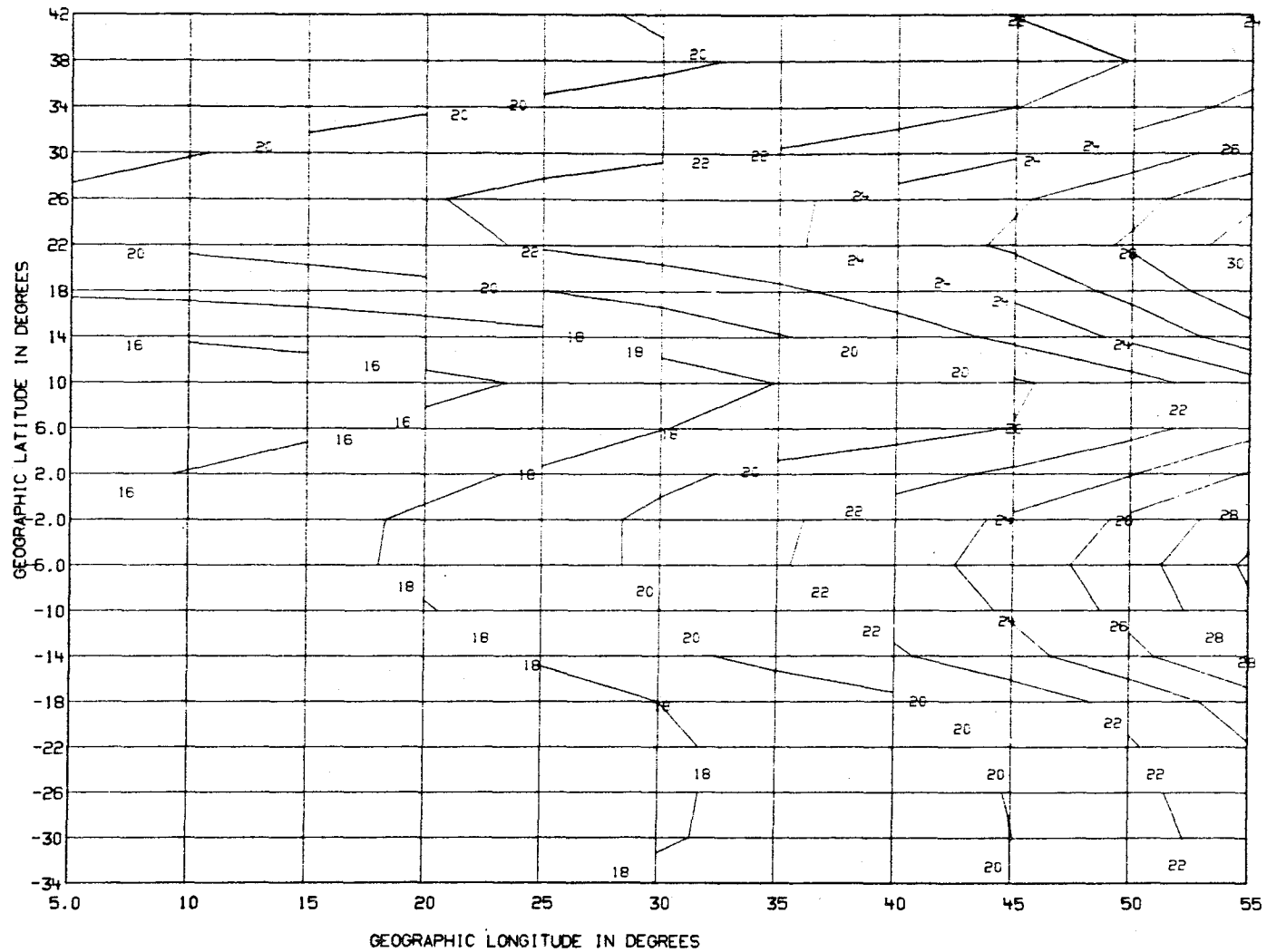
Figure 20. Frequencies (in MHz) that will penetrate the ionosphere above Zone 4, 90 percent of the time during October, 1600 hrs UT, SSN=120 from a geo-stationary satellite at 0° longitude.

41
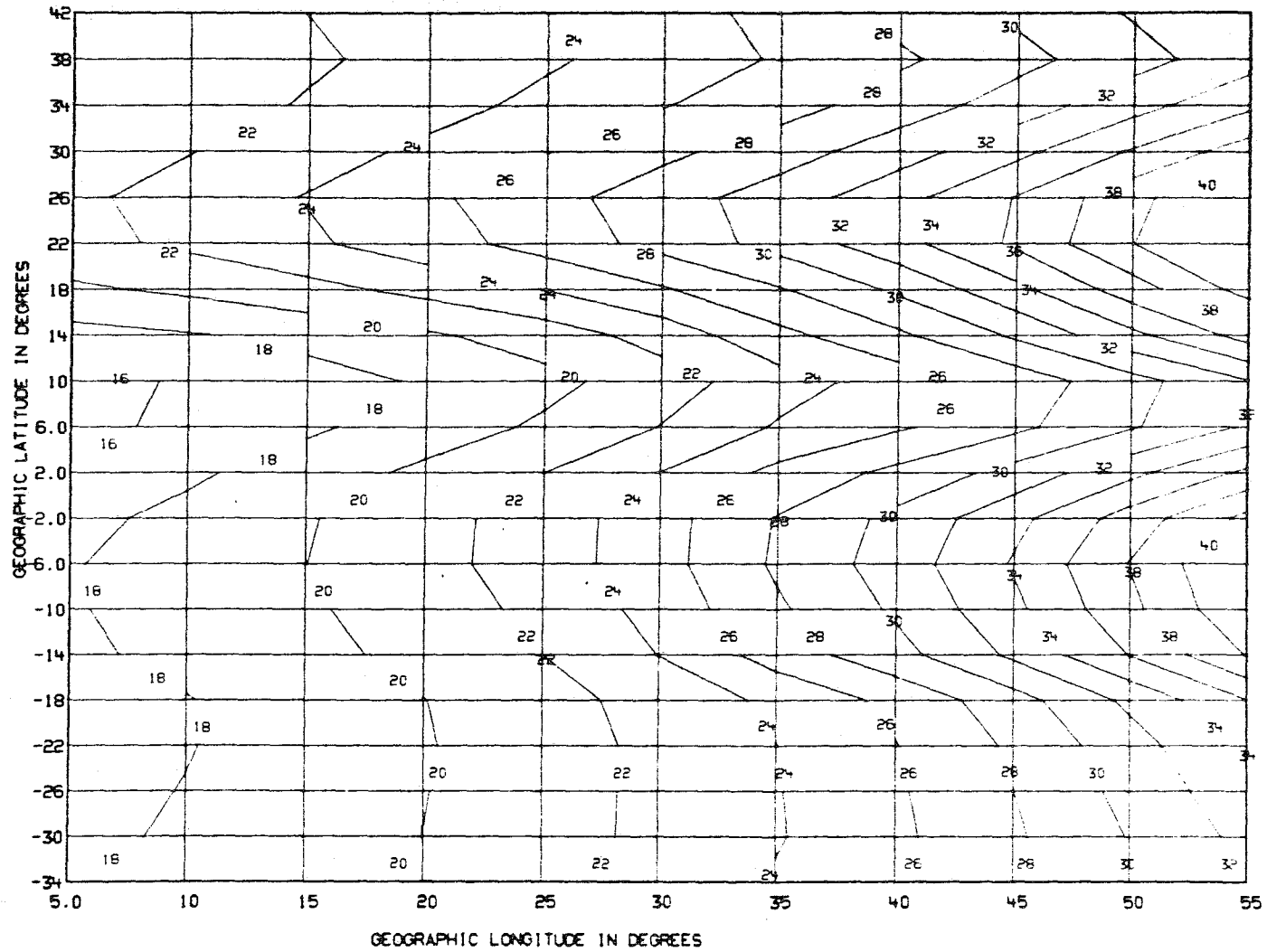
Figure 21. Frequencies (in MHz) that will penetrate the ionosphere above Zone 4, 90 percent of the time during October, 1600 hrs UT, SSN=120 from a geostationary satellite at 15°W longitude.
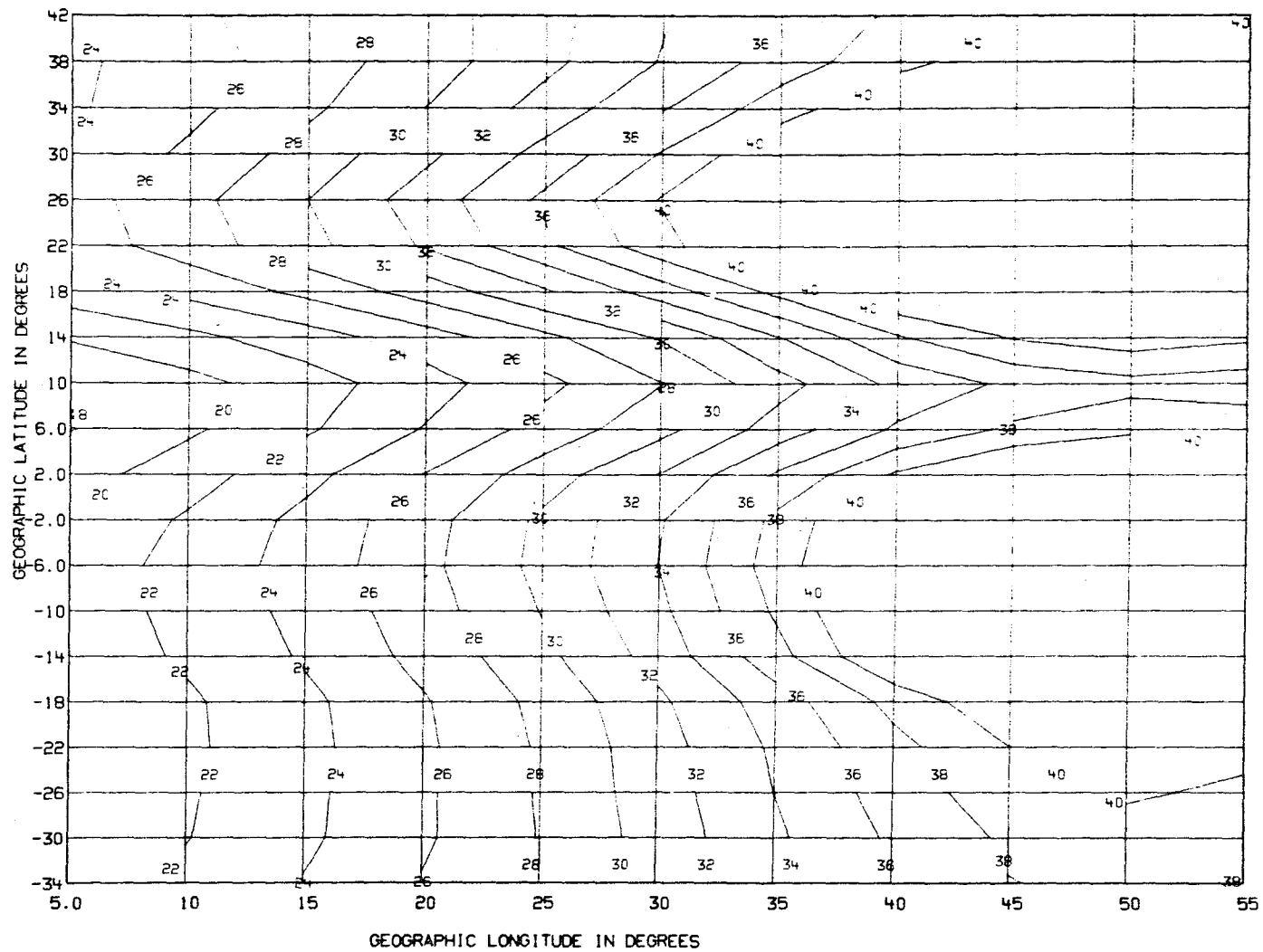
Figure 22. Frequencies (in MHz) that will penetrate the ionosphere above Zone 4, 90 percent of the time during October, 1800 hrs UT, SSN=120 from a geostationary satellite at 30°W longitude.

43
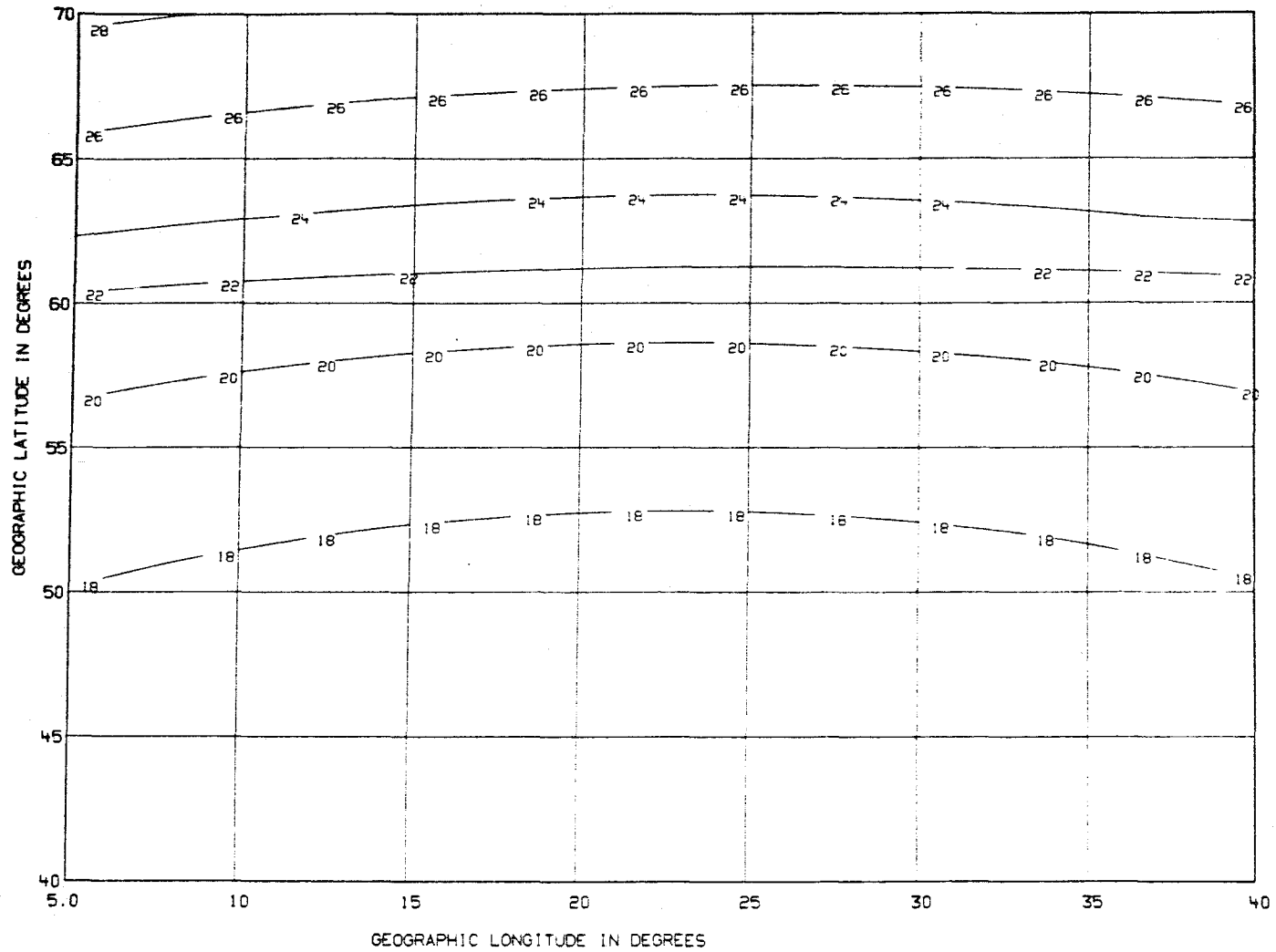
Figure 23. Frequencies (in MHz) that will penetrate the ionosphere above Zone 3, 90 percent of the time during October, 1800 hrs UT, SSN=120 from a geostationary satellite at 0° longitude.

44
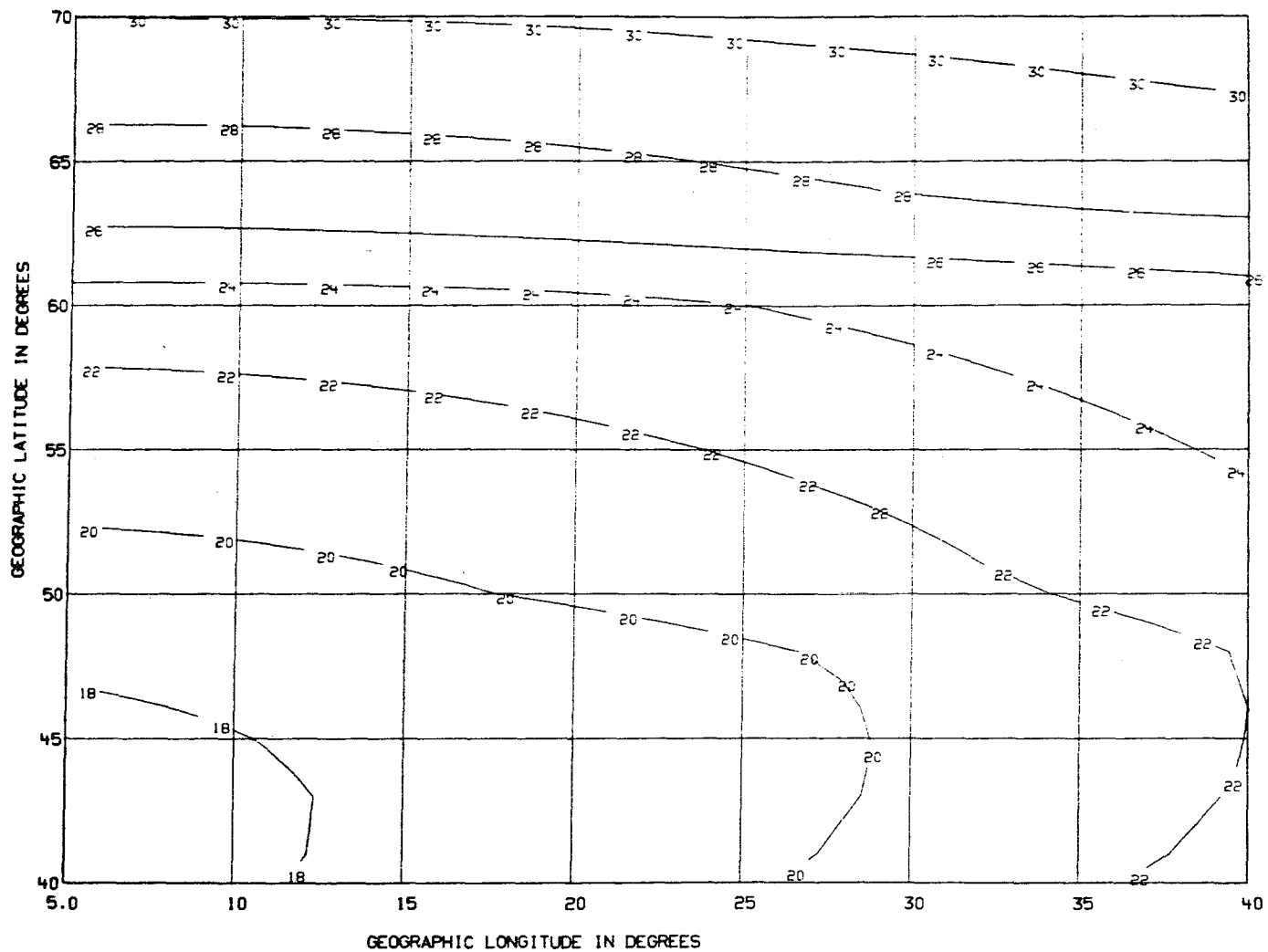
Figure 24.   Frequencies (in MHz) that will penetrate the ionosphere above Zone 3, 90 percent of the time during October, 1800 hrs UT, SSN=120 from a geostationary satellite at 15°W longitude.
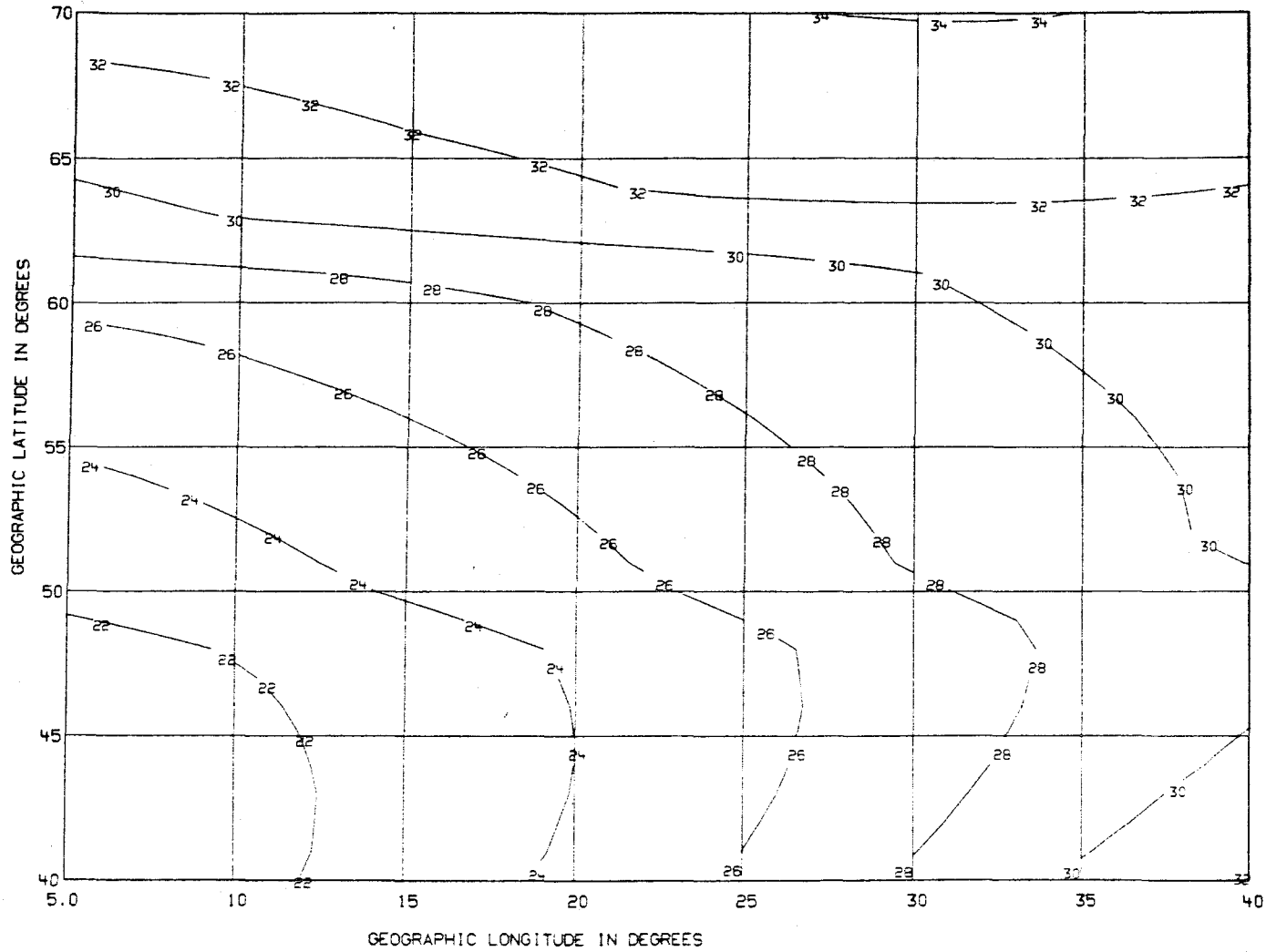
Figure 25.   Frequencies (in MHz) that will penetrate the ionosphere above Zone 3, 90 percent of the time during October, 1800 hrs UT, SSN=120 from a geostationary satellite at 30°W longitude.
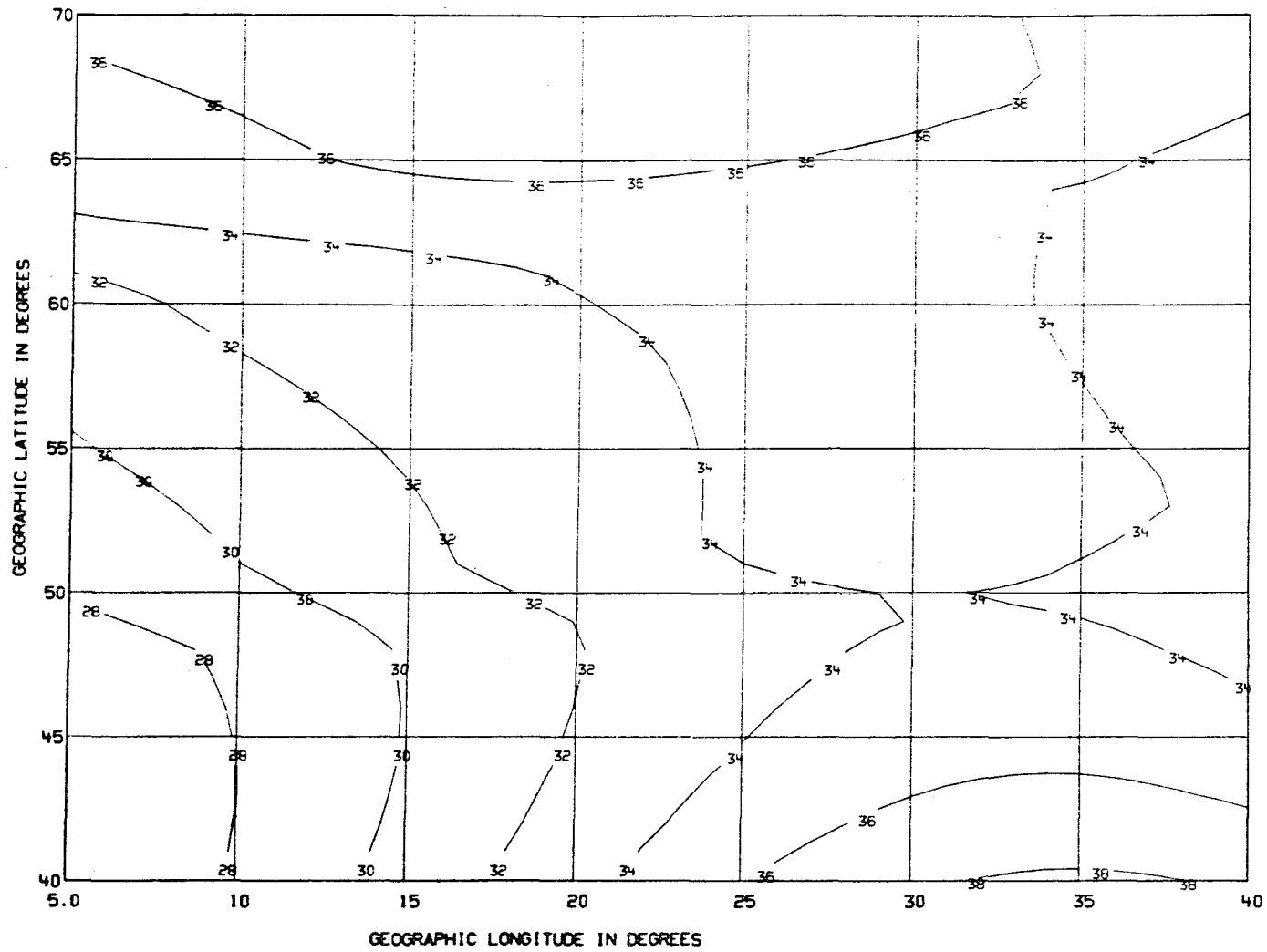
Figure 26. Frequencies (in MHz) that will penetrate the ionosphere above Zone 3, 90 percent of the time during October, 1800 hrs UT, SSN=120 from a geostationary satellite at 45°W longitude.

Table 7. Penetration Frequencies and Ionospheric Losses
for Zone 4 for Satellites in Nonoptimum Geostationary
Locations for October Solar Maximum, 1800 hrs UT

Satellite Location	Offset From Mid-Zone	Penetration Frequency (MHz) to Cover Entire Zone 90 Percent of Time	Ionospheric Loss (dB) for 90 Percent Penetration Frequencies
0°, 30°E	0°	20	2
0°, 15°E	-15°	22	2
0°, 0°	-30°	30	2
0°, 15°W	-45°	40	2
0°, 30°W	-60°	40	2

Table 8. Penetration Frequencies and Ionospheric Losses
for Zone 3 for Satellites in Nonoptimum Geostationary
Locations for October Solar Maximum, 1800 hrs UT

Satellite Location	Offset From Mid-Zone	Penetration Frequency (MHz) to Cover Entire Zone 90 Percent of Time	Ionospheric Loss (dB) for 90 Percent Penetration Frequencies
0°, 0°	-20°	34	2
0°, 15°W	-35°	38	2
0°, 30°W	-50°	40	2
0°, 45°W	-60°	40	2

to provide coverage over the entire solar cycle, frequencies greater than HF must be used if off-set geostationary orbits with low elevation angles are employed in DBS systems.

3.5.2 Effects of other DBS orbits

A satellite in a hovering orbit, such as a Molniya orbit, or a satellite in a sun-synchronous, low-altitude orbit can be used for DBS operations with certain advantage. A hovering and a Molniya orbit can be designed to ensure that the satellite hovers above the intended broadcast target area during the prime listening hours. This will be particularly advantageous for middle-latitude zones where frequencies greater than those allocated to the HF broadcasting service must be used if coverage is to be provided over 90 percent of all time (Sections 3.3 and 3.4). Lower penetration frequencies could be obtained by considering satellites that dwell at locations closer to the intended reception area.

Figures 27 and 28 illustrate the advantage afforded by use of a hovering-type orbit for broadcasting into Zone 5 during October solar maximum at 1600 hrs UT. The figures show the change in the 90 percent penetration frequencies for a satellite that is located along the 55°E meridian at the equator and at 40°N. In determining the penetration frequency, the satellite was assumed to be at a hovering altitude of 35860 km. The effect of moving the location of the satellite closer to the intended reception area is apparent. At 40°N latitude, the penetration frequency needed to provide coverage to the entire zone 90 percent of the time is 10 MHz compared to 26 MHz when the satellite is positioned on the equator in geostationary orbit.

Figures 29, 30, and 31 show the penetration frequencies for July solar maximum for Zones 3, 5, and 7 when a Molniya orbit is used. In determining the penetration frequencies, the satellite was assumed to hover at an altitude of 35860 km. Figure 29 shows results for 1800 hrs UT with the satellite hovering above the location 63°N, 20°E. Figure 30 shows results for 2000 hrs UT with the satellite hovering at 63°N, 70°E. Figure 31 shows comparable results at 0000 hrs UT for a hovering location of 63°N, 125°E. The universal times illustrated for Zones 3 and 5 correspond to local times that span the primary evening broadcasting hours. The results in Figure 31 for Zone 7 are illustrative of local times that span the primary morning broadcasting hours. It is seen that the frequencies greater than 10 MHz will penetrate the ionosphere 90 percent of the time. Calculations performed for other seasons illustrate the same behavior. Use of a Molniya-type orbit for DBS purposes enables frequencies as
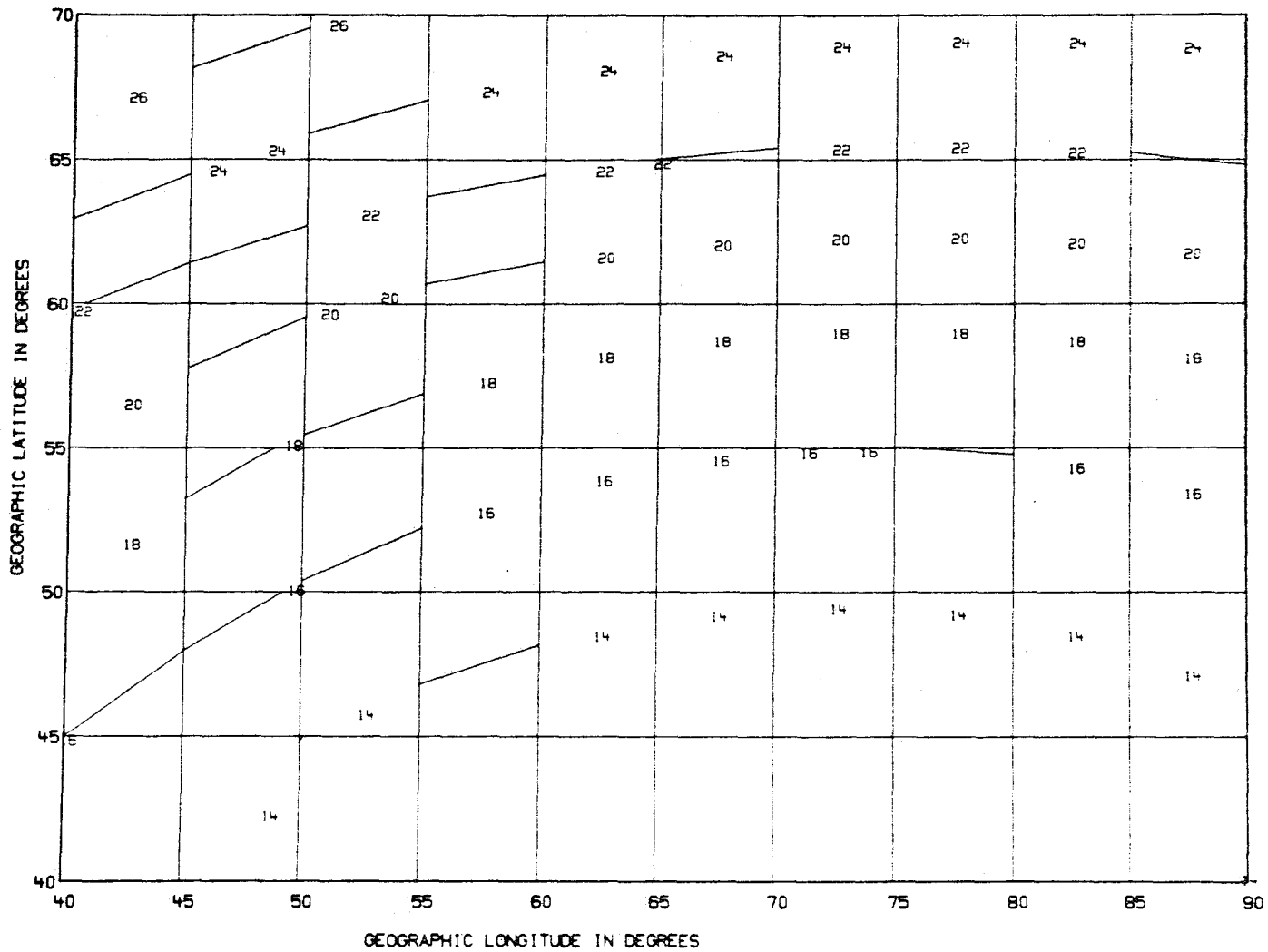
Figure 27. Frequencies (in MHz) that will penetrate the ionosphere above Zone 5, 90 percent of the time during October, 1600 hrs UT, SSN=120 from a satellite hovering at 35860 km, 0° latitude, and 55°E longitude (longitude offset of -10° from mid-zone).
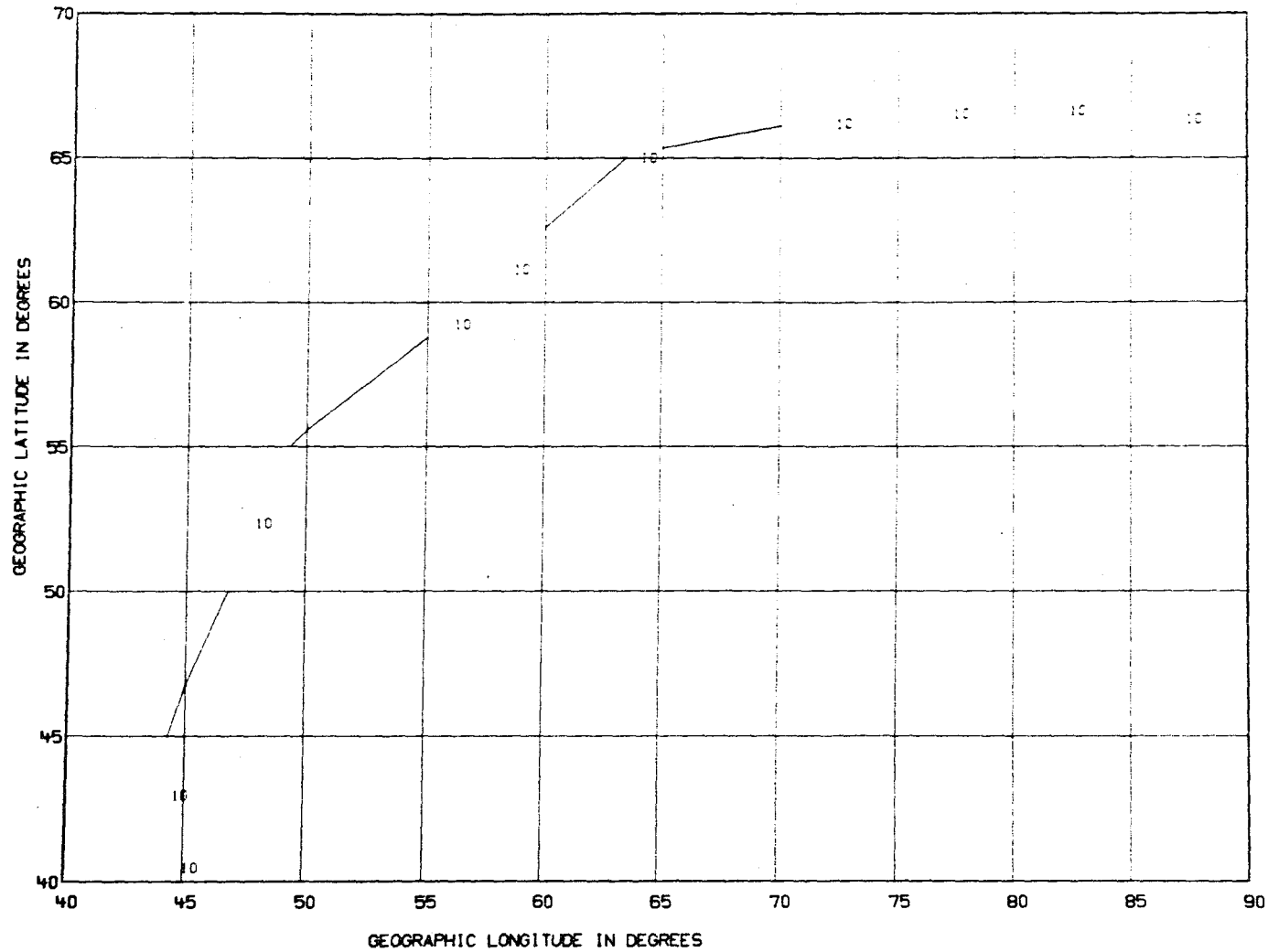
Figure 28.   Frequencies (in MHz) that will penetrate the ionosphere above Zone 5, 90 percent of the time during October, 1600 hrs UT, SSN=120 from a satellite hovering at 35860 km, 40°N latitude, and 55°E longitude (longitude offset -10° from mid-zone).
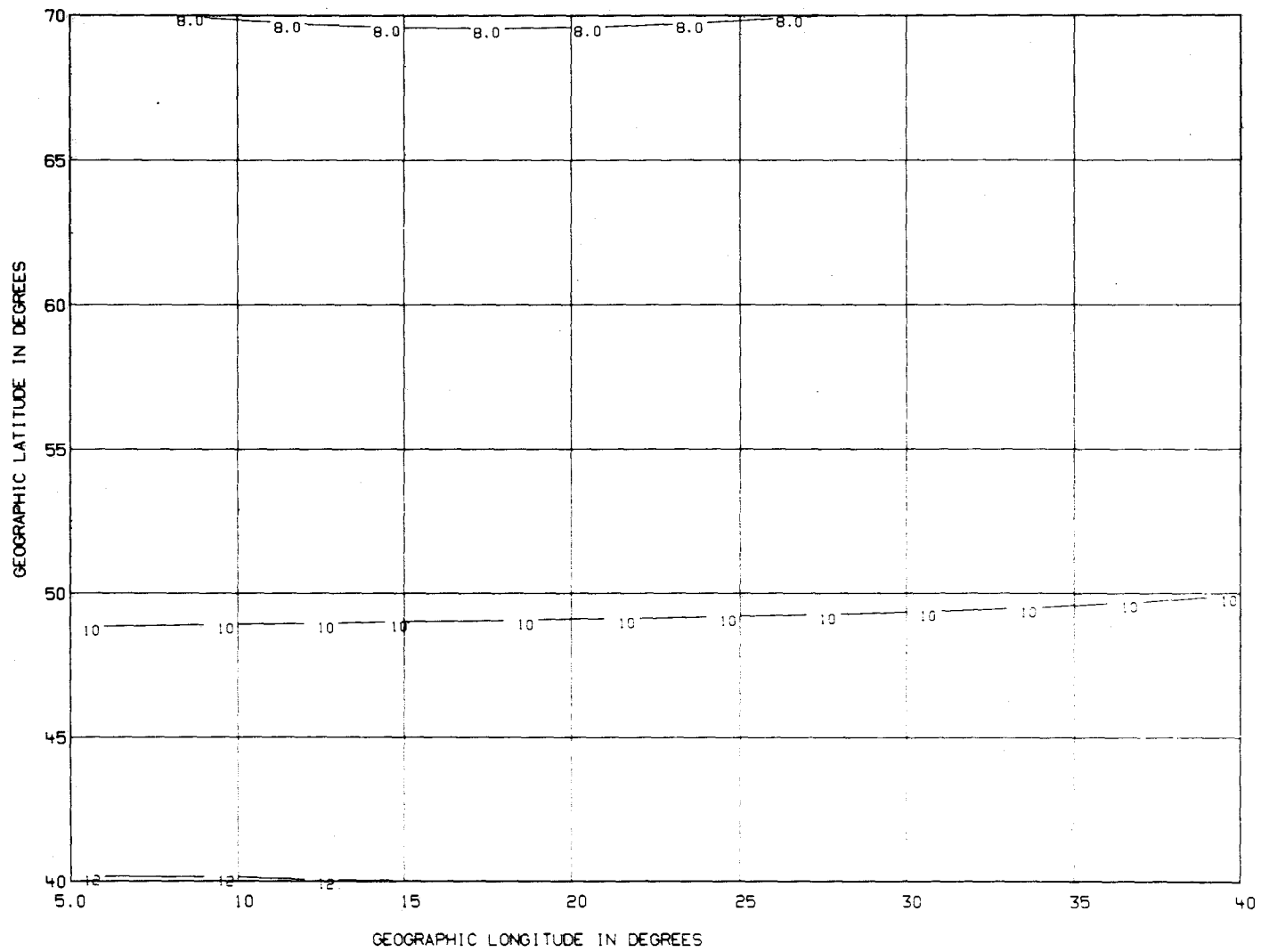
Figure 29.   Frequencies (in MHz) that will penetrate the ionospshere above Zone 3, 90 percent of the time during July, 1800 hrs UT, SSN=120 from a satellite hovering at 35680 km, 63°N latitude, and 20°E longitude.
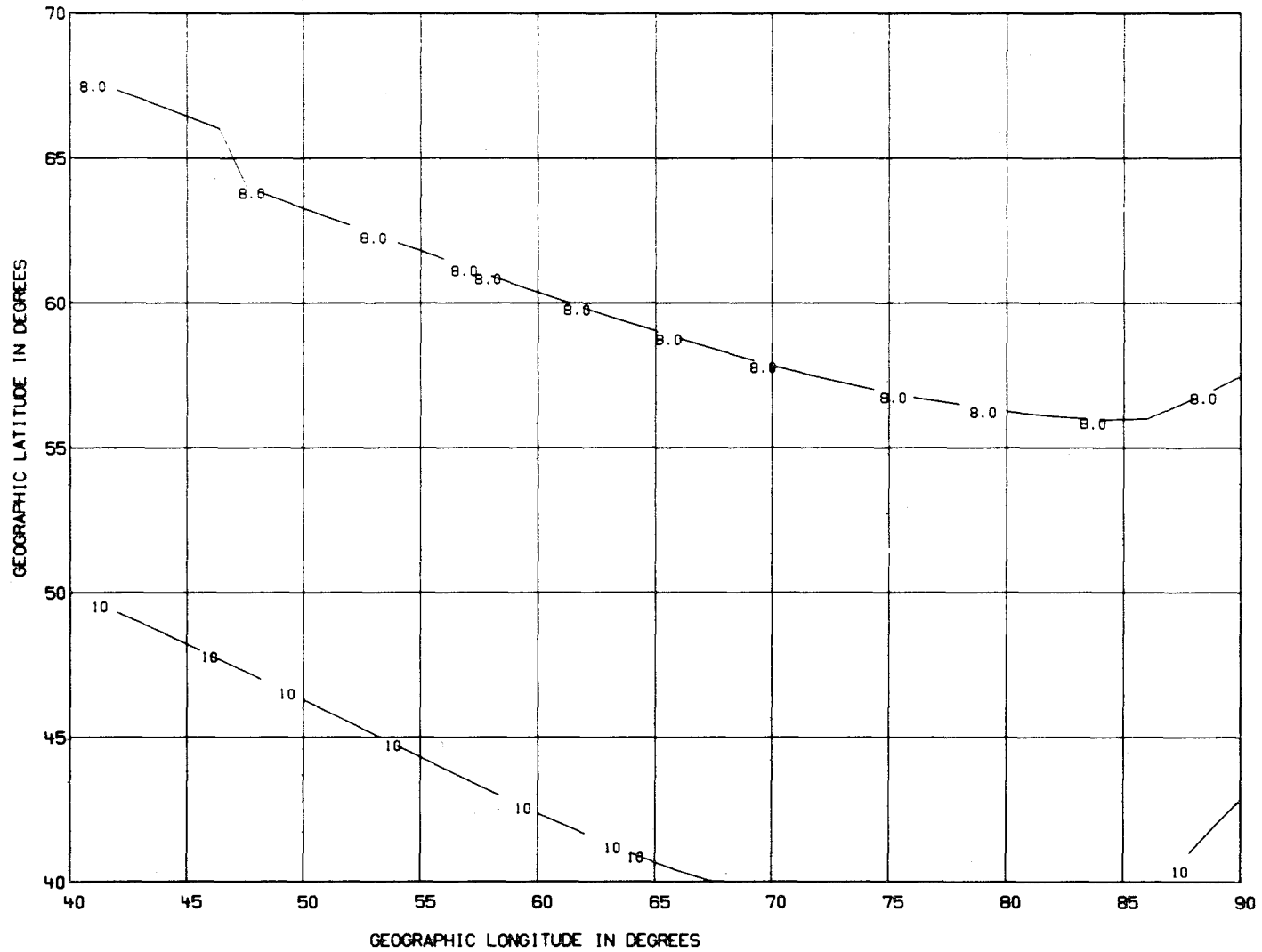
Figure 30. Frequencies (in MHz) that will penetrate the ionospshere above Zone 5, 90 percent of the time during July, 2000 hrs UT, SSN=120 from a satellite hovering at 35680 km, 63°N latitude, and 70°E longitude.

53
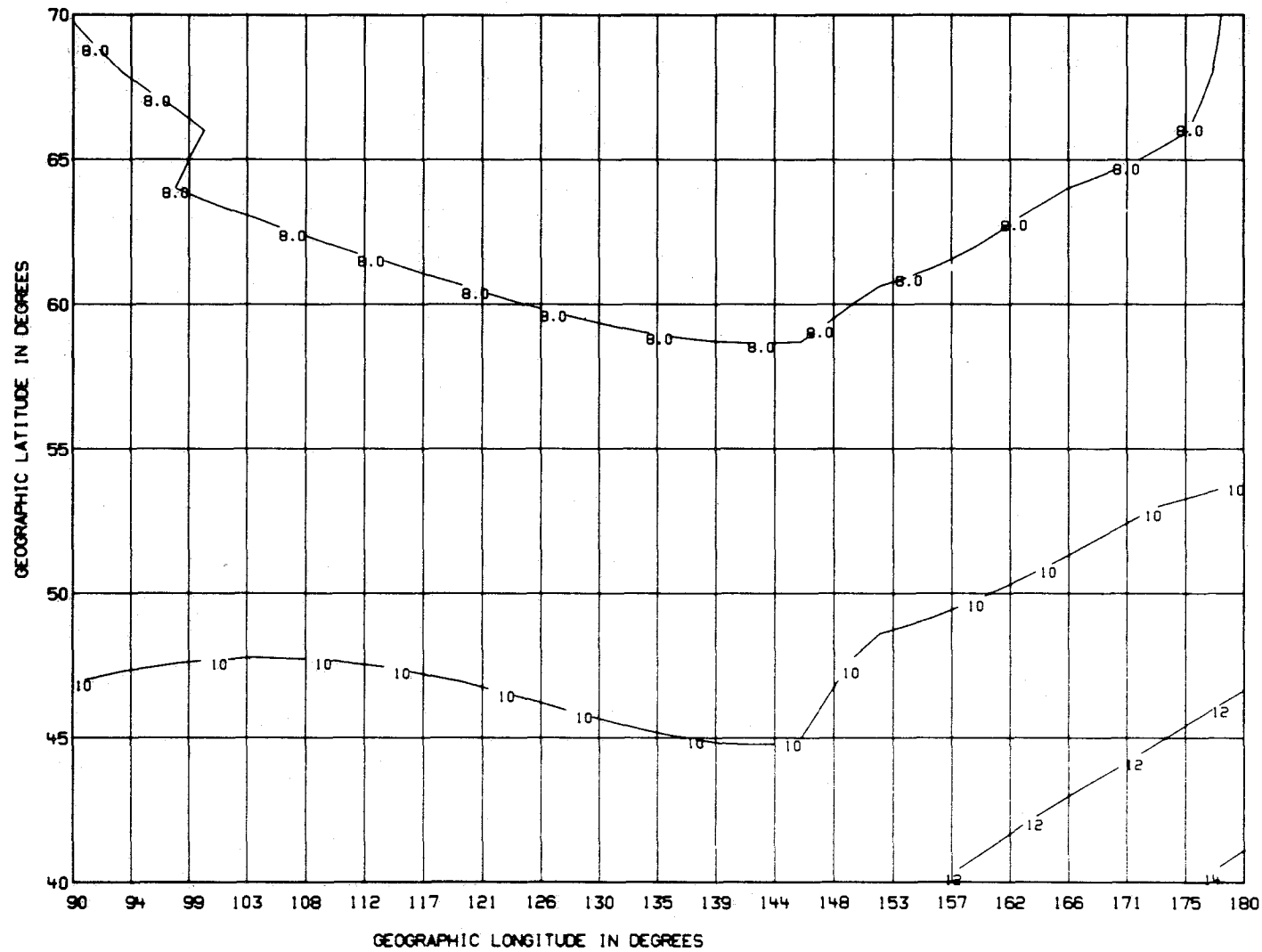
Figure 31.   Frequencies (in MHz) that will penetrate the ionospshere above Zone 7, 90 percent of the time during July, 0000 hrs UT, SSN=120 from a satellite hovering at 35680 km, 63°N latitude, and 125°E longitude.

low as 11.8 MHz (the closest band above 10 MHz that is allocated to the HF broadcast service) to be transmitted into the middle-latitude broadcast target areas over 90 percent of the time.

Similar calculations can be performed for different orbital configurations that provide other advantages over a geostationary orbit. It was mentioned that the use of an 8-hour orbit would enable the use of smaller spacecraft antenna. This is because the spacecraft would be at a lower altitude of 13900 km. In order to provide broadcast coverage to the entire zone with a satellite in an 8-hour orbit at a lower altitude, higher penetration frequencies must be employed than are associated with the operation of a satellite in a geostationary orbit. Figure 32 shows the penetration frequencies for Zone 5 for the 8-hour orbit with the satellite at 0°, 65°E for October solar maximum 1600 hrs UT. Frequencies that are about 2 MHz higher are needed for penetration and total coverage using an 8-hour orbit satellite than a geostationary satellite (see Table 4).

Figures 32 through 37 illustrate the effect of moving the 8-hour satellite location from the equator to 50°N along the 65°E meridian in 10-degree increments during October solar maximum 1600 hrs UT. This simulated the motion of a space-craft in the 8-hour orbit. The penetration frequency needed to cover the entire zone does not vary smoothly as the satellite moves northward. This is because of the relative location of the satellite with respect to the ionospheric structure at this time. The frequency needed to provide coverage to the northern section of Zone 6 more than 90 percent of the time changes quite dramatically as the satellite is positioned further north.

The ionospheric loss associated with the penetration frequencies given in Figures 18 through 37 was found to never exceed 3 dB and, in many instances, was less than 2 dB. Further calculations of the effects of satellite position and altitude on DBS operations can be readily performed. However, because there exists a plethora of orbital configurations and broadcast requirements, such calculations are most meaningful if undertaken with specific broadcasting operational objectives in mind.

4. EFFECTS OF SPORADIC E ON DBS OPERATION

In the previous section, results were presented showing frequencies that penetrate the ionosphere 90 percent of the time assuming that the F2-region ionization distribution controlled the penetration process. This is a legitimate assumption, because the F2-region critical frequency is generally the highest
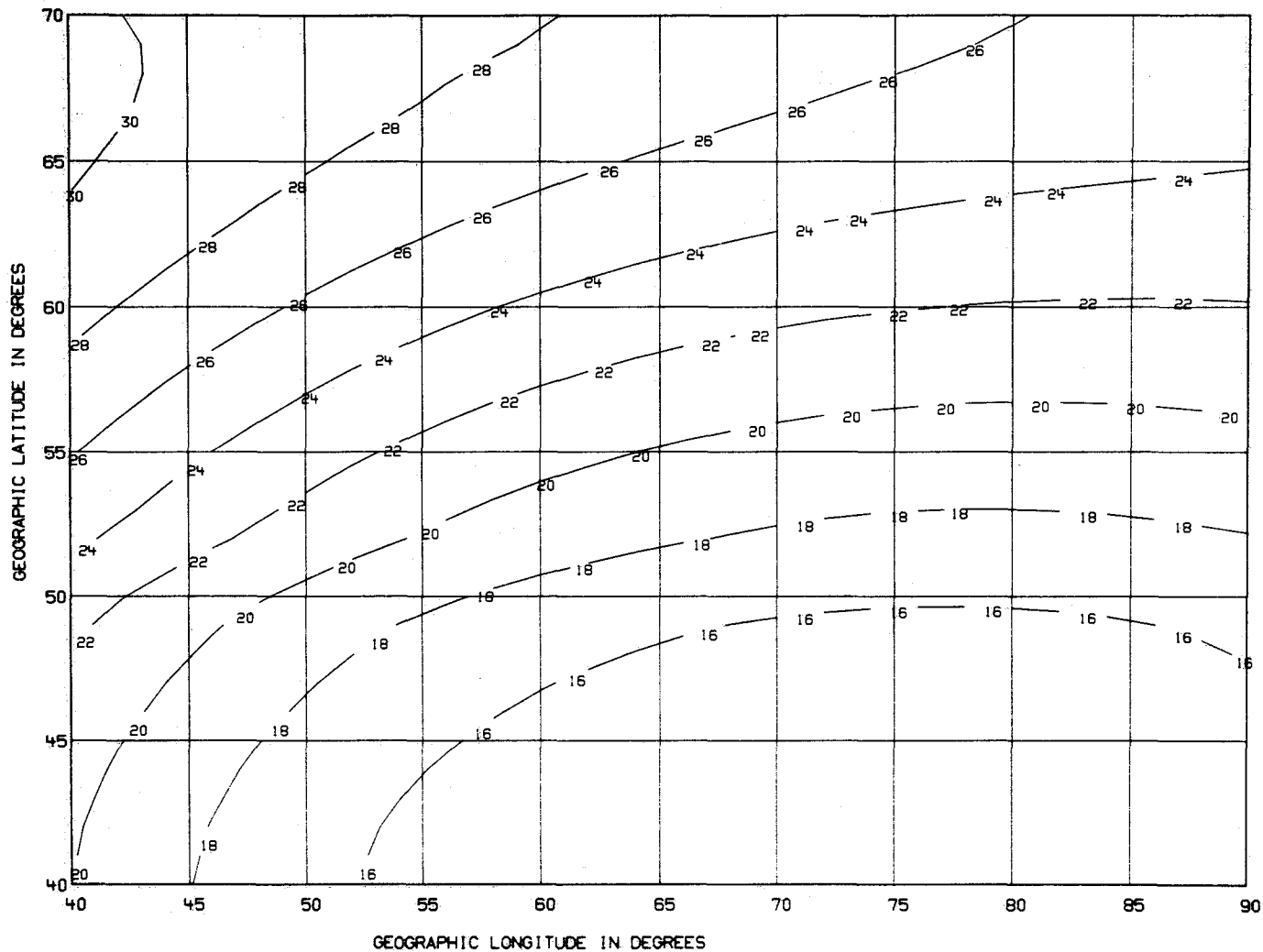
Figure 32. Frequencies (in MHz) that will penetrate the ionosphere above Zone 5, 90 percent of the time during October, 1600 hrs UT, SSN=120 from a satellite in an 8-hour orbit at 13900 km, 0° latitude, and 65°E longitude.
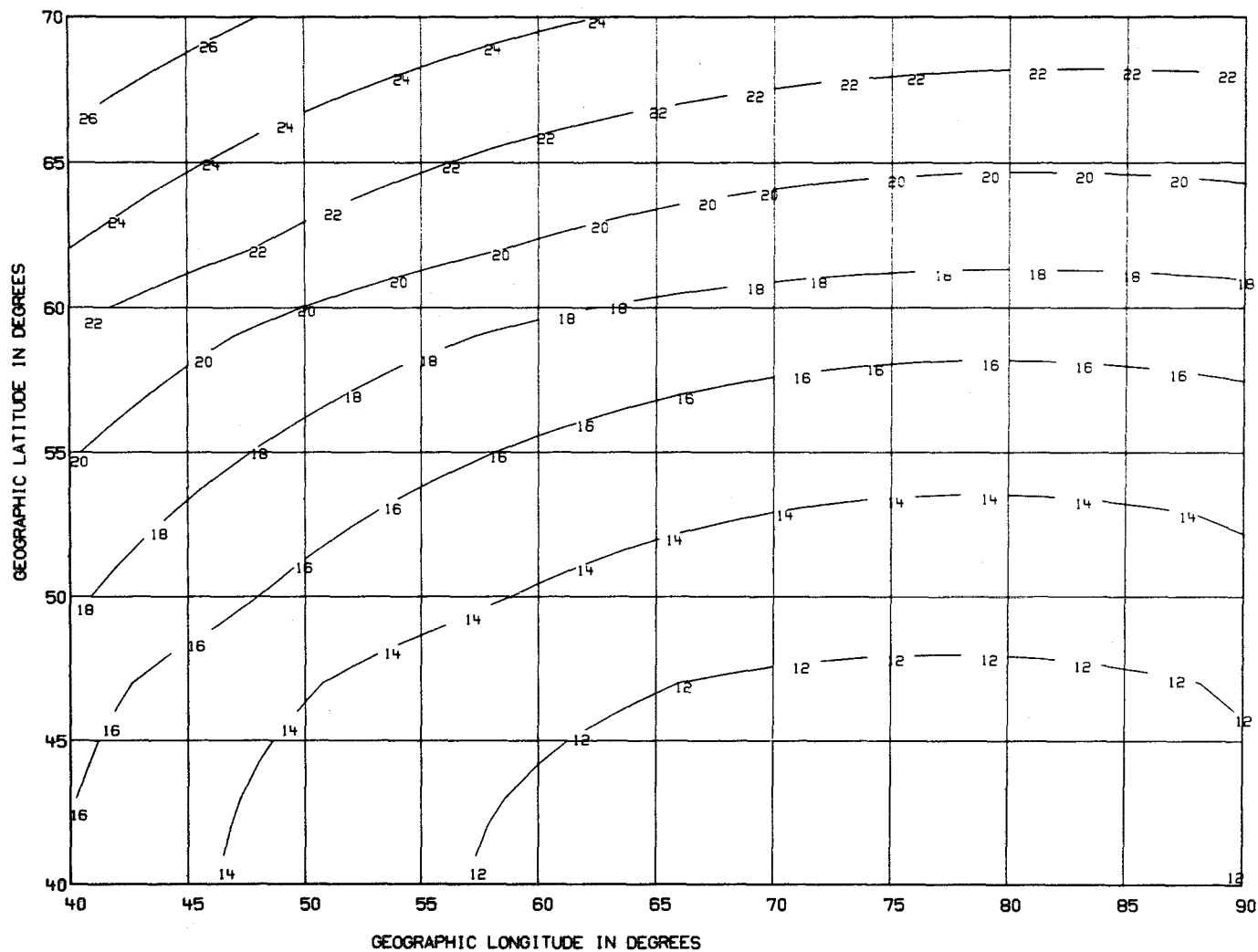
Figure 33. Frequencies (in MHz) that will penetrate the ionosphere above Zone 5, 90 percent of the time during October, 1600 hrs UT, SSN=120 from a satellite in an 8-hour orbit at 13900 km, 10°N latitude, and 65°E longitude.
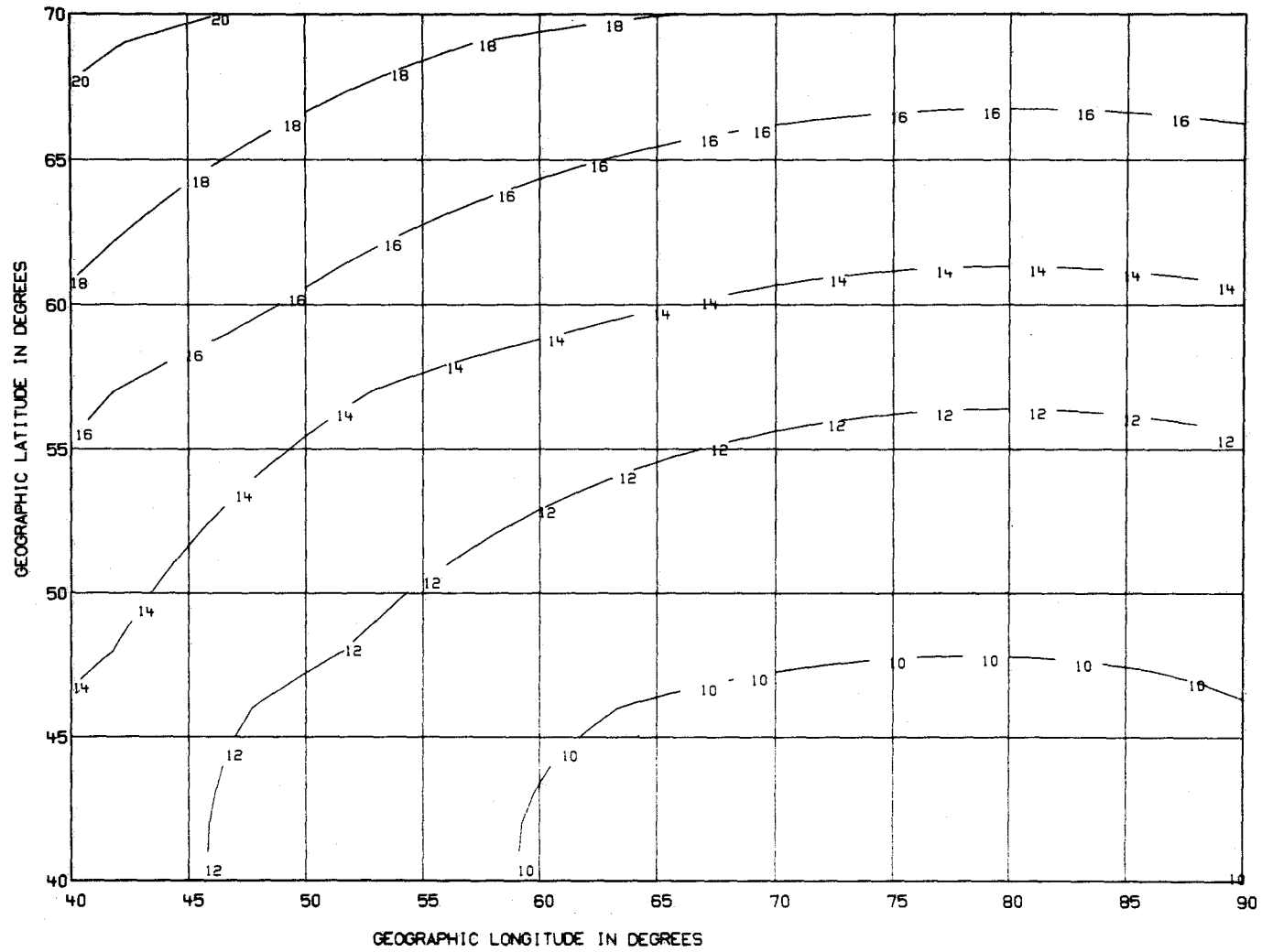
Figure 34. Frequencies (in MHz) that will penetrate the ionosphere above Zone 6, 90 percent of the time during October, 1600 hrs UT, SSN=120 from a satellite in an 8-hour orbit at 13900 km, 20°N latitude, and 65°E longitude.
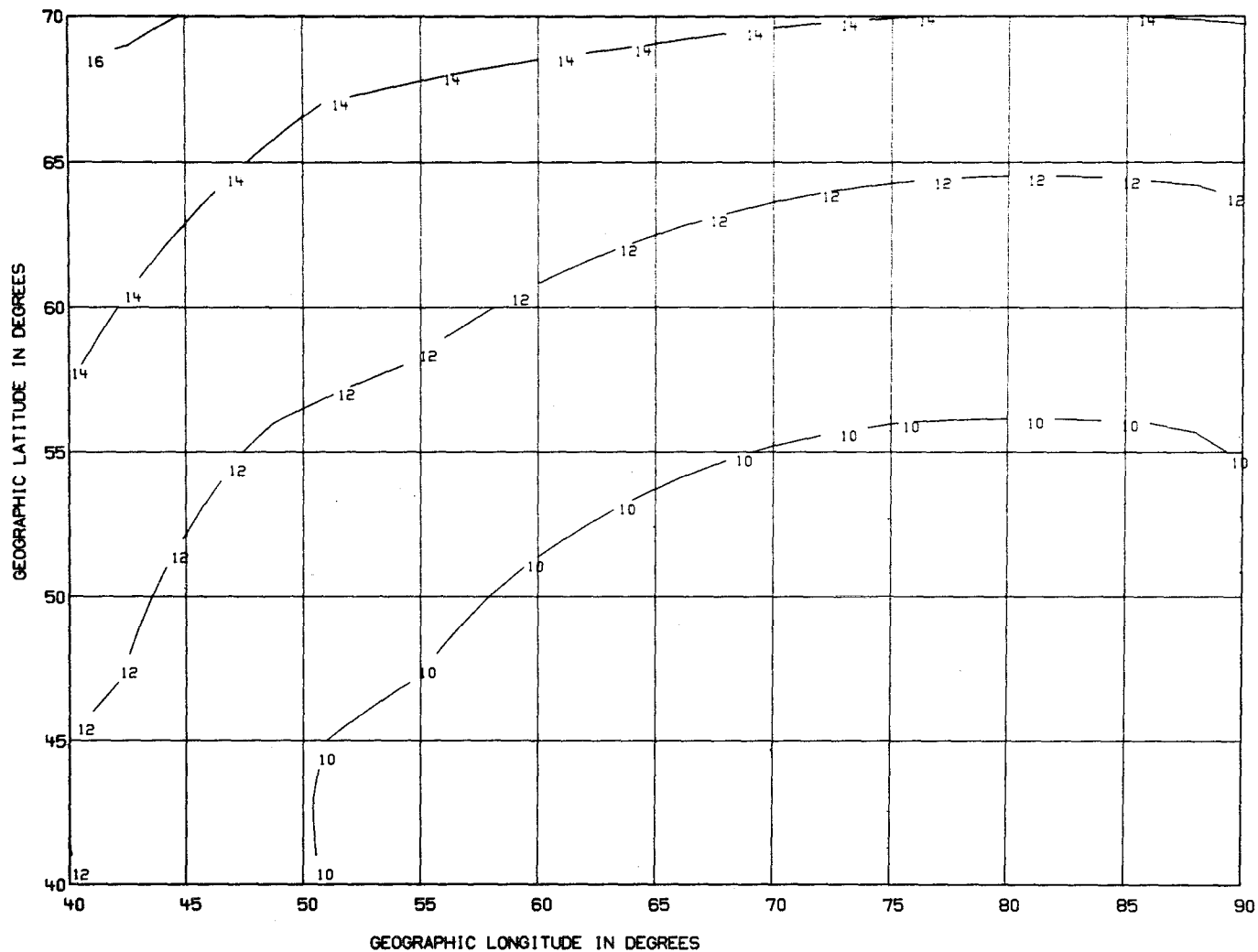
Figure 35.   Frequencies (in MHz) that will penetrate the ionosphere above Zone 6, 90 percent of the time during October, 1600 hrs UT, SSN=120 from a satellite in an 8-hour orbit at 13900 km, 30°N latitude, and 65°E longitude.
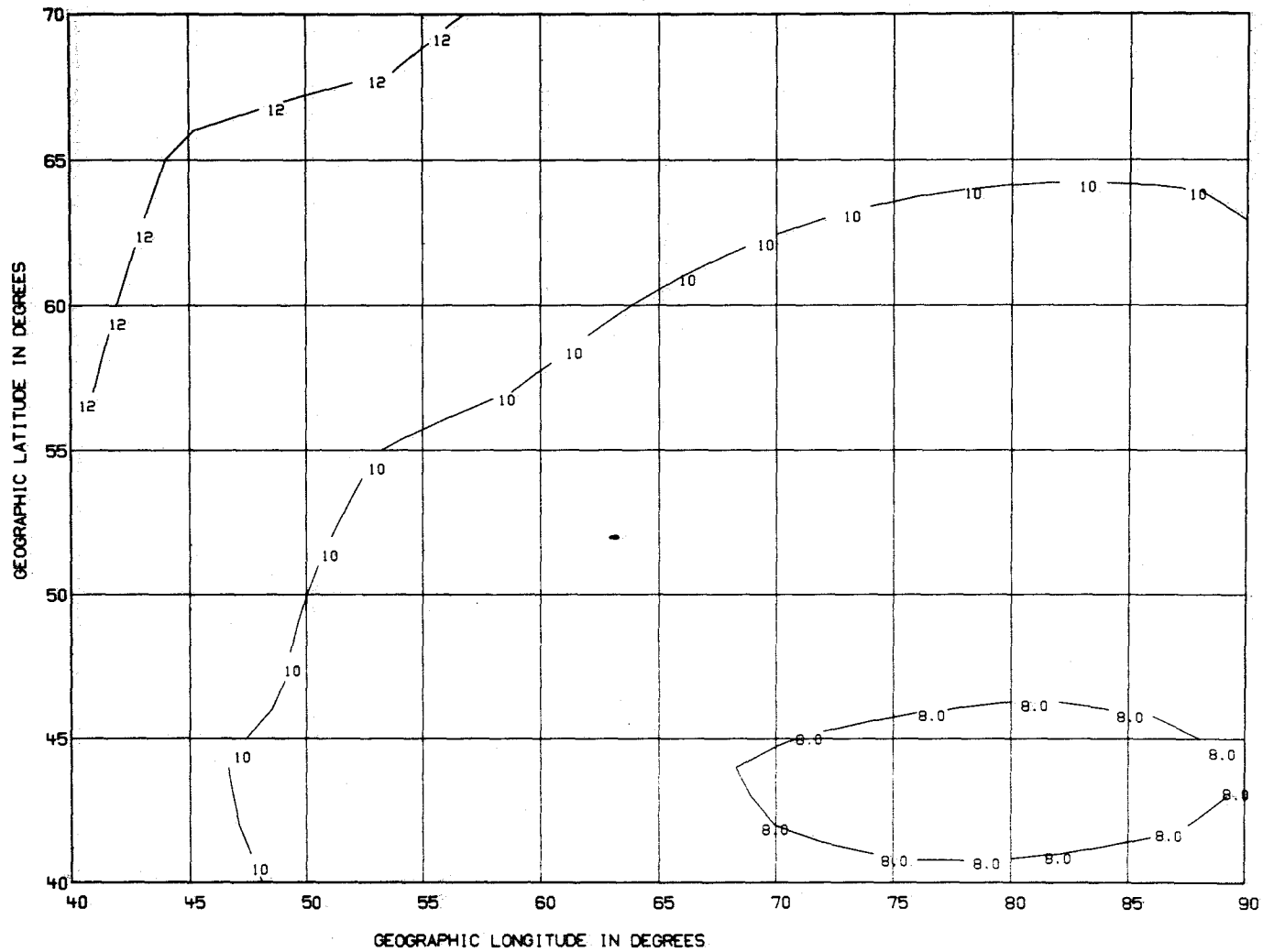
Figure 36.   Frequencies (in MHz) that will penetrate the ionosphere above Zone 5, 90 percent of the time during October, 1600 hrs UT, SSN=120 from a satellite in an 8-hour orbit at 13900 km, 40°N latitude, and 65°E longitude.
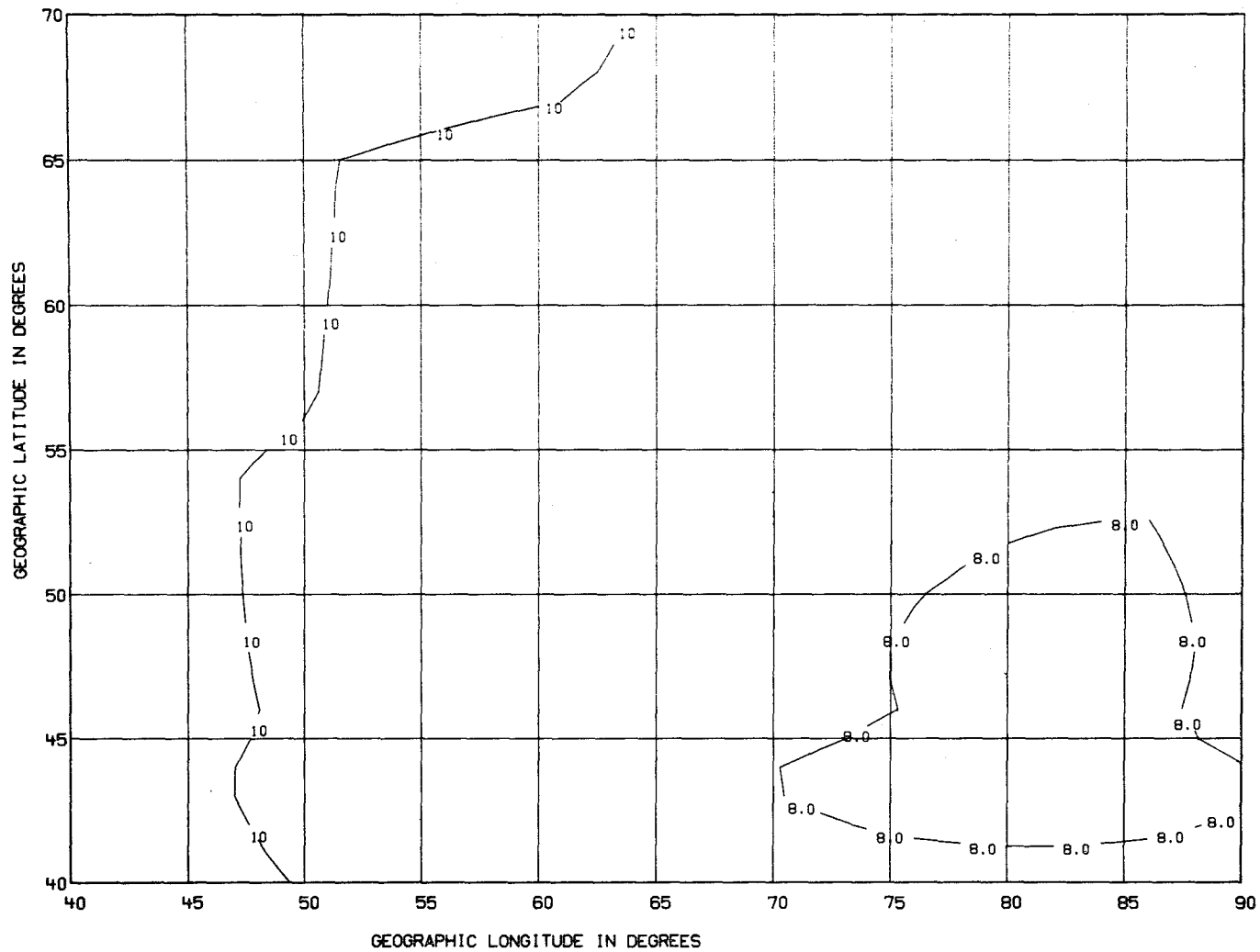
Figure 37. Frequencies (in MHz) that will penetrate the ionosphere above Zone 5, 90 percent of the time during October, 1600 hrs UT, SSN=120 from a satellite in an 8-hour orbit at 13900 km, 50°N latitude, and 65°E longitude.

critical frequency of the various ionospheric layers. There are times, however, when the ionization density in the lower ionosphere exceeds that in the F2 region. In particular, the number of electrons that are observed in sporadic-E layers can, at times, exceed that of the F2 region. The structure of sporadic-E ionization takes many different forms--it can appear sheet-like and essentially nonretarding to electromagnetic energy propagated through, or it can appear relatively thick with high refractive properties. The sheet-like sporadic-E structures can appear at all latitudes, while the thick structures are usually confined to the equatorial and polar ionospheric regions.

The name, sporadic E, derives from the early history of ionospheric observation. It was observed at middle latitudes that a thin layer of ionization appeared at E-region heights on vertical-incidence ionograms in a quasi-random or sporadic fashion. It is now known that sporadic E can occur regularly under certain conditions. The sheet-like structure of sporadic E is a regular feature of the daytime summer middle-latitude ionosphere. It can also occur with regularity in the equatorial and polar regions. The refracting type of sporadic E that occurs at the equatorial and polar latitudes is generally associated with some geophysical phenomena such as equatorial irregularities resulting from plasma instabilities, plasma interactions in the polar ionosphere, or auroral substorm activity.

The effect of sporadic E on signals transmitted from a satellite in a high-altitude orbit to the surface of the earth are twofold, depending upon the type of sporadic-E ionization:

    (a) It can refract and reflect signals that pass through the F2 region preventing them from reaching the intended target area, or

    (b) It can cause scattering of the signal resulting in a reduced signal strength at the surface of the earth.

In order to determine to what extent the results presented in Section 3 need to be modified to account for sporadic-E effects on transionospherically propagated signals, a study was conducted to determine how often the critical frequency of the sporadic-E layer was likely to exceed the critical frequency of the F2 region in the areas of the world of primary interest for DBS applications. Observations of the critical frequency of the F2 region and the critical frequency of the sporadic-E layer, foEs, that were observed at the locations given in Table 9 were used in the study.

In keeping with the procedures adopted in Section 3, the months of January, April, July, and October were considered to be representative of the four

Table 9. Stations Used in Study of Sporadic-E Effects on Transionospheric Signals

	Latitude (°) N	Longitude (°) E	Magnetic Dip
Leningrad, USSR	59.95	30.70	73.11
Moscow, USSR	55.47	37.32	70.72
Lindau, Fed. Rep. Germany	51.60	10.10	67.04
Poitiers, Belgium	46.60	.30	62.67
Genova, Italy	44.60	9.00	60.90
Khabarovdk, USSR	48.50	135.10	63.36
Wakkanai, Japan	45.40	141.70	59.03
Akita, Japan	39.70	140.10	53.24
Tokyo, Japan	35.67	139.55	48.54
Yamagawa, Japan	31.20	130.60	43.91
Okinawa	26.30	127.80	36.58
Grand Bahama Island	26.60	281.80	58.47
Djibouti	11.50	42.80	5.66
Bogota, Colombia	4.50	285.80	29.78
Huancayo, Peru	-12.05	284.67	- .05
Johannesburg, South Africa	-26.10	28.10	-63.42

seasons. In addition, the sporadic-E and foF2 data were analyzed for a year of low solar activity and a year of high solar activity in order to determine the solar cycle variability, if any, in the occurrence and magnitude of sporadic-E observations. Primary consideration was given to sporadic-E observations for the current solar cycle, Cycle 21. Data for the years 1975 and 1976 were used for minimum solar activity, and data for 1979 were used to represent maximum solar activity. In a few cases, due to the unavailability of ionospheric observations for the current cycle, observations from previous solar cycles, i.e., Cycles 19 and 20, were used for the analysis. For broadcast planning purposes, the primary listening hours were assumed to be 4 to 6 hours after sunrise and after sunset. Therefore, observations for only these hours are considered in this study.

The penetration frequency given by the methods in Section 2 is determined by the highest critical frequency encountered along the propagation path from the satellite to the ground. Although the refracting type of sporadic E could cause additional refraction of signals that penetrate the F2 region under conditions when foF2 exceeds foEs, for broadcast planning purposes, it can be assumed that the penetration frequency is determined either by foF2 or foEs. If foEs rarely exceeds foF2, then it can be assumed that the results given in Section 3 are valid even in the presence of sporadic E. Tables 10 and 11 show the percentage of time that sporadic-E ionization totally blankets the F2-region critical frequency (i.e., prevents it from being observed) for the 16 locations given in Table 9 for the four seasonal months for each of the two levels of solar activity.

From Table 10, it is seen that there is more blanketing sporadic E occurring in local summer than in local winter in the northern hemisphere. Blanketing sporadic E occurs more frequently for the hours after sunrise and at sunset in local summer, while in local winter it occurs more frequently at sunrise and the hours following sunset. This seasonal effect is probably due to the very low foF2 values observed during the night hours in local winter. Conversely, in local summer, the foF2 values are relatively lower after sunrise, and normally there is a secondary maximum in foF2 after sunset.

Geographically, the maximum occurrence of blanketing sporadic E is at the temperature latitudes between 30°-50°N in both summer and winter, and there is essentially no blanketing sporadic E at the magnetic equator (Djibouti and Huancayo) and the southern hemisphere station of Johannesburg. For the two equinoctial months, there is very little blanketing sporadic E observed. There are a

64

Table 10. Percentage of Time foF2 is Totally Blanketed by foEs at Solar Cycle Minimum

JANUARY / JULY

Station	SR	+1	+2	+3	+4	+5	SS	+1	+2	+3	+4	+5	SR	+1	+2	+3	+4	+5	SS	+1	+2	+3	+4	+5
Leningrad	7	3	0	0	0	0	0	0	10	15	8	24	0	0	0	7	7	3	0	0	0	0	0	3
Moscow	3	0	0	0	0	0	0	0	0	0	3	3	0	3	3	3	6	3	0	0	0	0	6	0
Lindau	0	0	0	0	0	0	0	0	0	0	6	0	0	0	6	13	23	13	17	3	0	6	3	3
Poitiers	3	0	0	0	0	0	3	0	3	0	6	0	0	0	10	16	23	13	6	10	3	7	10	7
Genova	0	0	0	0	0	0	0	0	0	0	0	3	7	0	0	18	7	45	3	3	0	0	6	10
Khabarovsk	0	6	0	0	0	0	3	3	3	10	6	0	0	3	20	20	33	30	26	13	3	0	10	7
Wakkanai	3	0	0	0	0	0	3	16	10	6	10	10	3	17	33	33	30	40	30	10	10	13	17	13
Akita	0	0	0	0	0	0	0	7	7	3	0	3	7	18	14	29	24	30	7	7	10	10	14	3
Tokyo	0	0	0	0	0	0	3	3	10	6	19	3	7	13	14	30	30	30	7	3	3	3	10	3
Yamagawa	3	0	0	0	0	0	0	3	3	0	0	0	7	18	7	7	30	40	0	7	13	17	17	10
Okinawa	20	0	0	0	0	0	0	10	10	3	3	3	6	6	0	6	0	17	0	10	7	10	6	10
Grand Bahama	0	0	0	0	0	0	0	0	0	3	3	3	3	10	6	6	3	10	0	0	3	3	0	0
Djibouti	10	0	0	0	0	0	0	0	0	0	0	0	10	0	0	0	0	0	0	0	0	0	0	0
Bogota	0	0	0	0	0	0	0	7	10	7	3	3	0	0	0	0	7	3	0	0	0	0	0	0
Huancayo	0	0	0	0	0	0	0	0	0	0	0	0	0	0	0	0	0	0	0	0	0	0	0	0
Johannesburg	0	0	0	0	0	0	0	0	0	0	0	0	0	0	0	0	0	0	0	0	0	0	0	0

APRIL / OCTOBER

Station	SR	+1	+2	+3	+4	+5	SS	+1	+2	+3	+4	+5	SR	+1	+2	+3	+4	+5	SS	+1	+2	+3	+4	+5
Leningrad	11	0	0	0	0	0	0	0	0	0	0	3	3	0	0	0	0	0	0	0	0	0	0	0
Moscow	0	0	0	0	0	0	0	0	0	3	3	3	0	0	0	0	0	0	0	0	0	0	0	0
Lindau	0	0	0	0	0	0	0	0	0	0	0	0	0	0	0	0	0	0	0	0	0	0	0	0
Poitiers	3	0	0	0	0	0	0	0	0	0	0	3	3	3	0	0	0	3	0	0	0	0	6	3
Genova	0	0	0	0	0	0	0	0	0	0	0	0	0	0	0	0	0	0	0	0	0	0	0	0
Khabarovsk	0	0	0	0	0	7	0	0	0	0	0	0	0	0	0	0	0	3	0	7	3	3	0	3
Wakkanai	3	3	0	7	3	0	0	0	0	0	0	0	0	3	3	0	0	0	0	3	3	13	10	3
Akita	0	0	0	0	3	3	0	0	3	0	0	0	0	0	0	0	0	0	0	0	3	3	3	3
Tokyo	3	0	0	3	3	7	0	0	0	0	0	0	0	0	0	0	0	0	0	0	0	0	0	3
Yamagawa	3	0	3	0	7	7	0	0	7	3	3	3	0	0	0	0	0	0	0	3	3	0	0	6
Okinawa	23	0	3	0	7	3	3	12	24	24	17	20	0	3	0	0	0	0	0	0	0	0	0	0
Grand Bahama	0	0	0	0	0	0	0	0	0	3	0	3	3	0	0	0	0	0	0	0	0	3	3	0
Djibouti	13	0	0	0	0	3	0	0	0	0	0	0	0	0	0	0	0	3	0	0	0	0	0	0
Bogota	0	0	0	3	0	0	0	0	0	0	0	0	3	0	0	0	0	0	0	0	3	3	0	0
Huancayo	0	0	0	0	0	0	0	0	0	0	0	0	0	0	0	0	0	0	0	0	0	0	0	0
Johannesburg	0	0	0	0	0	0	0	0	0	3	3	0	0	0	0	0	0	0	0	0	0	0	0	0

Table 11. Percentage of Time foF2 is Totally Blanketed by foEs at Solar Cycle Maximum

JANUARY

Station	SR	+1	+2	+3	+4	+5	SS	+1	+2	+3	+4	+5	SR	+1	+2	+3	+4	+5	SS	+1	+2	+3	+4	+5
		Time	(hrs)					Time	(hrs)					Time	(hrs)					Time	(hrs			
Leningrad	0	0	0	0	0	0	0	0	0	0	0	0	0	0	0	3	0	0	0	0	0	0	0	0
Moscow	0	0	0	0	0	0	0	0	0	0	0	0	0	0	0	0	0	0	0	0	0	0	0	0
Lindau	0	0	0	0	0	0	0	0	0	0	0	0	0	0	0	0	0	0	0	0	3	3	0	0
Poitiers	0	0	0	0	0	0	0	0	0	0	0	0	0	0	0	0	0	0	3	0	0	0	0	0
Genova	0	0	0	0	0	0	0	0	0	0	0	0	0	0	0	6	10	6	6	6	6	0	0	3
Khabarovsk	0	0	0	0	0	0	0	0	0	0	0	0	0	10	3	0	3	3	3	0	6	0	0	0
Wakkanai	0	0	0	0	0	0	0	0	0	0	0	0	0	0	0	7	13	10	10	3	0	0	0	0
Akita	0	0	0	0	0	0	0	0	3	0	0	0	0	0	3	6	6	23	13	13	10	0	0	0
Tokyo	0	0	0	0	0	0	0	0	0	0	0	0	0	0	0	10	0	10	6	3	0	0	0	0
Yamagawa	0	0	0	0	0	0	0	0	0	3	0	0	0	0	3	0	13	10	0	3	0	3	3	0
Okinawa	0	0	0	0	0	0	0	0	0	0	0	0	0	0	0	3	3	3	0	0	0	0	3	3
Grand Bahama	0	0	0	0	0	0	0	0	0	0	0	0	0	0	0	6	0	3	0	0	3	3	0	0
Djibouti	7	0	0	0	0	0	0	0	0	0	0	0	0	0	0	0	0	0	0	0	0	0	0	0
Bogota	0	0	0	0	0	0	0	0	0	0	0	0	0	0	0	0	0	0	0	0	0	0	0	0
Huancayo	0	0	0	0	0	0	0	0	0	0	0	0	0	0	0	0	0	0	0	0	0	0	0	0
Johannesburg	0	0	0	0	0	0	0	0	0	0	0	0	0	0	0	0	0	0	0	0	0	0	0	0

(JANUARY columns 1–12; JULY columns 13–24)

APRIL

Station	SR	+1	+2	+3	+4	+5	SS	+1	+2	+3	+4	+5	SR	+1	+2	+3	+4	+5	SS	+1	+2	+3	+4	+5
Leningrad	0	3	0	0	0	0	0	0	0	0	0	0	0	0	0	0	0	0	0	0	0	0	0	0
Moscow	0	0	0	0	0	0	0	0	0	0	0	0	0	0	0	0	0	0	0	0	0	0	0	0
Lindau	0	0	0	0	0	0	0	0	0	0	0	0	0	0	0	0	0	0	0	0	0	0	0	0
Poitiers	0	0	0	0	0	0	0	0	0	0	0	0	0	0	0	0	0	0	0	0	0	0	0	0
Genova	0	0	0	0	0	0	0	0	0	0	0	0	0	0	0	0	0	0	0	0	0	0	0	0
Khabarovsk	0	0	0	0	0	0	0	0	0	0	0	0	0	0	0	0	0	0	0	0	0	0	0	0
Wakkanai	0	0	0	0	0	0	0	0	0	0	0	0	0	0	0	0	0	0	0	0	3	0	0	0
Akita	0	0	0	0	0	0	0	3	0	0	0	0	0	0	0	0	0	0	0	0	0	0	0	0
Tokyo	0	0	0	0	0	0	0	0	0	0	0	0	0	0	0	0	0	0	0	0	0	0	0	0
Yamagawa	0	0	0	0	0	0	0	0	0	3	0	0	0	0	0	0	0	0	0	0	0	0	0	0
Okinawa	0	0	0	0	0	0	0	0	0	0	0	0	0	0	0	0	0	0	0	0	0	0	0	0
Grand Bahama	0	0	0	0	0	0	0	0	0	0	0	0	0	0	0	0	0	0	0	0	0	0	0	0
Djibouti	0	0	0	0	0	0	0	0	0	0	0	0	0	0	0	0	0	0	0	0	0	0	0	0
Bogota	0	0	0	3	0	0	0	0	0	0	0	0	0	0	0	0	0	0	0	0	0	0	0	0
Huancayo	0	0	0	0	0	0	0	0	0	0	0	0	0	0	0	0	0	0	0	0	0	0	0	0
Johannesburg	3	0	0	0	0	0	0	0	0	0	0	0	0	0	0	0	0	0	0	0	0	0	0	0

(APRIL columns 1–12; OCTOBER columns 13–24)

few occurrences in the Asian sector only and, seasonally, it is more prevalent during the hours after sunrise in April and the hours following sunset in October.

The percentage of time that foF2 is totally blanketed by foEs at solar maximum is given in Table 11. It is evident (because of the increased magnitudes of foF2) that sporadic E never totally blankets or obscures the F2 layer, except in the Asian sector during local summer (July).

Tables 12 and 13 show how often foEs exceeds foF2 at the same locations given in Tables 10 and 11. In general, the seasonal variations apparent in Table 12 are similar to those mentioned above for Table 10. Geographically, it is interesting to note that at Huancayo, where sporadic E never blanketed the F2 layer at solar minimum, quite frequently sporadic E is observed at frequencies greater than the F2-layer critical frequencies. This is particularly true for the sunrise period for July and April and to a lesser extent for January.

The results given in Tables 11 and 13 indicate that (except for the Asian sector, local summer) sporadic E would not be expected to blanket the F2 layer or would foEs exceed foF2 for a significant percentage of the time at solar maximum.

This is demonstrated quite markedly in Figures 38 and 39. These figures show the cumulative distribution of foF2, foEs, and fbEs (the sporadic-E blanketing frequency) during July solar minimum (1975) and solar maximum (1979) activity levels for Moscow and Akita. The results are shown for the month (July) at which sporadic E exerts its layers and effect and for local times in the middle of the primary broadcasting hours. Figure 38 shows that only for a few hours after sunrise during solar minimum (1975) are foEs and fbEs greater than foF2 for more than 10 percent of the time at Moscow. During the evening hours (Fig. 38b), foEs and fbEs at Moscow never exceed foF2 more than a few percent of the time. The results for Akita, shown in Figure 39 (39a and 39b), indicate that during solar minimum, foEs and fbEs can exceed foF2 for substantial periods of time in the morning and evening hours. During solar maximum, however, foEs and fbEs rarely exceed foF2 for more than 10 percent of the time.

The results that were presented in Section 3 were derived in a manner to maximize the influence of the ionosphere on the penetration frequency and are assumed to be valid for 90 percent of all time. The results were determined for ionospheric conditions found during solar minimum and solar maximum. In light of the findings presented in Tables 11 and 13, the penetration frequencies determined solely by considering foF2 appear to be appropriate for solar maximum even in the presence of sporadic E. During solar minimum conditions, sporadic-E

Table 12. Percentage of Time foEs Exceeds foF2 at Solar Cycle Minimum

JANUARY / JULY

Station	SR	+1	+2	+3	+4	+5	SS	+1	+2	+3	+4	+5	SR	+1	+2	+3	+4	+5	SS	+1	+2	+3	+4	+5
Leningrad	7	7	0	0	0	0	0	3	13	15	11	27	27	30	13	10	10	13	19	0	6	0	10	19
Moscow	13	6	0	0	0	0	3	6	16	10	14	30	29	19	10	13	16	29	10	3	6	13	19	29
Lindau	10	0	0	3	0	0	0	3	26	6	23	26	47	29	39	48	74	52	27	30	10	19	26	17
Poitiers	6	0	0	0	0	0	3	6	3	3	13	0	10	6	16	20	32	13	6	13	10	17	17	10
Genova	0	0	0	0	0	0	0	0	3	3	3	7	23	41	14	33	35	52	21	10	31	14	36	37
Khabarovsk	3	10	0	0	0	0	3	19	19	29	13	6	6	3	23	40	47	53	45	27	19	10	17	10
Wakkanai	6	6	0	0	0	0	19	39	35	42	23	23	27	37	57	67	63	67	50	40	13	20	33	30
Akita	3	0	3	0	0	0	3	13	20	23	13	7	27	40	50	53	52	83	40	38	21	17	34	41
Tokyo	0	0	3	3	0	0	3	7	10	17	23	20	21	38	46	55	57	46	31	14	14	17	21	16
Yamagawa	30	0	0	0	3	3	0	3	7	0	10	7	30	33	26	33	68	63	24	38	24	31	32	22
Okinawa	33	0	0	0	0	0	0	10	13	3	17	13	42	26	16	26	45	55	13	23	13	23	13	29
Grand Bahama	6	6	3	3	0	6	0	3	26	26	19	13	52	32	16	23	29	29	10	10	10	35	26	26
Djibouti	13	0	0	0	3	3	0	0	0	0	0	0	20	7	7	0	3	7	0	0	0	3	3	7
Bogota	17	0	0	3	0	0	3	10	20	17	10	20	7	7	3	10	10	7	0	0	0	0	0	0
Huancayo	50	3	0	3	6	23	0	0	0	0	0	0	50	7	7	23	30	52	0	3	0	0	0	3
Johannesburg	26	9	17	9	0	0	9	0	9	4	4	13	43	0	0	0	3	0	0	3	16	16	13	3

APRIL / OCTOBER

Station	SR	+1	+2	+3	+4	+5	SS	+1	+2	+3	+4	+5	SR	+1	+2	+3	+4	+5	SS	+1	+2	+3	+4	+5
Leningrad			No Data						No Data				3	0	0	0	0	0	0	0	10	10	6	0
Moscow	0	3	0	0	0	0	3	3	0	10	13	3	3	0	0	0	0	0	0	0	3	10	13	13
Lindau	0	3	3	0	0	3	0	0	0	0	0	0	6	0	0	3	3	16	3	0	0	0	6	10
Poitiers	3	0	0	0	0	0	0	0	0	0	0	3	3	3	3	0	0	3	0	0	0	0	6	3
Genova	0	0	0	0	0	0	0	0	0	0	0	0	0	0	0	0	0	0	3	0	6	3	0	3
Khabarovsk	0	0	0	0	0	7	0	0	0	0	0	0	0	0	0	0	0	3	0	10	3	3	10	6
Wakkanai	3	10	0	13	7	10	0	0	0	3	0	0	0	3	3	6	3	0	3	3	6	19	10	13
Akita	3	0	6	7	10	10	13	10	3	7	3	3	0	0	6	0	3	0	3	10	14	17	21	24
Tokyo	3	0	7	10	7	7	0	7	7	10	3	13	0	0	0	0	3	0	0	13	19	16	13	10
Yamagawa	20	0	3	3	10	10	3	0	13	20	20	10	19	10	0	0	0	3	0	3	10	13	6	10
Okinawa	36	0	3	9	10	7	3	12	24	33	17	20	14	17	0	0	0	0	0	0	3	3	3	3
Grand Bahama	3	3	0	0	3	0	0	0	0	7	3	3	20	23	3	0	0	3	7	10	27	30	13	13
Djibouti	23	3	0	0	3	7	0	0	0	0	0	0	7	7	0	0	0	3	0	0	0	0	0	0
Bogota	0	0	0	3	0	0	0	0	0	0	0	0	3	0	0	0	0	0	3	6	3	6	13	13
Huancayo	63	40	3	3	33	60	7	0	3	0	0	0	23	0	0	0	3	7	0	0	0	0	0	0
Johannesburg	10	6	0	0	0	0	0	0	0	3	3	3	8	0	3	0	0	0	0	0	0	0	0	0

Table 13. Percentage of Time foEs Exceeds foF2 at Solar Cycle Maximum

JANUARY / JULY

Station	Time (hrs)						Time (hrs)						Time (hrs)						Time (hrs					
	SR	+1	+2	+3	+4	+5	SS	+1	+2	+3	+4	+5	SR	+1	+2	+3	+4	+5	SS	+1	+2	+3	+4	+5
Leningrad	0	0	0	0	0	0	0	0	0	0	0	0	0	0	0	6	0	0	3	0	0	0	6	3
Moscow	0	0	0	0	0	0	0	0	0	0	0	3	0	0	0	0	3	3	3	3	0	0	0	3
Lindau	3	3	0	0	0	0	0	0	0	0	0	0	3	3	0	0	6	10	6	7	6	6	6	3
Poitiers	0	0	0	0	0	0	0	0	0	0	0	0	0	0	3	0	0	0	6	0	0	0	0	0
Genova	3	3	0	0	0	0	0	0	0	0	0	0	0	0	0	10	13	10	10	13	6	3	0	7
Khabarovsk	0	0	0	0	0	0	0	0	0	0	0	3	0	10	3	3	3	6	6	0	6	0	0	0
Wakkanai	0	0	0	0	0	0	0	0	0	10	6	0	3	3	3	17	30	23	19	17	17	10	10	0
Akita	0	0	0	0	0	0	0	0	0	6	3	3	0	0	6	16	23	33	13	23	16	19	13	6
Tokyo	0	0	0	0	0	0	0	0	0	0	0	0	0	0	3	16	10	16	10	6	10	3	10	10
Yamagawa	0	0	0	0	0	0	0	0	0	0	0	0	0	3	3	6	28	13	10	13	10	3	10	3
Okinawa	0	0	0	0	0	0	0	0	0	0	0	0	6	6	3	6	16	23	0	0	0	3	0	0
Grand Bahama	10	0	0	0	0	0	0	0	0	0	0	3	6	0	0	17	3	6	0	3	3	3	0	0
Djibouti	7	0	0	0	0	0	0	0	0	0	0	0	0	0	0	0	0	0	3	0	0	0	0	0
Bogota	0	0	0	0	0	0	0	0	0	0	0	0	0	3	10	0	0	0	0	0	0	0	0	0
Huancayo	7	0	0	0	0	0	0	0	0	0	0	0	0	0	0	0	0	0	0	0	0	0	0	0
Johannesburg	0	0	0	0	0	0	0	0	0	0	0	0	0	0	0	0	0	0	0	0	0	0	0	3

APRIL / OCTOBER

Station	Time (hrs)						Time (hrs)						Time (hrs)						Time (hrs					
	SR	+1	+2	+3	+4	+5	SS	+1	+2	+3	+4	+5	SR	+1	+2	+3	+4	+5	SS	+1	+2	+3	+4	+5
Leningrad	0	3	0	0	0	0	0	0	0	3	3	0	0	0	0	0	0	0	0	0	0	0	0	0
Moscow	0	0	0	0	0	0	3	3	0	0	0	0	0	0	0	0	0	0	0	0	0	0	0	0
Lindau	0	3	0	0	0	0	0	0	0	0	0	0	3	0	0	0	0	0	0	0	0	0	0	0
Poitiers	0	0	0	0	0	0	0	0	0	0	0	0	0	0	0	0	0	0	0	0	0	0	0	0
Genova	0	0	0	0	0	0	0	0	0	0	0	0	0	0	0	0	0	0	0	0	0	0	3	0
Khabarovsky	0	0	0	0	0	0	0	0	0	0	0	0	0	0	0	0	0	0	0	0	0	3	3	0
Wakkanai	0	0	0	0	0	0	0	0	0	0	0	0	0	0	0	0	0	0	0	0	3	0	3	3
Akita	0	0	0	0	0	0	3	3	0	3	0	0	0	0	0	0	0	0	0	0	0	0	0	0
Tokyo	0	0	0	0	0	0	0	7	0	3	0	0	0	0	0	0	0	0	3	6	0	0	0	0
Yamagawa	0	0	0	0	0	0	0	0	0	3	0	0	0	0	0	0	0	0	3	0	0	0	0	0
Okinawa	0	0	0	0	0	0	0	0	0	0	0	0	0	0	0	0	0	0	0	0	0	0	0	0
Grand Bahama	0	0	0	0	0	0	0	0	0	0	0	0	0	0	0	0	0	0	0	0	0	0	0	0
Djibouti	0	0	0	0	0	0	0	0	0	0	0	0	0	0	0	0	0	0	0	0	0	0	0	0
Bogota	0	0	0	0	0	0	0	0	0	0	0	0	0	0	0	0	0	0	0	0	0	0	0	0
Huancayo	0	0	0	0	0	0	0	0	0	0	0	0	0	0	0	0	0	0	0	0	0	0	0	0
Johannesburg	3	0	0	0	0	0	0	0	0	0	0	0	0	0	0	0	0	0	0	0	0	0	0	0

69

Figure 38a. Cumulative distribution of foF2, foEs, and fbEs at Moscow during July for the time period 0700-0900 LMT.
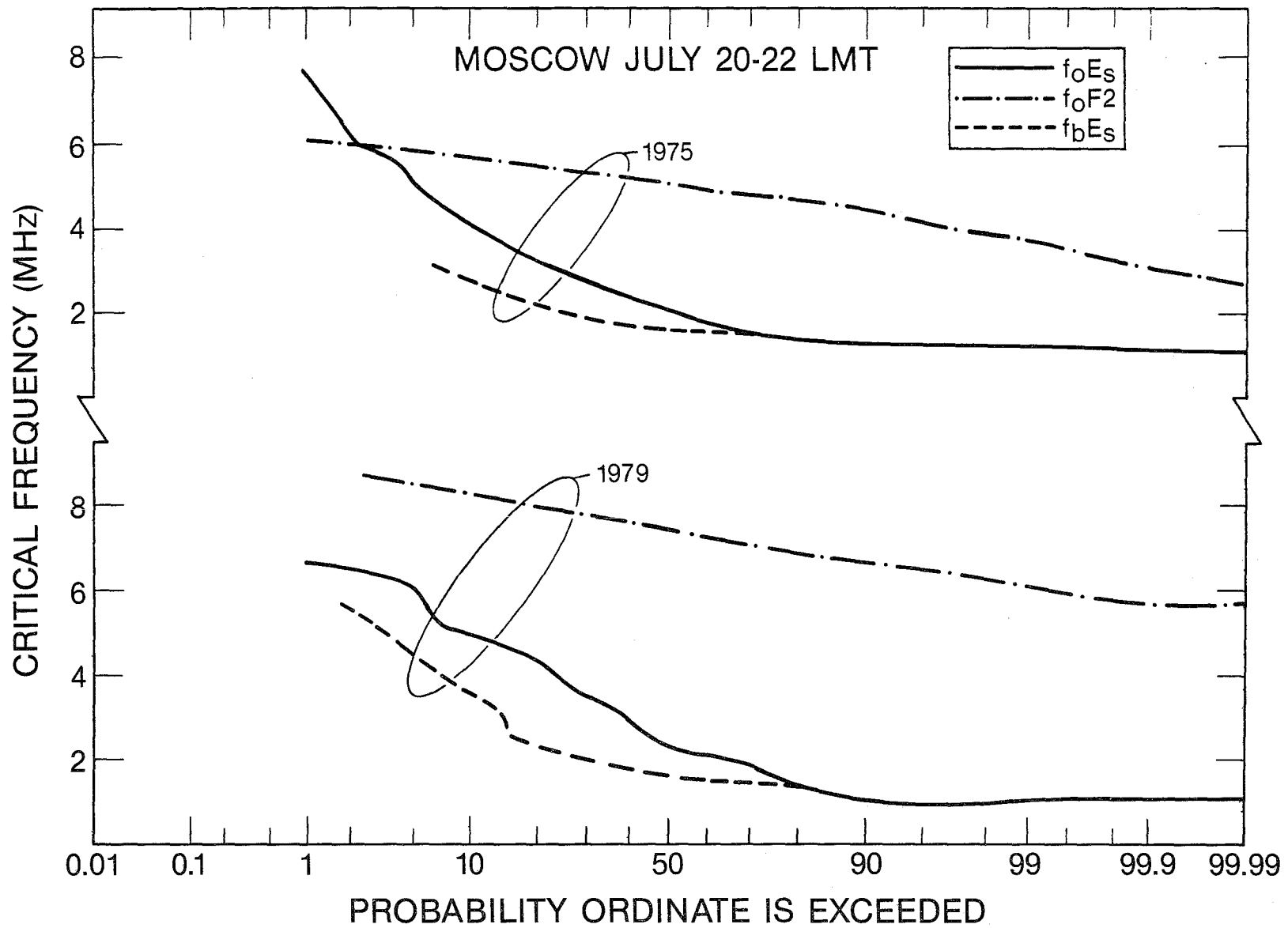
Figure 38b. Cumulative distribution of foF2, foEs, and fbEs at Moscow during July
for the time period 2000-2200 LMT.
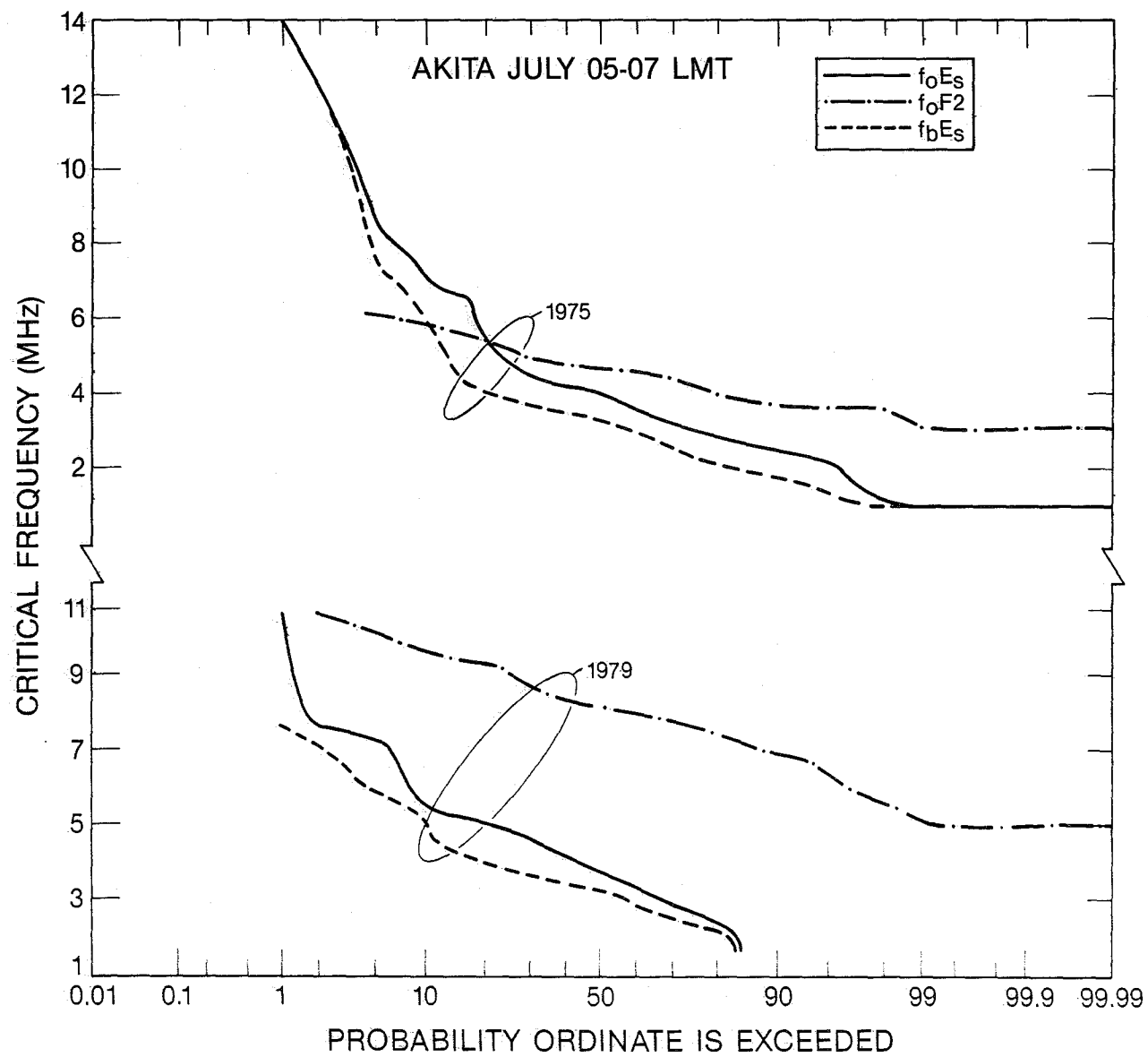
Figure 39a. Cumulative distribution of foF2, foEs, and fbEs at Akita during July
for the time period 0500-0700 LMT.
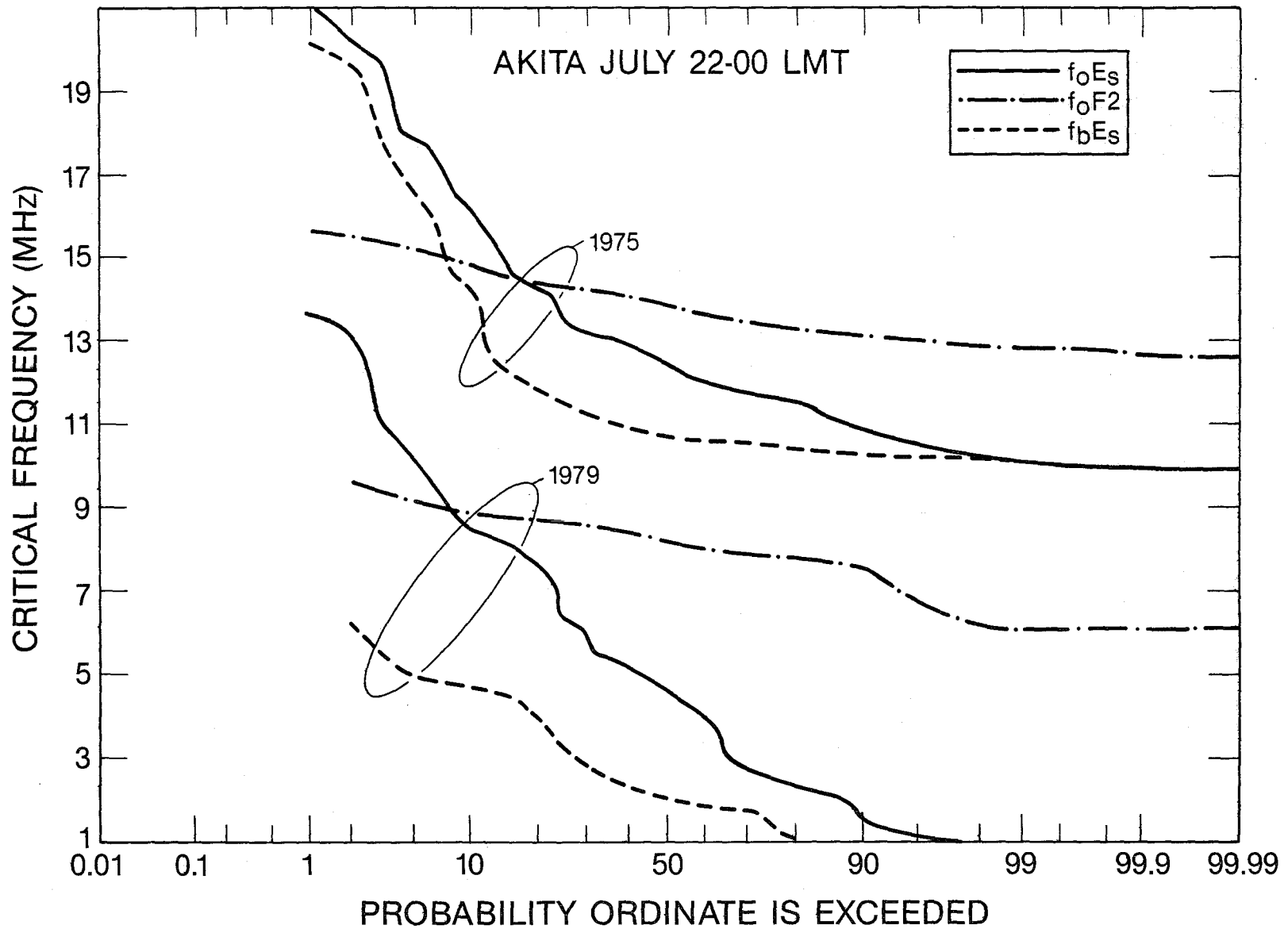
Figure 39b. Cumulative distribution of foF2, foEs, and fbEs at Akita during July
for the time period 2200-0000 LMT.

ionization can dominate the propagation conditions particularly in summer. However, if a DBS system is designed using the penetration frequencies that are appropriate for 90 percent of all time (i.e., for solar maximum conditions), shielding of frequencies by sporadic E will be of little consequence over the entire solar cycle.

In addition to shielding, sporadic E can affect the amplitude of transionospheric signals that penetrate through it. The passage of a signal through the sporadic-E layer can give rise to increased absorption. Most HF propagation prediction programs, including the one based on the work of Stewart et al. (1983) and used in this study, take into account the absorption caused by sporadic E when determining field strength. However, sporadic-E absorption is significant only when sporadic E dominates the propagation modes. For the case of normal ground-based HF propagation, this occurs when the sporadic-E layer reflects the radio energy incident on the ionosphere. For transionospheric signals that penetrate the ionosphere at least 90 percent of all time, it is not likely that absorption due to sporadic E would be significant compared to that resulting from the normal E- and F-region absorption processes. The results of Phillips and Knight (1978) bear this out.

For direct broadcast satellite planning purposes, it appears that the effects of sporadic E can be neglected in determining the penetration frequencies and the ionospheric losses associated with DBS operations.

5. INTERFERENCE EFFECTS AND IONOSPHERIC DUCTING

5.1 General Comments

In planning any new telecommunication service, it is necessary to assess the degree to which the proposed new service would interfere with the operation of existing systems. For the purposes of this report, this assessment can be confined to determining the likelihood that a satellite-based broadcasting service will interfere with the operation of the existing ground-based broadcasting service. It is assumed that a DBS service would operate in the same frequency bands as are allocated to the current ground-based broadcasting service.

Any DBS operation that involves the transmission of a given radio frequency directly into an area serviced by a ground-based broadcasting service transmitting on the same frequency may result in cochannel interference to the existing service. It is reasonable to assume that the broadcasting requirements for DBS

74

operation would be subjected to the same procedures and coordination processes as are the existing ground-based broadcasting service requirements.

For the case of a VHF satellite direct broadcasting service, interference could be avoided by assuring that the DBS frequencies beamed into the target service area were not the same as used by ground-based broadcast transmitters in the area. To avoid interference altogether, it would be necessary to operate the DBS service at frequencies that are not cochannel or adjacent channel with those of the ground-based broadcast service in the target area.

The avoidance of interference with an HF DBS service is not as straight-forward. It is possible that signals transmitted in conventional HF broadcasting could arrive at the target area with the same frequencies as could penetrate the ionosphere directly from a DBS. This is due to the fact that the ground-based signals could be reflected at ionospheric locations that support the same frequency as being used in DBS operations. Such a signal could provide an adequate ground-based service into the same target area using the same frequency as the direct broadcast satellite. Coordination would have to be effected to avoid intentional harmful interference.

Under certain conditions, HF radio waves can propagate to parts of the earth that are not directly visible from a broadcasting satellite. It is possible, for example, that signals from a DBS could penetrate the ionosphere but be reflected by the ionosphere at a location away from the penetration point and reach parts of the earth's surface not directly illuminated by the satellite. It is also possible that signals could propagate to long distances away from the intended target area as a result of being ducted by the ionosphere. Such signals could arrive at distant locations with little attenuation after they have been injected into ionospheric ducts. They could give rise to substantial interference if the propagation conditions are proper to support ducted radio waves.

The potential interference effects of radio signals that propagate away from the intended target areas by ionospheric reflection and by ionospheric ducting are discussed separately below.

5.2 Potential Interference Effects Due to Ionospheric Reflection

The ability of the ionosphere to reflect HF radio signals incident upon it from below forms the basis for the long-distance HF broadcasting service. It is also the same process that gives rise to the potential for interference, because radio signals can propagate into unintended regions causing disruption to the existing broadcast service. In order to assess the degree to which the existing

HF broadcast service could be interfered with by signals penetrating the iono-
sphere from a DBS, a number of simulations of broadcasting scenarios were con-
ducted. In developing these simulations, use was made of the HF propagation
prediction program IONCAP, developed at the Institute for Telecommunication
Sciences and described by Teters et al. (1983).

It was assumed that a signal emitted from a DBS would be incident on the
earth and then reradiate in all directions and at all possible take-off angles.
This provides the worst-case simulation as far as interference is concerned,
because it does not take into account preferred radiation angles resulting from
the relative location of the satellite and the target area. Values of the pene-
tration frequencies discussed in Section 3 were used in the IONCAP program to
determine their likelihood of propagating to distances beyond the intended
zone. A good indication of the potential interference created by a DBS frequency
is to compare it to the maximum usable frequency (MUF) for a specific distance
that is applicable to the ground-based HF broadcasting circuit. Only frequencies
that are less than the MUF are likely to be used for ground-based broadcasting
purposes. If a frequency that penetrates the ionosphere is greater than the MUF
for a specific distance, it is not likely that the same frequency would be used
for ground-based broadcasting purposes.

Table 14 shows a summary of results for the July, solar minimum (SSN=5)
simulation for Zone 1. For this particular case, it was assumed that a satellite
was located in geostationary orbit and was broadcasting directly into Zone 1 at
1200 and 2400 hrs UT. Table 1 shows that under these conditions frequencies
greater than 16 MHz would penetrate into the area for all seasons. The frequen-
cies above 16 MHz that are allocated to the broadcasting service can be charac-
terized by midband values of 17.7, 21.6, and 25.6 MHz. The universal times of
1200 and 2400 hrs correspond to about 0800 hrs local time and 2000 hrs local time
in the center of Zone 1. Results are shown in Table 14 for two azimuths of
propagation to illustrate the effect of varying the local time with distance from
the center of the zone. Those instances when a likely penetration frequency is
less than the ground-based MUF are marked with an "X." The penetration frequency
is less than the MUF only for the 2400 hr UT results at the 270° azimuth (heading
into daylight hours) and the 1200 hrs UT results at the 90° azimuth (also heading
into daylight).

Table 15 gives results for the case of a geostationary DBS broadcasting into
a middle-latitude zone (in this case Zone 5) during July and October, solar
minimum at 0800 hrs and 2300 hrs UT. Reference to Table 3 shows that under these

Table 14. Instances When Broadcast Frequencies are Less Than MUF
(marked by an X) for July, SSN=5, Zone 1, Geostationary DBS

Time UT	Distance (km)	AZ = 90° MUF (MHz)	Frequency (MHz) 17.7	21.6	25.6	Time UT	Distance (km)	AZ = 270° MUF (MHz)	Frequency (MHz) 17.7	21.6	25.9
1200	500	6.6	-	-	-	1200	500	6.4	-	-	-
	1000	9.4	-	-	-		1000	8.7	-	-	-
	2000	14.4	-	-	-		2000	13.1	-	-	-
	3000	17.5	-	-	-		3000	15.7	-	-	-
	4000	19.6	X	-	-		4000	11.9	-	-	-
	5000	15.7	-	-	-		5000	11.5	-	-	-
	7500	19.2	X	-	-		7500	8.7	-	-	-
	10000	18.3	X	-	-		10000	9.3	-	-	-
	15000	19.2	X	-	-		15000	13.1	-	-	-
2400	500	7.1	-	-	-	2400	500	7.7	-	-	-
	1000	9.4	-	-	-		1000	11.1	-	-	-
	2000	13.2	-	-	-		2000	18.4	X	-	-
	3000	15.0	-	-	-		3000	24.2	X	X	-
	4000	14.9	-	-	-		4000	27.5	X	X	X
	5000	10.6	-	-	-		5000	23.2	X	X	-
	7500	13.1	-	-	-		7500	23.5	X	X	-
	10000	13.2	-	-	-		10000	18.9	X	X	-
	15000	9.9	-	-	-		15000	20.9	X	-	-

Table 15. Instances When Broadcast Frequencies are Less Than MUF (marked by an X) for July and October, SSN=5, Zone 5, Geostationary DBS

JULY

Time UT	Distance (km)	AZ = 90° MUF (MHz)	Frequency (MHz) 21.6	25.6		Time UT	Distance (km)	AZ = 270° MUF (MHz)	Frequency (MHz) 21.6	25.9
1800	500	6.6	–	–		1800	500	6.6	–	–
	1000	10.6	–	–			1000	9.8	–	–
	2000	15.9	–	–			2000	15.0	–	–
	3000	18.3	–	–			3000	18.5	–	–
	4000	20.6	–	–	–		4000	14.9	–	–
	5000	16.8	–	–			5000	14.9	–	–
	7500	20.3	–	–			7500	12.7	–	–
	10000	19.4	–	–			10000	12.1	–	–
	15000	20.3	–	–			15000	12.0	–	–
2300	500	5.2	–	–		2300	500	5.3	–	–
	1000	7.0	–	–			1000	7.4	–	–
	2000	10.5	–	–			2000	11.6	–	–
	3000	12.7	–	–			3000	14.6	–	–
	4000	13.5	–	–			4000	16.2	–	–
	5000	11.2	–	–			5000	13.8	–	–
	7500	13.1	–	–			7500	16.0	–	–
	10000	9.2	–	–			10000	15.6	–	–
	15000	13.4	–	–			15000	16.0	–	–

OCTOBER

Time UT	Distance (km)	AZ = 90° MUF (MHz)	Frequency (MHz) 21.6	25.6	Time UT	Distance (km)	AZ = 270° MUF (MHz)	Frequency (MHz) 21.6	25.9
1800	500	6.5	–	–	1800	500	6.4	–	–
	1000	10.6	–	–		1000	9.8	–	–
	2000	15.9	–	–		2000	14.0	–	–
	3000	17.7	–	–		3000	17.3	–	–
	4000	20.5	–	–		4000	13.9	–	–
	5000	17.0	–	–		5000	15.0	–	–
	7500	20.2	–	–		7500	12.7	–	–
	10000	19.5	–	–		10000	12.1	–	–
	15000	20.2	–	–		15000	12.0	–	–
2300	500	5.2	–	–	2300	500	5.3	–	–
	1000	7.1	–	–		1000	7.4	–	–
	2000	10.6	–	–		2000	11.7	–	–
	3000	12.7	–	–		3000	14.6	–	–
	4000	13.5	–	–		4000	16.2	–	–
	5000	11.3	–	–		5000	13.9	–	–
	7500	13.1	–	–		7500	16.0	–	–
	10000	9.2	–	–		10000	15.6	–	–
	15000	13.4	–	–		15000	16.0	–	–

conditions the penetration frequency must be greater than 18 MHz. Only frequencies of 21.6 and 25.9 MHz need to be considered for interference assessment. It is clear that in this case the MUF for each distance is below the frequencies that can penetrate into Zone 5. It is not very likely that frequencies of 21.6 and 25.9 MHz would be used by the ground-based HF broadcasting services at this time and the potential for interference would be minimal.

Table 16 shows the results of transmitting from a satellite in a Molniya-type orbit in Zone 5 during October solar maximum for 0400 hrs and 1800 hrs UT. According to the discussion presented in Section 3.5.2, frequencies greater than 10 MHz would penetrate the ionosphere 90 percent of the time under these conditions. It is clear from the results presented in Table 16 that many of the frequencies that penetrate into Zone 5 are less than the MUF for distances as great as 10000 km from the center of Zone 5.

5.3 Ionospheric Ducting

As was discussed above, signals that propagate away from the intended target areas by normal ionospheric reflection are not likely to cause interference to the existing broadcasting service. However, it is possible that signals could reach unintended areas on the earth as a result of propagation to great distances without intervening ionospheric reflections. Such signals could be trapped or ducted by the ionosphere and propagated to great distances with little attenuation. Gurevich and Tsedilina (1979) have estimated the field strength of these modes.

A great deal of study has been directed toward understanding and predicting the processes involved in ionospheric ducting. The work of Toman (1979) and Elkins et al. (1980) summarizes the status of the current understanding of ducted ionospheric propagation. The subject has been treated at some length by the CCIR in its Report 250-5 (CCIR, 1982). For this study, we need to be concerned with ducted propagation modes that result from ionospheric tilts and from guide propagation in the ionosphere.

Ducted propagation is supported by longitudinal ionospheric tilts. These tilts result from variations in layer heights and/or variations in layer critical frequency. An ionospheric tilt can cause a radio ray to be either refracted back to the earth or refracted so as to travel above the earth's surface before reentering the ionosphere to undergo further refraction back to the ground. Observations of HF signals propagating to the antipodal point of a transmitter (Bold, 1969) have demonstrated the importance of ducted propagation supported by

Table 16.   Instances When Broadcast Frequencies are Less Than MUF
(marked by an X) for October SSN=120, Zone 5, Molniya Orbit

Time UT	Distance (km)	MUF (MHz)	AZ = 90° Frequency (MHz) 11.8	13.7	15.4	17.7	21.6	25.9	Time UT	Distance (km)	MUF (MHz)	AZ = 270° Frequency (MHz) 11.8	13.7	15.4	17.7	21.6	25.9
0400	500	9.1	-	-	-	-	-	-	0400	500	8.9	-	-	-	-	-	-
	1000	12.1	X	-	-	-	-	-		1000	11.6	-	-	-	-	-	-
	2000	18.3	X	X	X	X	-	-		2000	17.1	X	X	X	-	-	-
	3000	23.4	X	X	X	X	X	-		3000	20.8	X	X	X	X	-	-
	4000	26.6	X	X	X	X	X	X		4000	22.4	X	X	X	X	X	-
	5000	21.5	X	X	X	X	-	-		5000	17.6	X	X	X	-	-	-
	7500	26.1	X	X	X	X	X	X		7500	20.3	X	X	X	X	-	-
	10000	24.9	X	X	X	X	X	-		10000	18.3	X	X	X	X	-	-
	15000	26.1	X	X	X	X	X	X		15000	21.9	X	X	X	X	X	-
1800	500	8.9	-	-	-	-	-	-	1800	500	8.9	-	-	-	-	-	-
	1000	11.7	-	-	-	-	-	-		1000	11.8	-	-	-	-	-	-
	2000	17.7	X	X	X	-	-	-		2000	18.1	X	X	X	X	-	-
	3000	21.9	X	X	X	X	X	-		3000	22.8	X	X	X	X	X	-
	4000	24.1	X	X	X	X	X	-		4000	25.6	X	X	X	X	X	-
	5000	19.9	X	X	X	X	-	-		5000	21.3	X	X	X	X	X	-
	7500	23.7	X	X	X	X	X	-		7500	25.2	X	X	X	X	X	-
	10000	21.6	X	X	X	X	-	-		10000	24.3	X	X	X	X	X	-
	15000	12.7	X	-	-	-	-	-		15000	25.2	X	X	X	X	X	-

80

longitudinal ionospheric tilts. Observations by Hortenbach and Rogler (1979) on a transantipodal path revealed unexpectedly high signal intensities resulting from tilt-supported propagation modes. Coupling into and out of the duct evidently was via layer tilts existing in the twilight regions near both terminals of the path.

Certain long-distance modes of propagation have been attributed to channeling in the ionosphere analogous to a waveguide. These modes arise from:

(a) an electron density profile characterized by a monotonic increase of the electron density with height. The waveguide has an upper boundary, usually within the F layer, but no lower boundary. Guided waves propagate inside the concavity of the reflecting sphere; the earth's lower ionosphere acts as a spherical whispering-gallery path for radio waves, or

(b) an electron density profile characterized by relative minima, like the one between the E and F layers. The waveguide possesses an upper and lower wall, and ducting occurs in the space between the two concentric spheres, a double-walled duct.

The propagation mechanism of whispering-gallery and double-walled ducts is indistinguishable observationally. Generalizations about the whispering-gallery type of propagation are (CCIR, 1982):

(a) whispering-gallery propagation is possible in any phase of the solar cycle,

(b) at the most favorable frequency, a ray must make an angle not larger than 7° to 8° with the tangent to the layer for guidance to occur,

(c) the guided paths are not reachable from the ground unless scattering or refracting (or reflecting) centers perform as wave couplers between ground and whispering gallery,

(d) the total calculated losses, inclusive of absorption, are relatively insensitive to terminal separation and are of the order of magnitude of 125 dB to 138 dB from 25 MHz to 45 MHz.

For ducted propagation to occur, radio waves must be injected into the ionospheric duct. For the case of a radio transmission from a satellite, the energy can be injected directly into the duct or after a bounce from the earth's surface. The reception at the ground of HF signals radiated by a satellite orbiting above the F2 region of the ionosphere from long ranges and beyond the horizon has been discussed by Beni et al. (1978). Signals from the 1970-34A

satellite were received in Florence, Italy, over ranges greater than 10000 km. High propagation probability from the North Atlantic zone occurred when the satellite was above the F2 maximum (445-1500 km altitude) and when the sunset transition was near the receiving station. Another favorable situation occurred when the satellite was high (800-1600 km) in the night zone south of the receiving station; both the satellite and receiving station were situated along the twilight zone. Free-space propagation losses were reduced by as much as 6 dB over ranges of 12000 km and up to 8 dB for nearly antipodal satellite passes. Evidence of HF ducting phenomena has been seen in the Ariel 3 satellite data discussed by Horner and Bent (1969). This satellite orbited the earth at a height of about 800 km. On the other hand, HF observations made on board the RAE-1 satellite (at 6000 km altitude) and reported by Herman et al. (1973) show no evidence of ducting phenomena. Evidence of HF ducting has only been observed for satellites orbiting below 2000 km. It is possible that energy from a DBS could be directed into an ionospheric duct if the DBS were transmitting at a very low incidence angle. There are little or no data to provide a basis for discussion of ducting from high-altitude satellites.

Energy can be trapped in a duct as a result of reradiating the signal into the intended target area. For this to occur, natural mechanisms must be able to perform injection of HF radio waves into the ionospheric-ducted modes. These mechanisms are ionospheric tilts, sporadic-E ionization, auroral columns and curtains, meteor trails, and equatorial F-region ionization troughs. Comparable mechanisms must be able to effect removal of the signals from the duct.

Toman and Miller (1977) have shown that ionospheric wave ducting of HF rays does not require, but is facilitated by, the continued presence of an ionization valley in the plane of the ray trajectory. Burtnyk et al. (1962) observed that F-layer sunset tilts last longer, are larger in maximum amplitude, and are seen more often than sunrise tilts. Gerson et al. (1969) noted a decline before and an increase after sunrise in antipodal reception.

Ionospheric ducting phenomena have been observed for over 50 years (Toman, 1979). While it is a subject of great interest, there is little evidence that the conventional ground-based HF broadcasting service is degraded by ionospheric ducting per se. It is difficult to envision conditions for DBS applications where the impact of ionospheric ducting on broadcast service interference would be substantially different, although Phillips and Knight (1970) have pointed out some situations where interference and distortion could occur.

82

6. FARADAY ROTATION

6.1 General Comments

Faraday rotation is a well-known effect in transionospheric propagation. This rotation of the plane of polarization of linearly polarized waves, due to the presence of free electrons and the geomagnetic field in the earth's ionosphere, has been used since the 1950's in studies of ionospheric electron content, n_T. Davies (1980) has reviewed many of the results of ionospheric studies using Faraday rotation of VHF transmissions from geostationary satellites of opportunity as well as the results from the ionospheric beacon placed on board the ATS-6 geostationary satellite. The beacon on the ATS-6 satellite allowed multifrequency Faraday rotation measurements in addition to group delay and differential carrier phase measurements to be made.

Even though the Faraday rotation effect is well known, its possible impact on a DBS system operating at standard short wave or FM frequencies in the VHF band has not been specifically considered. Faraday rotation can cause the received polarization to be orthogonal to the transmitted polarization resulting in total loss of received signal. When the rate of Faraday rotation is fast, the effect on the received signal is a fade from signal maximum to a complete null as the polarization rotates through 90 degrees. Faraday rotation is of great concern in attempts to receive linearly-polarized signals from satellites. In this section, we present results showing typical magnitudes of Faraday rotation and its rate of change at three representative ground stations monitoring satellite broadcasts.

6.2 The Faraday Rotation Effect

The Faraday effect is a rotation of the plane of polarization of linearly polarized radio waves due to the birefringent properties of the earth's ionosphere in the presence of the earth's magnetic field. Simple Faraday rotation only occurs under conditions when the quasi-longitudinal approximation to the Appleton-Hartree equation is valid. This is a function of the ratio of the satellite frequency to the maximum plasma frequency, f_c, and the angle which the ray from the satellite makes with the earth's magnetic field in the ionosphere. In the general case, a linearly-polarized, transmitted radio wave will become elliptically polarized on its path through the ionosphere. For the locations investigated in this study, the mode of propagation is quasi-longitudinal and only a simple rotation of the plane of polarization would occur.

The amount of Faraday rotation can be found by considering the expression for the phase refractive index in the ionosphere when collisions can be neglected and by considering the quasi-longitudinal case. The refractive index of the ionosphere can then be expressed (see Davies, 1965) as

$$\mu^2 = 1 - \frac{2X(i-X)}{2(1-X) - Y_T^2 \pm \sqrt{Y_T^4 + 4(1-X)^2 Y_L^2}} \qquad (33)$$

where $X = \dfrac{f_c^2}{f^2}$, $Y_L = \dfrac{f_H}{f} \cos\theta$ and $Y_T = \dfrac{f_H}{f} \sin\theta$.

For frequencies much higher than f_c, the inequality $(Y_T)^4 \ll 4(1-X)^2 Y_L^2$ is satisfied and the refractive index can be expressed as

$$\mu = \left(1 - \frac{X}{1 \pm Y_L}\right)^{1/2}, \text{ or } \mu = 1 \pm \frac{XY_L}{2} . \qquad (34)$$

The two solutions to phase refractive index occur due to the birefringent property of the ionosphere in the presence of the earth's magnetic field. Faraday rotation results from the difference between the phase path of the ordinary ray and the extraordinary ray, or

$$\Omega = \frac{\pi}{\lambda} \int (\mu_o - \mu_x) \, ds = \frac{\pi}{\lambda} XY_L = \frac{K}{f^2} \int B \cos\theta \, N \cdot dl . \qquad (35)$$

In the practical case, the quantity $B \cos\theta$ varies much more slowly than $N \cdot dl$ along the path from the satellite to the ground. Thus, we can write $\Omega = \frac{K}{f^2} \overline{B \cos\theta} \int N \cdot dl$ where $\overline{B \cos\theta}$ is the mean value equal to the actual value taken at some mean height, usually from 350 to 450 km. Numerous studies have been made of the integrated electron content, here called TEC, from observations made at various locations throughout the world. Many of these locations measured Faraday rotation from satellites that were launched for some other purpose, but which had continuously emitting, linearly polarized VHF telemetry transmitters on board. These transmitters were the sources of stable polarization for measuring the changes in the Faraday effect. Using the Faraday effect, measurements of the TEC have been made at many stations, and models of the TEC behavior have been constructed to represent its average behavior over the world.

84

6.3 Results of Calculations of Faraday Rotation

The locations used to determine the Faraday rotation were Boulder, Colorado; Moscow, USSR; and Nairobi, Kenya, with the geostationary satellite located at 105°W longitude for the Boulder broadcast service area and the satellite located at the Greenwich meridian, 0° longitude, for the latter two broadcast areas. Two solar activity conditions were used, solar minimum (SSN=10) and an average solar maximum corresponding to a sunspot number equal to 100. Seasonal changes have been investigated by using an equinox (March) month, one summer (June) month, and one winter (December) month. In order to estimate the average amount of Faraday rotation at the three locations chosen for this study, we have used the Bent ionospheric model (Llewellyn and Bent, 1973), which is a good representation to the actual average TEC. The amount of Faraday rotation, as given in equation (35), is proportional to the cosine of the propagation angle, θ, which is a function of the satellite and the station location so that for the two mid-latitude stations there is significantly more rotation than is observed from the Nairobi station where the ray path from the satellite is more nearly transverse to the magnetic field. Three frequencies were chosen for calculating the amount of Faraday rotation: 15, 26, and 90 MHz. Results of the amount of Faraday rotation in radians, and its rate of change in radians per minute are given in Figures 40 through 42. In each figure, the amount of Faraday rotation and its rate of change is given for solar flux values corresponding to solar minimum and solar maximum for the three frequencies and the three months indicated. Note that in all cases the Faraday rotation calculated from the Bent model was many radians. Receiving antennas not aligned with the orientation of the received plane of polarization will suffer signal loss due to this nonalignment. In the worst case, the receiving antenna will be aligned orthogonally with the received electric field vector and no signal will be received. In actual practice, broadcast receiving antennas are rarely exactly linearly polarized, but are elliptically polarized with an unknown orientation so that the receiving antenna will actually still pick up some small amount of signal. Linearly polarized receiving antennas of good design will be thwarted by the Faraday effect!

An obvious and simple solution to the potential problem of Faraday rotation effects on reception of satellite broadcast signals is to transmit circularly polarized radio waves in a DBS system. Circularly polarized radio waves suffer little or no Faraday rotation effects and, even in the small geographic region of the earth in the vicinity of the magnetic equator where quasi-longitudinal
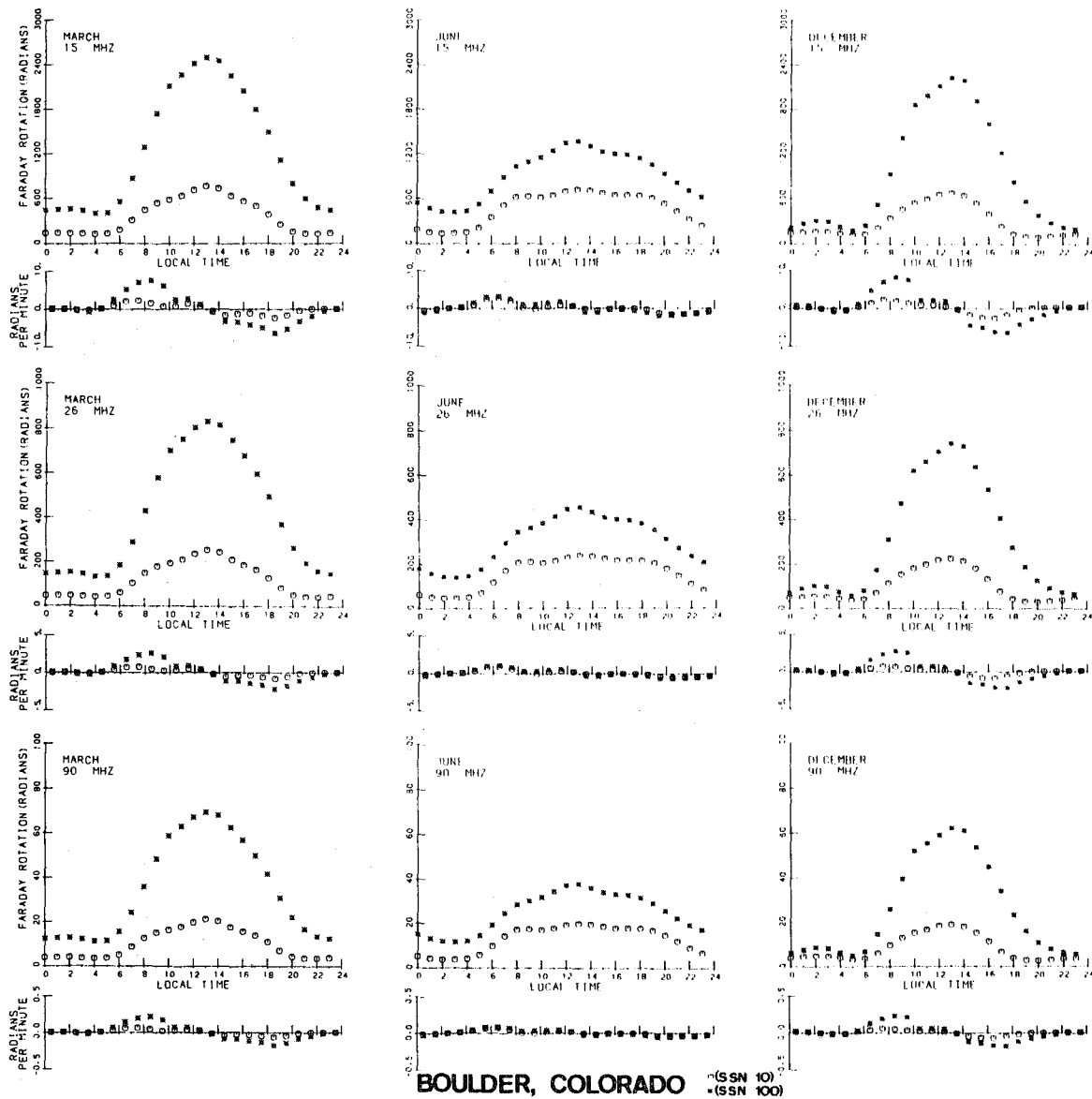
Figure 40. Monthly median Faraday rotation and its rate of change at 15, 26, and 90 MHz for March, June, and December for solar minimum (SSN=10) and solar maximum (SSN=100) at Boulder, Colorado, using a geostationary satellite at 105°W longitude.
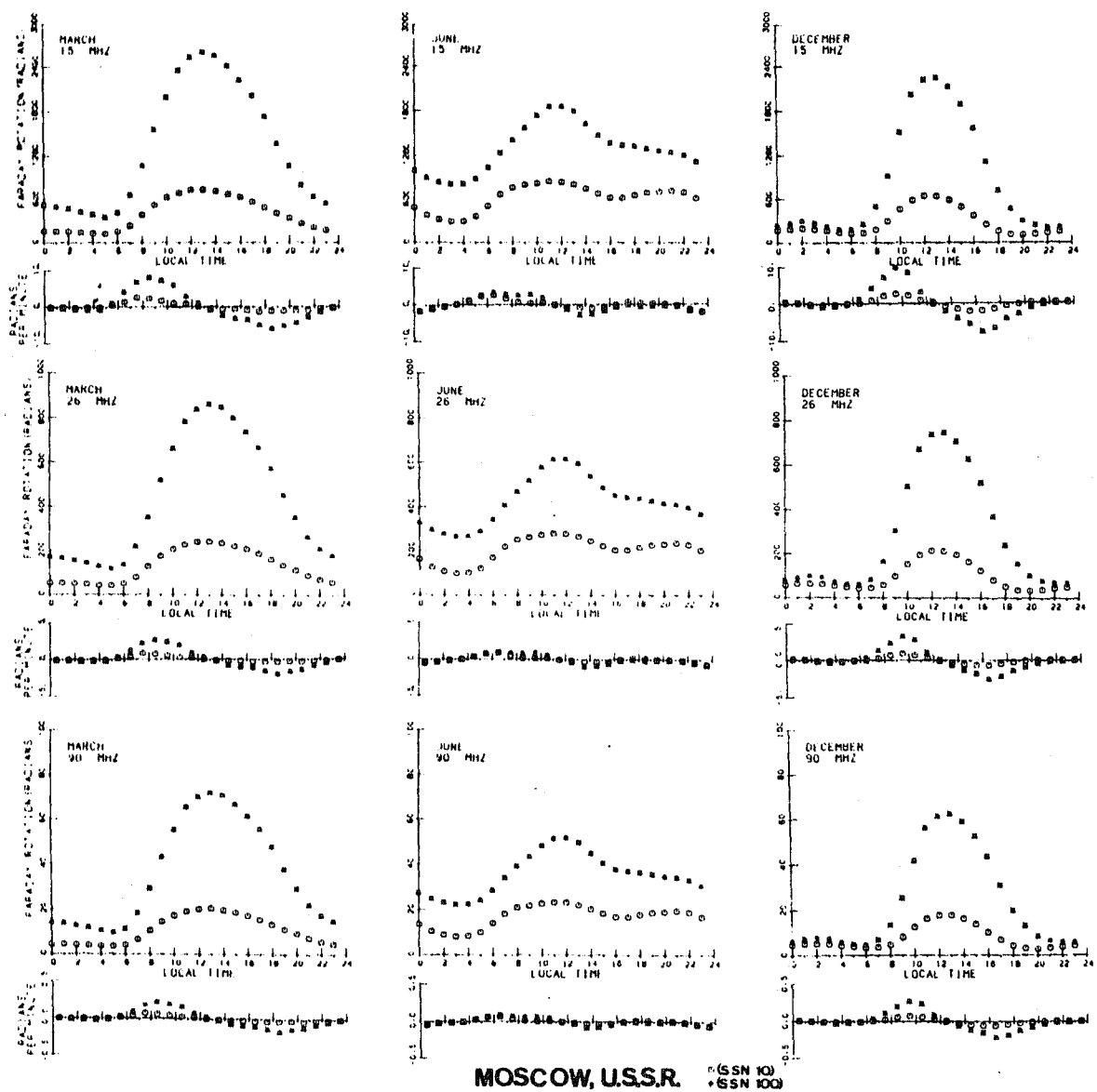
Figure 41. Monthly median Faraday rotation and its rate of change at 15, 26, and 90 MHz for March, June, and December for solar minimum (SSN=10) and solar maximum (SSN=100) at Moscow, USSR, using a geostationary satellite at 0° longitude.

Figure 42. Monthly median Faraday rotation and its rate of change at 15, 26, and 90 MHz for March, June, and December for solar minimum (SSN=10) and solar maximum (SSN=100) at Nairobi, Kenya, using a geostationary satellite at 0° longitude.

propagation does not apply, the received polarization will still be nearly circularly polarized. At the frequencies of potential use for DBS operation in the HF and VHF bands, the use of circularly polarized transmitting polarization is the only reasonable solution to this potentially serious fading problem. Thus, for the price of additional satellite transmitting complexity and about 3 dB of power, the problem of Faraday rotation fading is eliminated. Fortunately, it is a complete solution.

7. IMPACT OF IONOSPHERIC SCINTILLATION ON DBS OPERATION

7.1 Background

In the previous sections, it was assumed that the radio signal traveled from the satellite through an ionosphere characterized by the absence of irregular- ities in the electron density distribution. It is well known, however, that electron density irregularities in the ionosphere, particularly in the F2 region, occur at specific times and locations around the globe (Crane, 1977; Aarons, 1982). These irregularities produce amplitude fading or scintillation on signals that traverse the ionosphere. The effects vary with frequency, time of day, magnetic and solar activity, season and latitude. The signal both increases and decreases in level as a result of passing through the irregularities. Increases can be up to 10 dB above the quiet level; fades, or decreases, have been recorded to 50 dB below the quiet level. The maximum fade depth that has been observed frequently is a function of the signal-to-noise ratio of the system being observed. In many experiments for which data are available, the signal-to-noise ratio has been of the order of 15 dB. Thus, the utility of these data is limited for setting margins.

An example of scintillation activity as encountered on a steady-state signal is shown in Figure 43. Normal 137 MHz signals from the synchronous satellite ATS-5 are shown where the thickness of the lines is due to the spin of the satellite. The onset of scintillation activity brings both fades and increases in signals with fading rates of the order of seconds in this particular case.

Most of the data that exist concerning scintillation is the result of monitoring satellite transmissions at the frequencies of 136 MHz or greater. These data have been used extensively to develop the global morphology of ionospheric scintillation. Figure 44 provides a pictorial representation of the depth of the global scintillation activity during low and moderate solar activity. The geomagnetic field governs the intensity with which scintillation
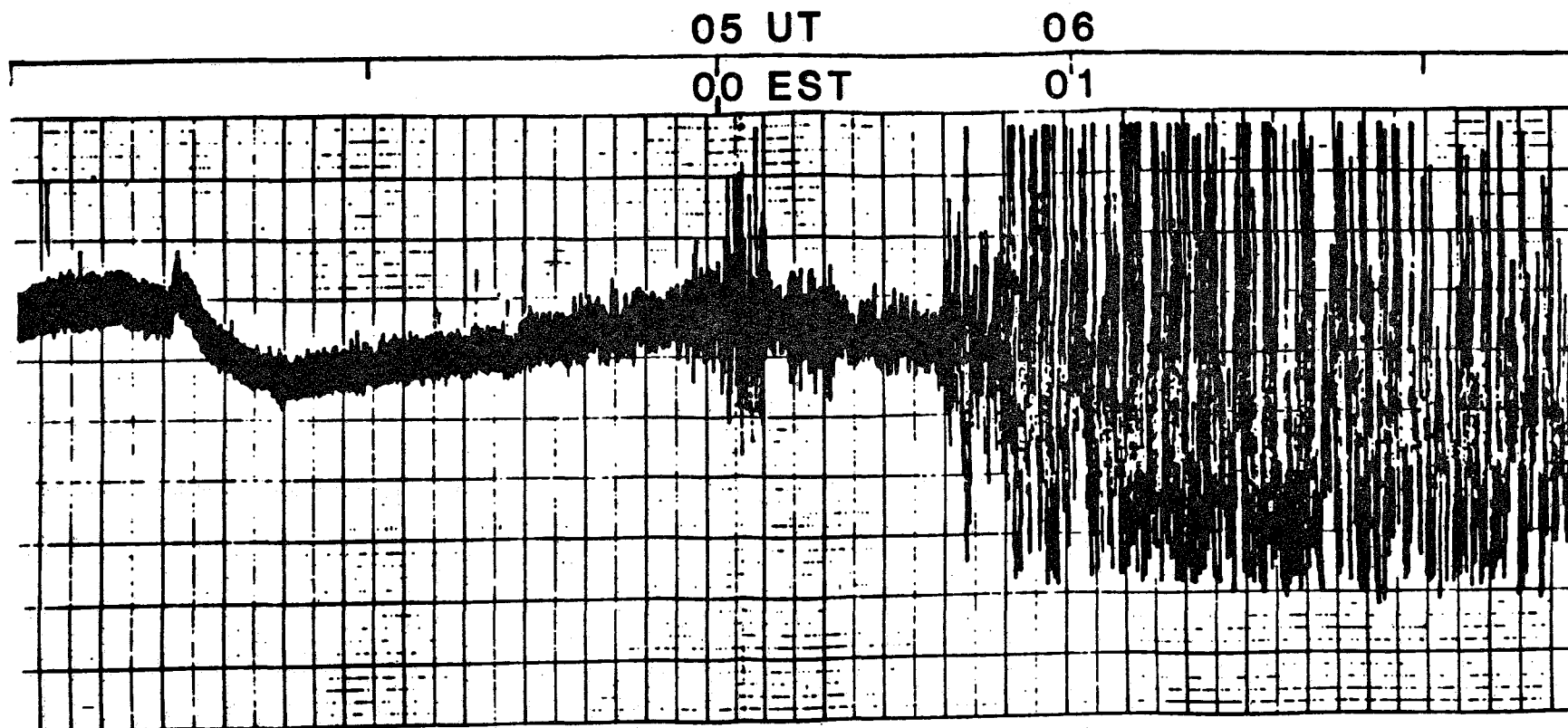
Figure 43. Example of ionospheric scintillation observed at Sagamore Hill, Massachusetts, from ATS-5 satellite, 137 MHz. Peak-to-peak fluctuations are saturated and are of the order of 20 dB.
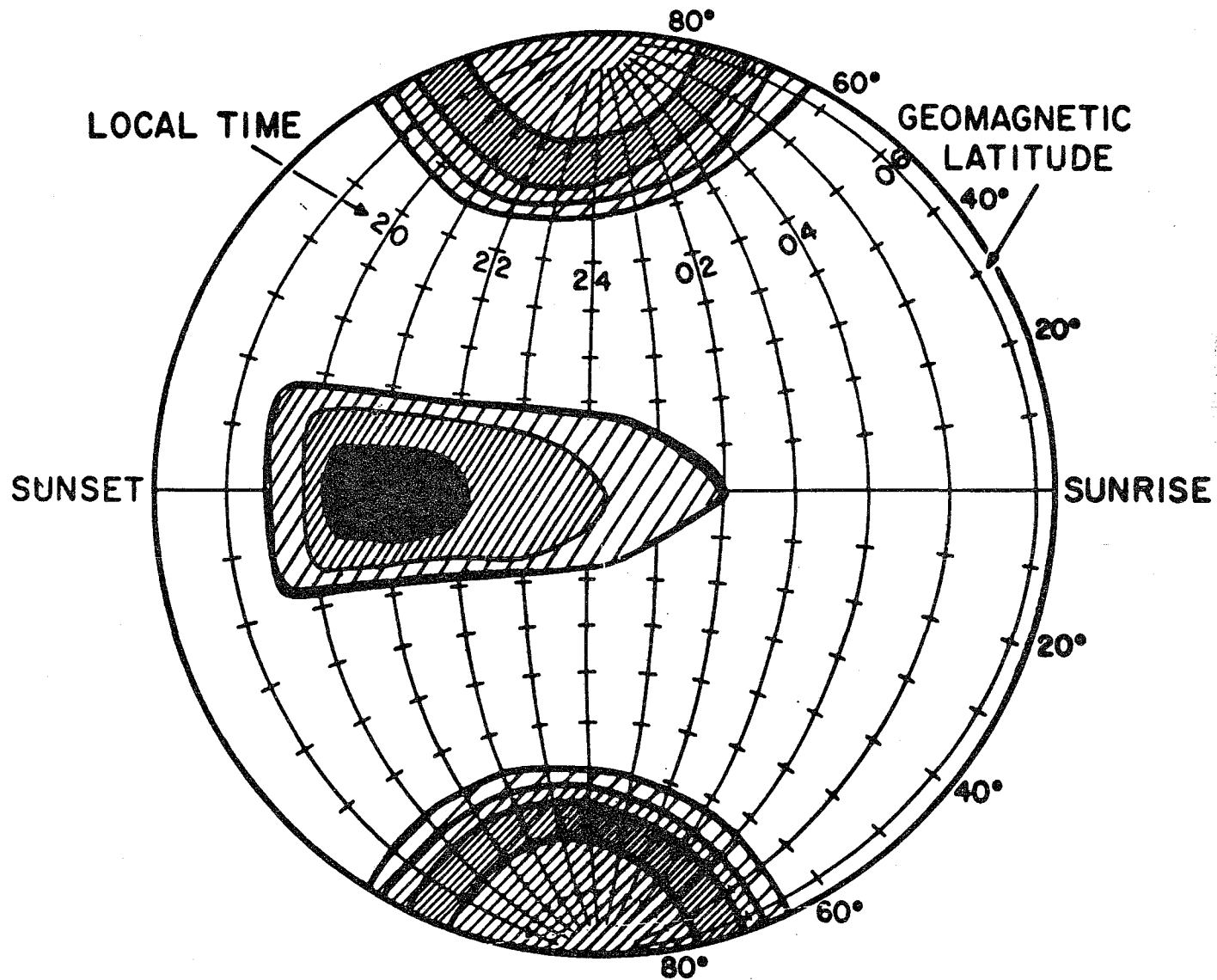
Figure 44. Depth of scintillation fading (proportional to density of crosshatching): low sunspot years.

is observed. Figure 45 provides a general picture of the magnetic latitude as a function of geographic coordinates. Using Figure 45, the sectors of interest in this study have been replotted into magnetic coordinates and are shown in Figure 46. It can be seen that the majority of sectors cover the equatorial region. For those sectors in equatorial regions, areas where there are afternoon or early evening increases in electron density relative to the magnetic equator, are shown crosshatched in Figure 46. The other latitude regions that can be affected by magnetic activity effects are shown hatched.

In the auroral region, irregularities of interest in this study appear at heights from 100 km to 1000 km and are governed by various plasma instability processes. The extent of the scintillation activity changes as a function of magnetic activity. Affected regions at high latitudes are shown hatched for the appropriate sectors in Figure 46.

7.2 Indices and Measurements Used in Scintillation Studies

Since the advent of satellite transmissions, recordings have been made of amplitude scintillation. It was recognized that scintillation resulted from scattering from irregularities in the ionosphere and various indices were used to record the increase and decrease of signals. These ranged from a qualitative index from 0 to 2 to an index called the scintillation index, SI, which is the difference in decibels from the third highest signal peak to the third lowest minimum within an observation period. A more precise measure of scintillation is the mean square deviation of the scattered signal from the mean, termed S4 in the literature.

The best characterization of amplitude scintillation is the Nakagami distribution, originally developed to describe HF fading characteristics (Herbert Whitney, private communication). We shall refer to characterization of scintillation using Nakagami m values (Nakagami, 1960). However, in surveying the various observations as a function of latitude, longitude, magnetic conditions, etc., we are forced to show the levels of scintillation activity in their original form, which is generally in the SI units.

In general terms, we have weak scattering when the peak-to-peak fading is below about 10 dB. With strong scattering, the frequency dependence law that will be outlined begins to fail. Finally, we find that the maximum fading is Rayleigh fading. All frequency dependence equations (given subsequently) are to be viewed as "worst cases."
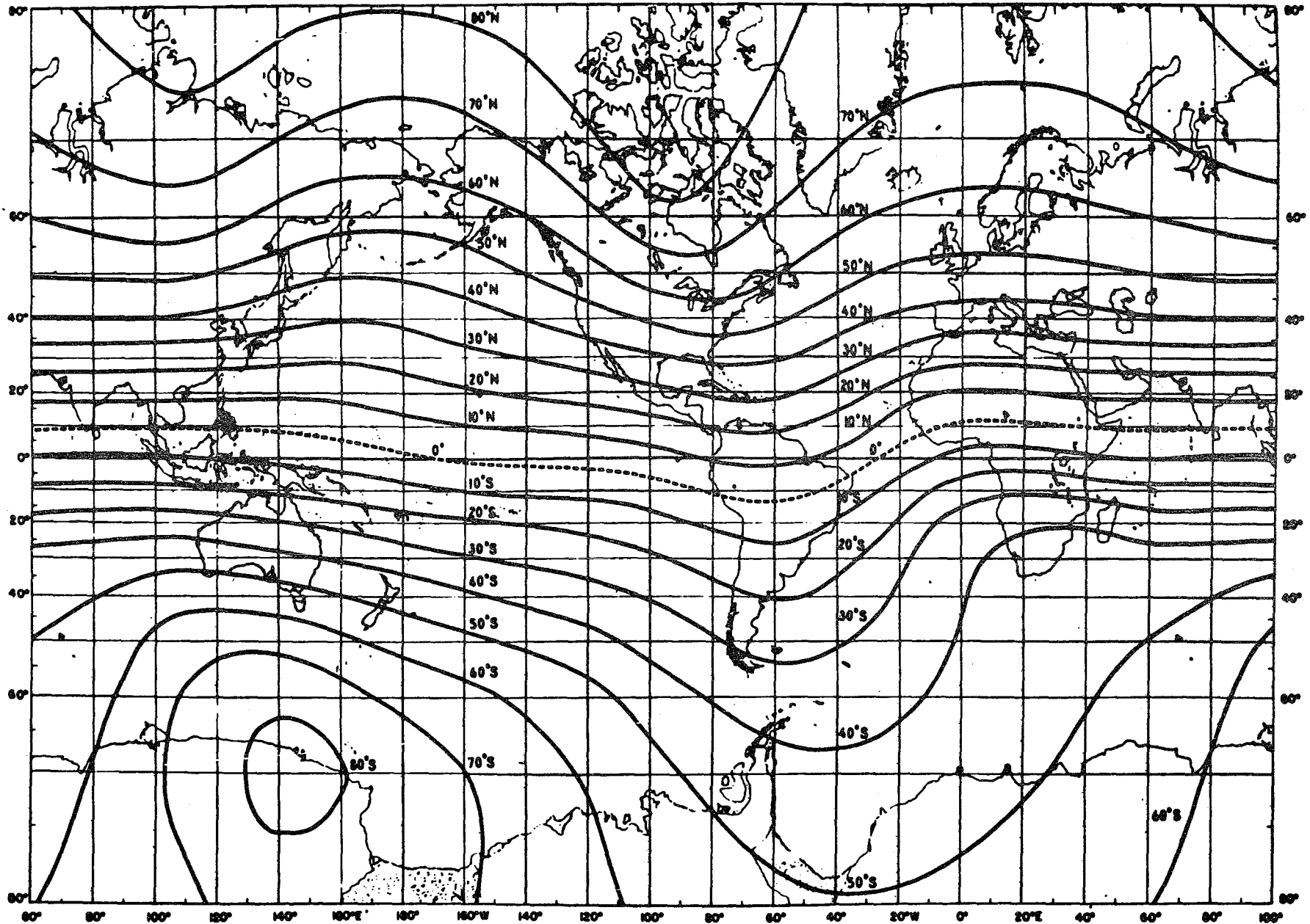
Figure 45.   Global variation of the magnetic latitude (dashed line is the dip equator).
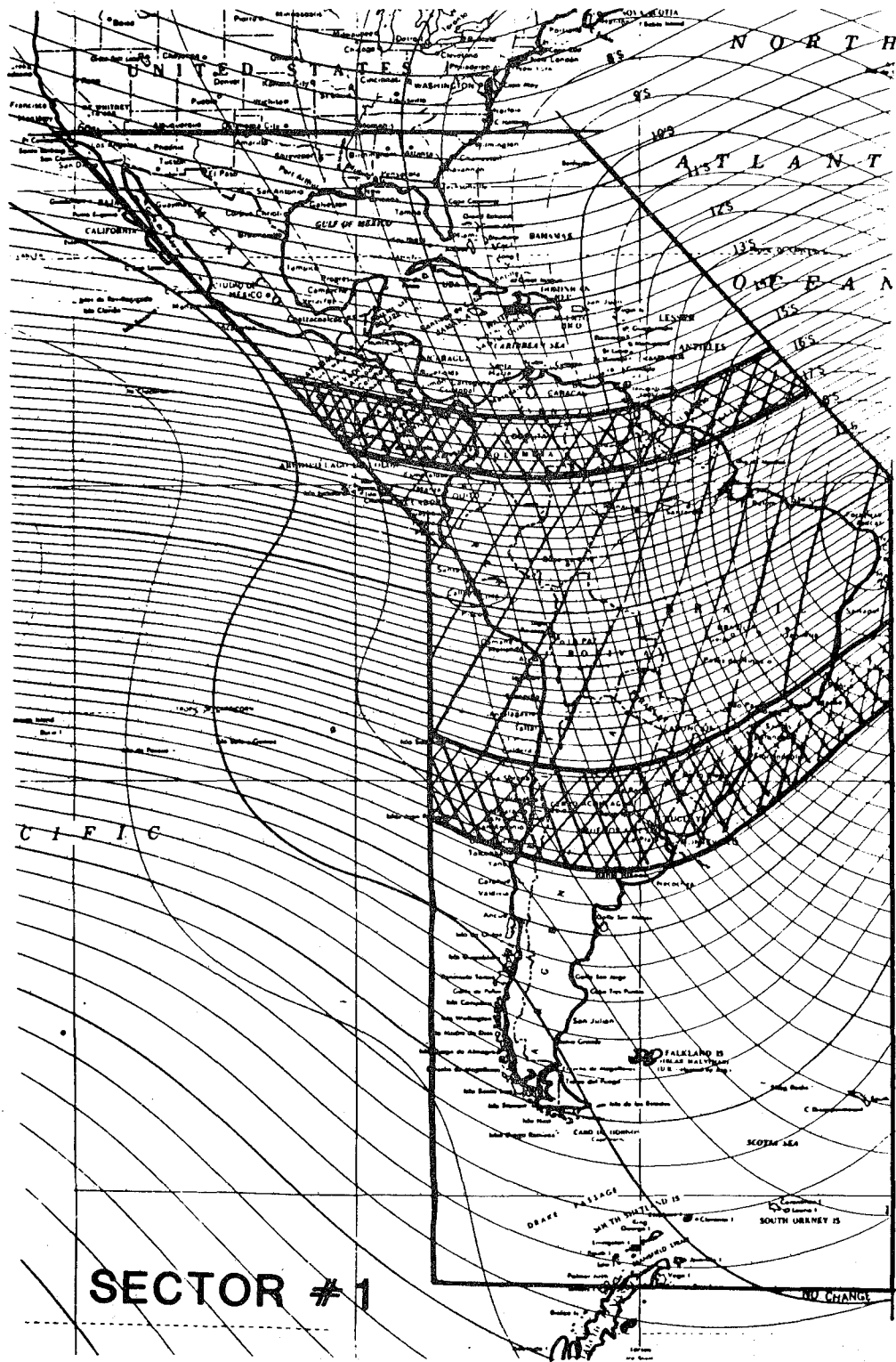
Figure 46a. Variation of magnetic dip and declination in
Zone 1. Crosshatched areas are locations where
maximum nighttime scintillation intensity
occurs. Hatched areas are regions of scintil-
lation intensity but are of lower level than
crosshatched areas.

94
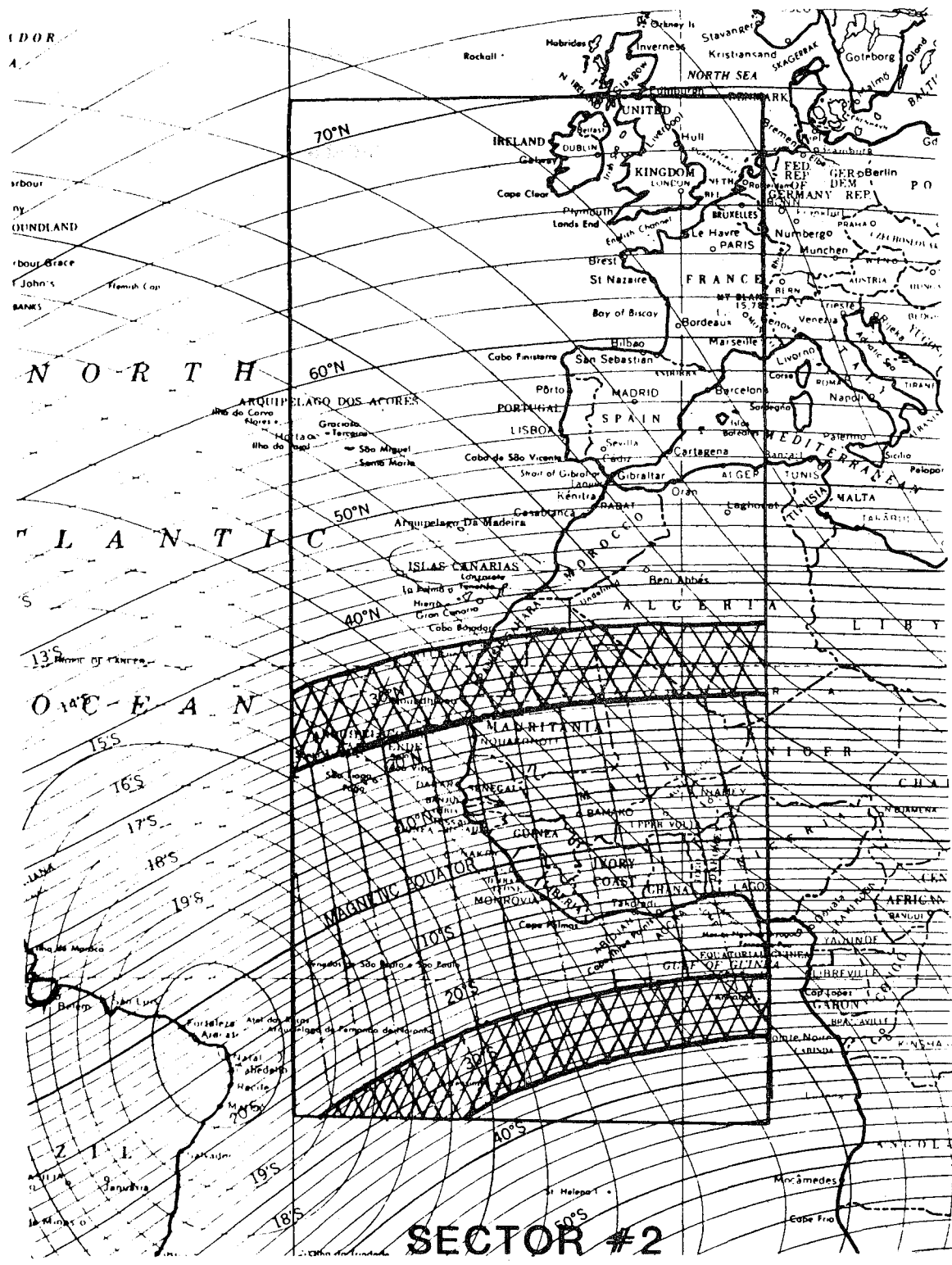
Figure 46b. Variation of magnetic dip and declination in
Zone 2. Crosshatched areas are locations where
maximum nighttime scintillation intensity
occurs. Hatched areas are regions of scintil-
lation intensity but are of lower level than
crosshatched areas.
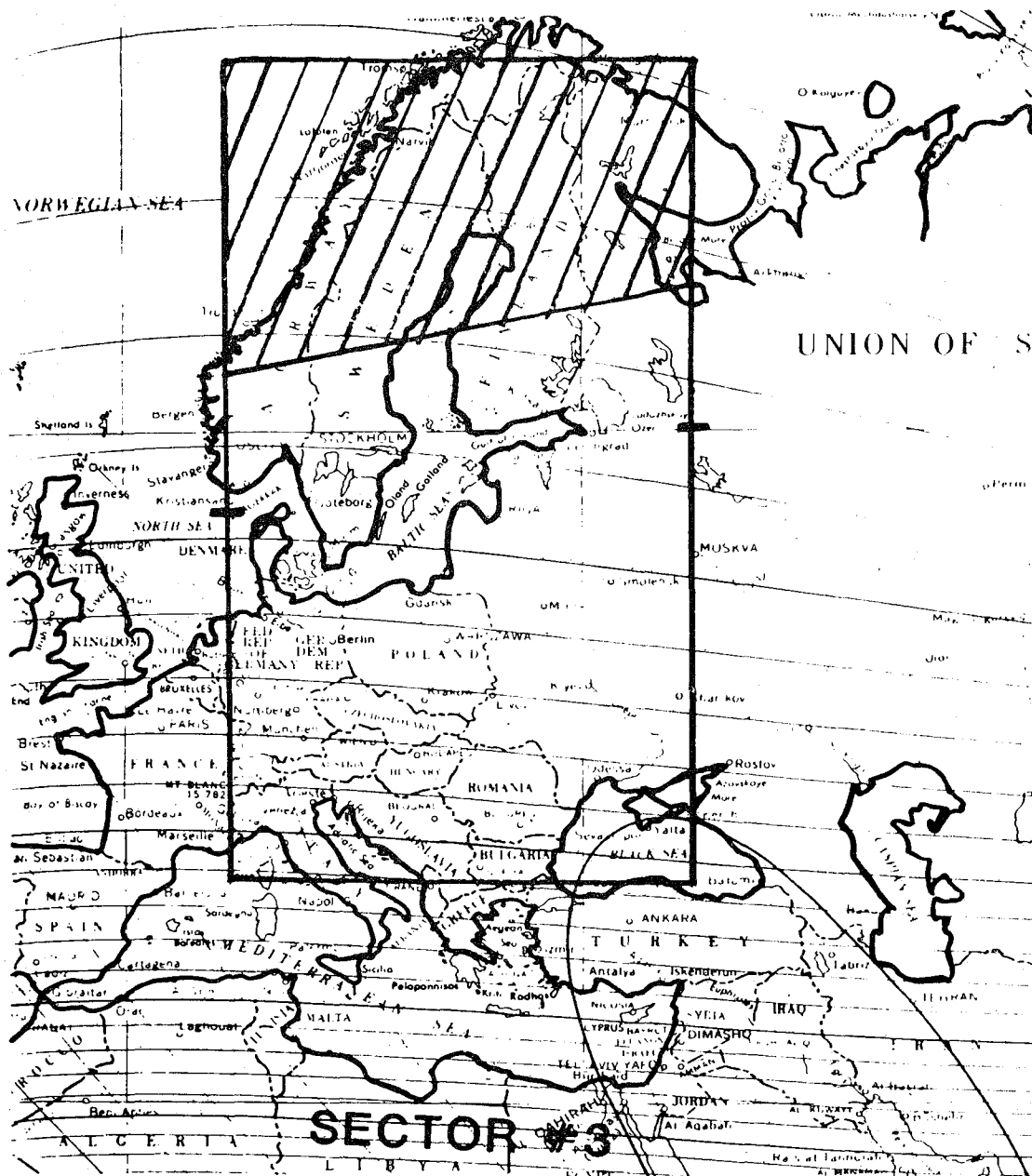
Figure 46c. Variation of magnetic dip and declination in Zone 3. Hatched areas are locations where high latitude scintillation effects are likely to occur.
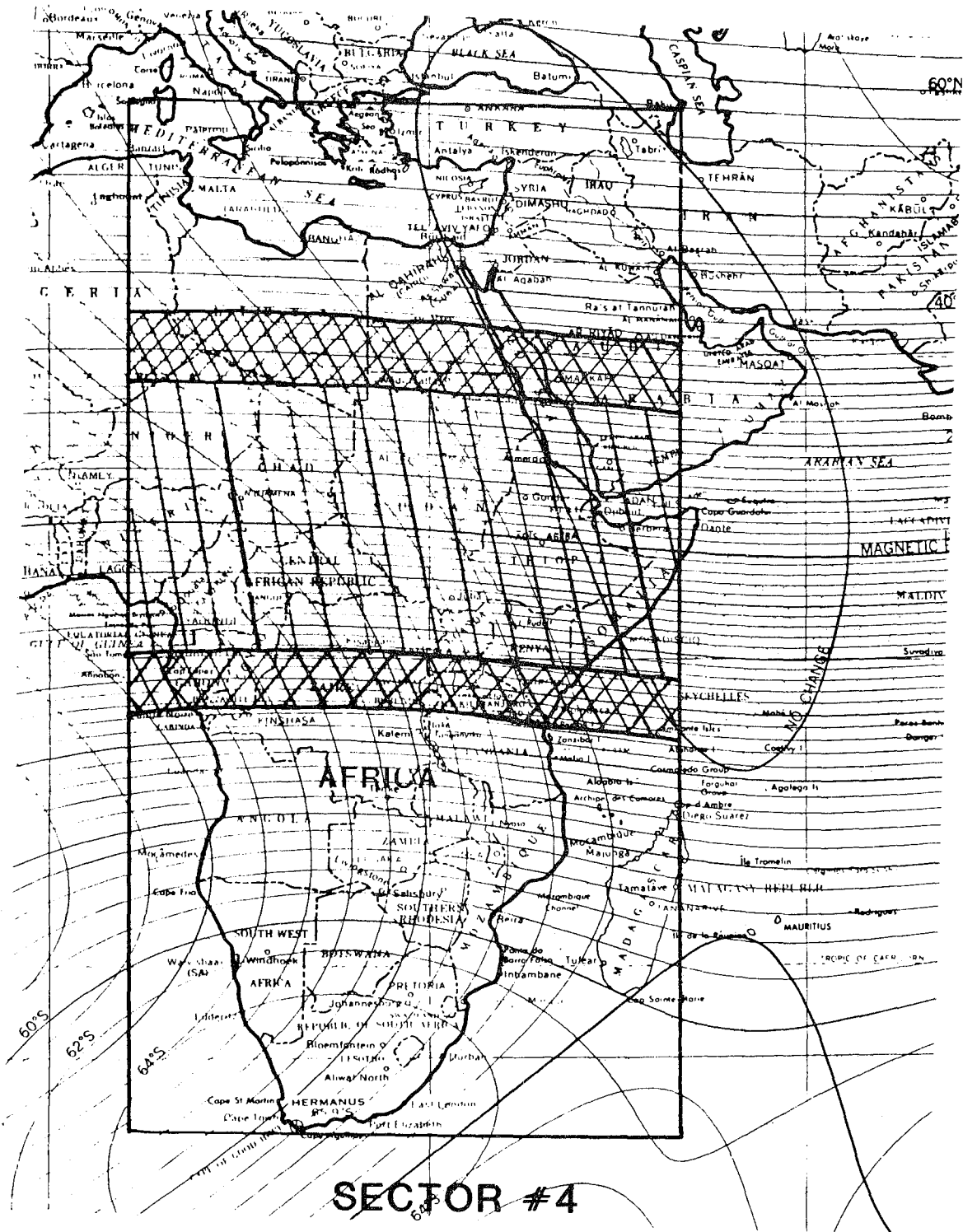
Figure 46d.   Variation of magnetic dip and declination in
              Zone 4.   Crosshatched areas are locations where
              maximum nighttime scintillation intensity
              occurs.   Hatched areas are regions of scintil-
              lation intensity but are of lower level than
              crosshatched areas.

97
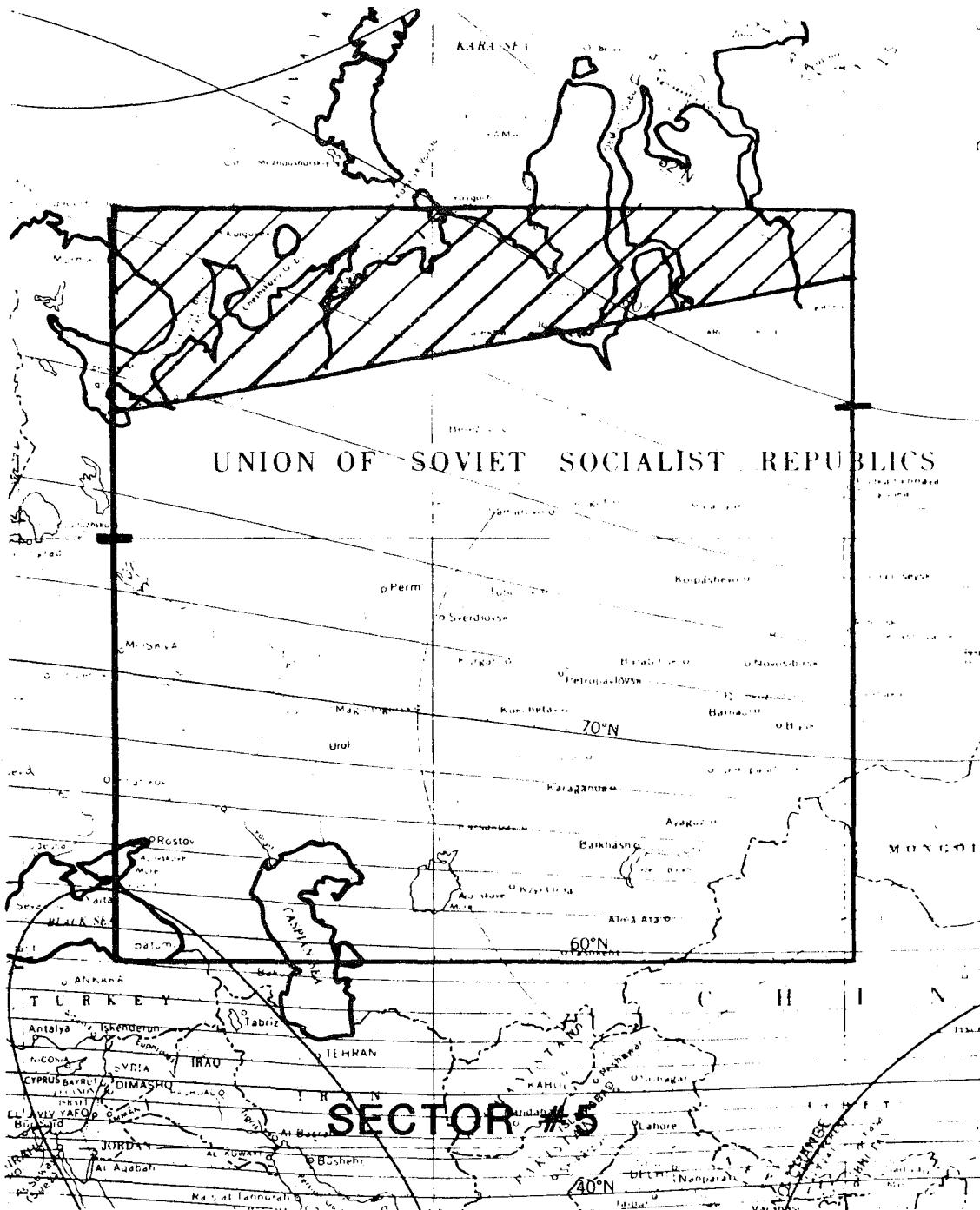
Figure 46e. Variation of magnetic dip and declination in
Zone 5. Hatched areas are locations where high
latitude scintillation effects are likely to
occur.

Figure 46f. Variation of magnetic dip and declination in Zone 6. Crosshatched areas are locations where maximum nighttime scintillation intensity occurs. Hatched areas are regions of scintillation intensity but are of lower level than crosshatched areas.
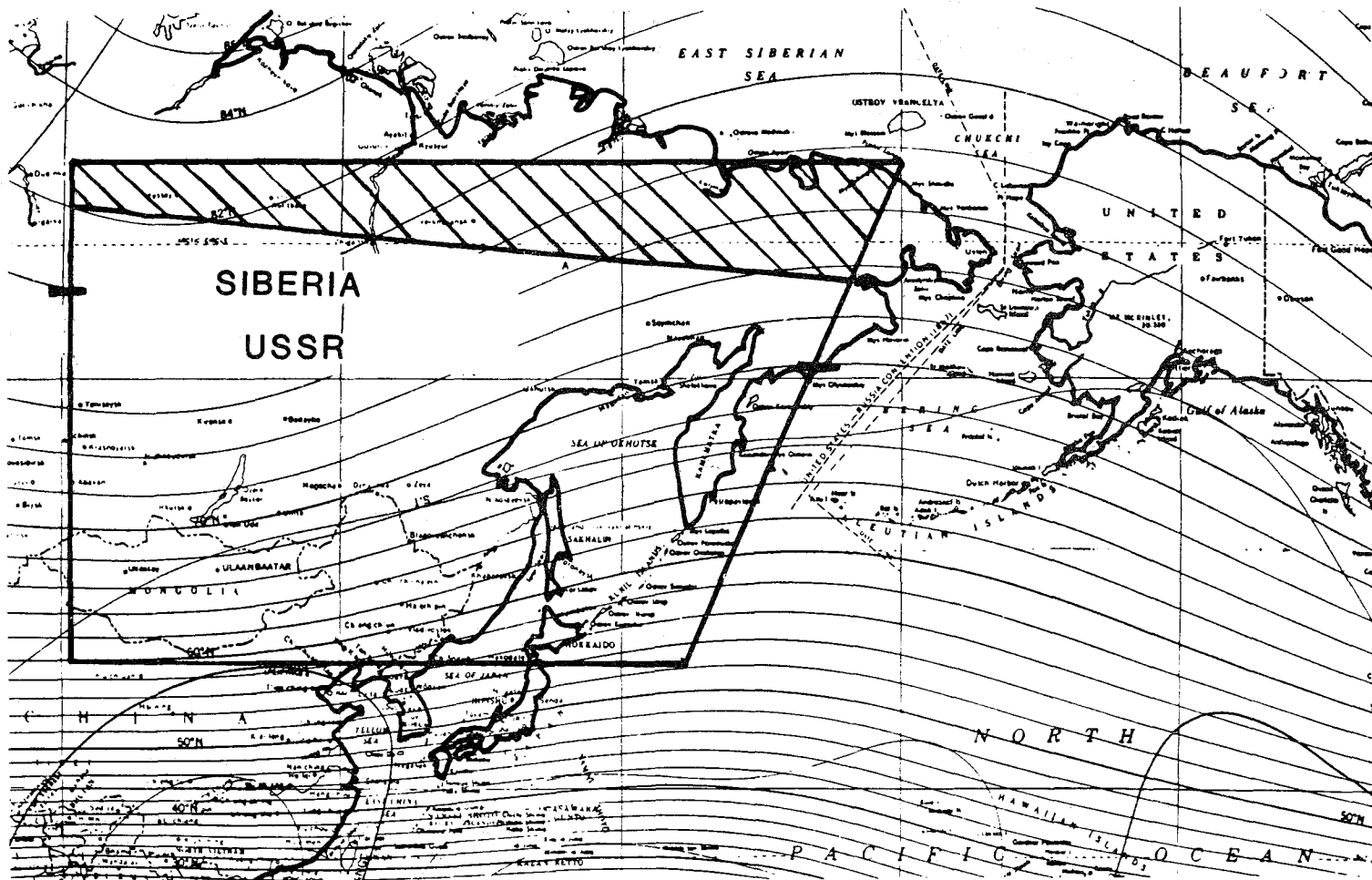
SECTOR #7

Figure 46g. Variation of magnetic dip and declination in Zone 7. Hatched areas are locations where high latitude scintillation effects are likely to occur.
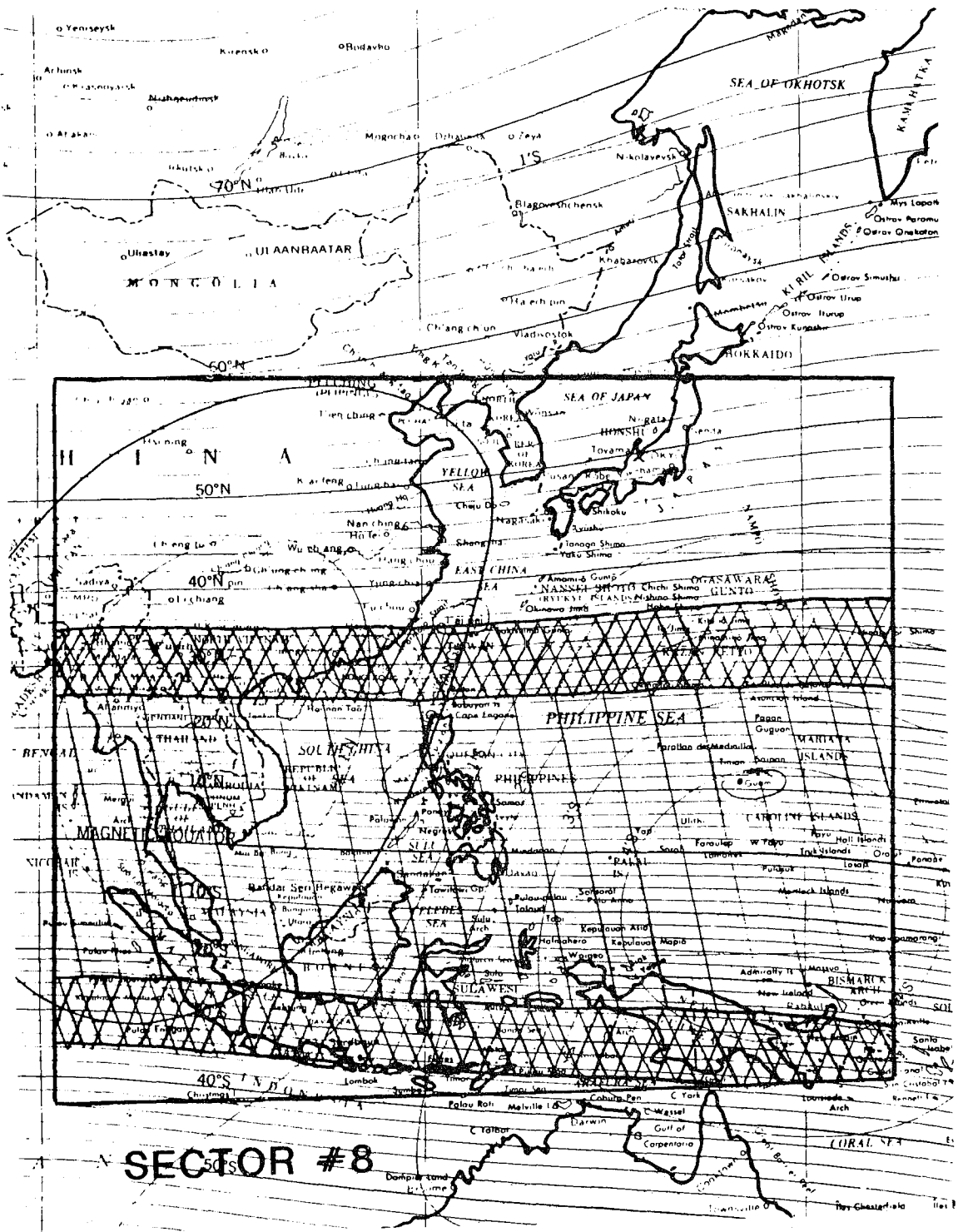
Figure 46h. Variation of magnetic dip and declination in
Zone 8. Crosshatched areas are locations where
maximum nighttime scintillation intensity
occurs. Hatched areas are regions of scintil-
lation intensity but are of lower level than
crosshatched areas.

101

In the VHF/UHF range, scintillations have been experimentally shown to follow a Nakagami distribution with the Rayleigh distribution (m=1) a limiting "worst" case. (There is some evidence particularly for HF that scintillations can exceed Rayleigh scattering, $0.5 < m < 1$, most likely due to focusing.)

Although data are limited, we expect that the Nakagami distribution would also describe HF (i.e., 30 MHz) scintillations. Under that assumption, the probability of a fade being deeper than various fade levels is given:

Probablity (%)	80	95	99	99.9	99.99	99.999
30 MHz fade level in dB (m=1)	5	12	18.5	27.5	35	50

The frequency dependence of the m parameter has been determined to be $f^{2.6}$. Using this to estimate fade levels at 30 MHz from measured scintillation at 136 MHz, where a considerable amount of amplitude scintillation data are available on SI > 2.5 dB at 136 MHz will produce Rayleigh fading at 30 MHz.

The most commonly used form of scintillation measurement prior to the mid-70's was simply the peak-to-peak excursion of signal amplitude. Converting peak-to-peak measurements of scintillations to fade information has been explored by Whitney (1974). He found theoretically that a 9.5 dB peak-to-peak scintillation would result in a 6 dB fade.

Table 17 shows the relationship between peak-to-peak excursions and fade depth as a function of peak-to-peak excursion. These and other measurements of scintillations have been utilized in this study in order to make full use of available data.

Table 17. Relation Between Peak-to-Peak Excursion
and Fade Depth

Peak-to-Peak Excursion in Decibels	Fade Depth in Decibels
2	1
4	2.15
6	3.5
10	6
16	9.7
20	12.25

Peak-to-peak excursions can also be scaled with frequency following a $1/f^{2.6}$ relationship (Whitney, 1974). However, this relationship fails for sufficiently intense scintillations, and the peak-to-peak excursions saturate at a constant value. A list of peak-to-peak values derived from similar considerations

(including saturation effects) is shown in Table 18. This table will be of
assistance in translating from scintillation indices at one frequency (the
frequency of observations for the studies reported) to other frequencies. Values
greater than 20 dB are shown for illustrative purposes only.

7.3 Scintillation at Equatorial Latitudes

7.3.1 General concepts

Equatorial scintillations are of much greater intensity than at high lati-
tudes. Fluctuations as high as 14 dB peak-to-peak have been noted on 4 GHz
signals. Maximum scintillation levels reported in the literature indicate that
the anomaly regions show scintillation activity higher than levels either at high
latitudes or near the magnetic equator. In the sector maps in Figure 46, the
anomaly regions, the areas where in the afternoon or early evening electron
densities are very high, are crosshatched. During years of high solar activity,
these regions show maximum scintillation activity. The scintillation levels of
14 dB peak-to-peak at 4 GHz mentioned above are for anomaly regions, while at the
magnetic equator maximum levels are of the order of 7-9 dB peak-to-peak at
1.6 GHz during solar maximum. During solar minimum, scintillations greater than
1 dB have not been observed at 4 GHz.

7.3.2 Scintillation observations at 40 MHz

Observations of scintillations at frequencies in the HF band are minimal.
Data from the fundamental and second harmonic of Sputnik III were taken at 20 and
40 MHz. Observations were made at 20 and 40 MHz of the transmissions of the BE-B
and BE-C 1000 km altitude satellites and data were taken from ATS-6 transmissions
at 40 MHz. However, due to restricted signal-to-noise ratios and to an absence
of data reduction, only a limited amount of data are available in useful form.
(In addition, most of the data were taken at middle latitudes where minimal scin-
tillation effects occurred.)

In Africa (Area 4) data have been taken at Addis Ababa, Nairobi, and Dar es
Salaam at 40 MHz in a year of moderate sunspot number. Addis Ababa is on the
magnetic equator, Nairobi has a dip of 27°S (14° magnetic latitude) and Dar es
Salaam has a dip of 38°S (21° magnetic latitude).

From Figures 47a, b, and c and the work of Kelleher and Sinclair (1968), the
following information can be noted:

1. Daytime levels: The 0530-0900 hr Local Standard Time (LST) period shows
slow fading with periods of minutes on synchronous satellite recordings but with
depths lower than those observed at night. Nairobi data showed only a few

103

Table 18: Conversion of Peak-to-Peak Excursions

PEAK-TO-PEAK EXCURSIONS

100	40 (MHz)	30
1	4.5	7.1
2	8.9	14.2
3	13.4	21.4
4	17.8	28.5
5	22.3	35.6
6	26.7	42.7
7	31.2	49.8 (dB)
8	35.6	56.9
9	40.1	61.0
10	44.5	61.0
11	49.0	61.0
12	53.4	61.0
13	57.9	61.0
14	61.0	61.0
15	61.0	61.0
16	61.0	61.0
17	61.0	61.0
18	61.0	61.0
19	61.0	61.0
20	61.0	61.0
21	61.0	61.0
22	61.0	61.0
23	61.0	61.0
24	61.0	61.0
25	61.0	61.0
26	61.0	61.0
27	61.0	61.0
28	61.0	61.0
29	61.0	61.0
30	61.0	61.0

PEAK-TO-PEAK EXCURSIONS

137	100	40 (MHz)	30
1	1.7	7.4	11.9
2	3.3	14.9	23.8
3	5.0	22.3	35.7
4	6.7	29.8	47.6
5	8.4	37.2	59.4
6	10.0	44.6	61.0
7	11.7	52.1	61.0
8	13.4	59.5	61.0
9	15.0	61.0	61.0 (dB)
10	16.7	61.0	61.0
11	18.4	61.0	61.0
12	20.0	61.0	61.0
13	21.7	61.0	61.0
14	23.4	61.0	61.0
15	25.1	61.0	61.0
16	26.7	61.0	61.0
17	28.4	61.0	61.0
18	30.1	61.0	61.0
19	31.7	61.0	61.0
20	33.4	61.0	61.0
21	35.1	61.0	61.0
22	36.8	61.0	61.0
23	38.4	61.0	61.0
24	40.1	61.0	61.0
25	41.8	61.0	61.0
26	43.4	61.0	61.0
27	45.1	61.0	61.0
28	46.8	61.0	61.0
29	48.4	61.0	61.0
30	50.1	61.0	61.0

(61 = + 60)

PEAK-TO-PEAK EXCURSIONS

254	137	100	40 (MHz)	30
1	2.7	4.6	20.3	32.5
2	5.5	9.1	40.7	61.0
3	8.2	13.7	61.0	61.0
4	10.9	18.3	61.0	61.0
5	13.7	22.8	61.0	61.0
6	16.4	27.4	61.0	61.0
7	19.1	32.0	61.0	61.0
8	21.9	36.6	61.0	61.0 (dB)
9	24.6	41.1	61.0	61.0
10	27.4	45.7	61.0	61.0
11	30.1	50.3	61.0	61.0
12	32.8	54.8	61.0	61.0
13	35.6	59.4	61.0	61.0
14	38.3	61.0	61.0	61.0
15	41.0	61.0	61.0	61.0
16	43.8	61.0	61.0	61.0
17	46.5	61.0	61.0	61.0
18	49.2	61.0	61.0	61.0
19	52.0	61.0	61.0	61.0
20	54.7	61.0	61.0	61.0
21	57.4	61.0	61.0	61.0
22	61.0	61.0	61.0	61.0
23	61.0	61.0	61.0	61.0
24	61.0	61.0	61.0	61.0
25	61.0	61.0	61.0	61.0
26	61.0	61.0	61.0	61.0
27	61.0	61.0	61.0	61.0
28	61.0	61.0	61.0	61.0
29	61.0	61.0	61.0	61.0
30	61.0	61.0	61.0	61.0
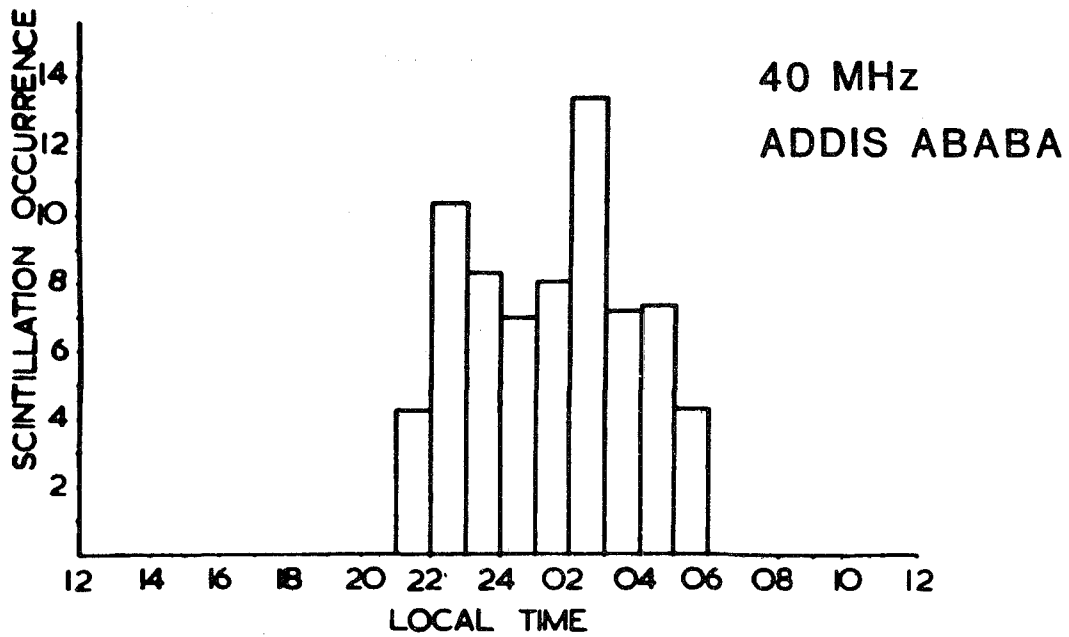
Figure 47a. Local time occurrence of scintillation at 40 MHz observed at Addis Ababa during 1966 and 1967.
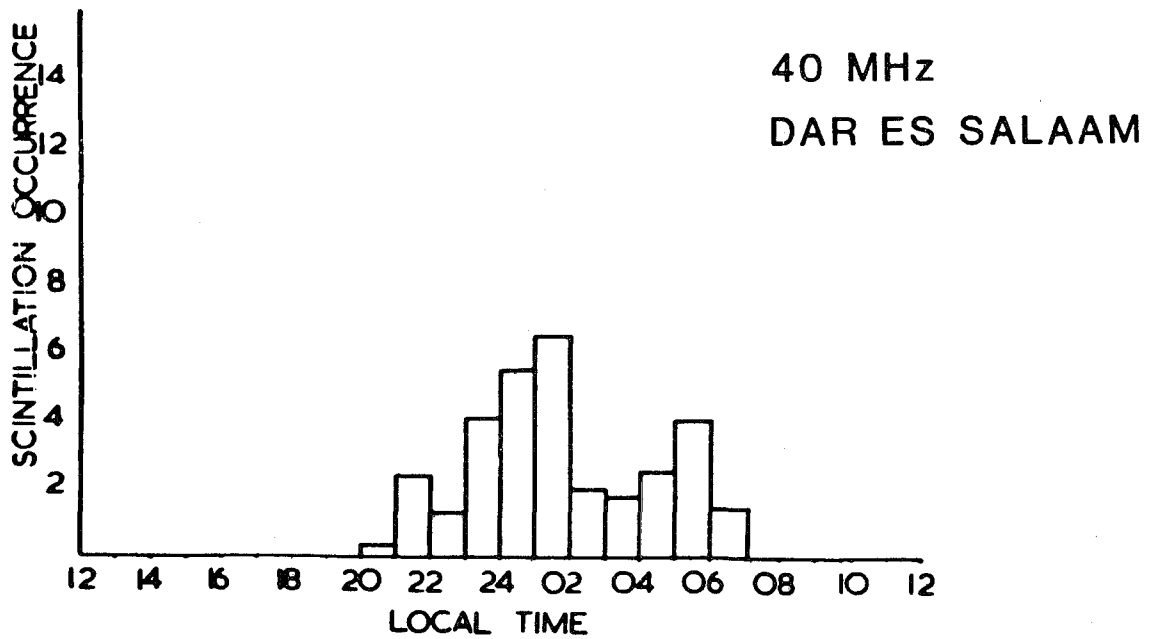
Figure 47b. Local time occurrence of scintillation at at 40 MHz scintillation at Dar es Salaam during 1966 and 1967.

40 MHz-NAIROBI
1966-1967
MODERATE SS #
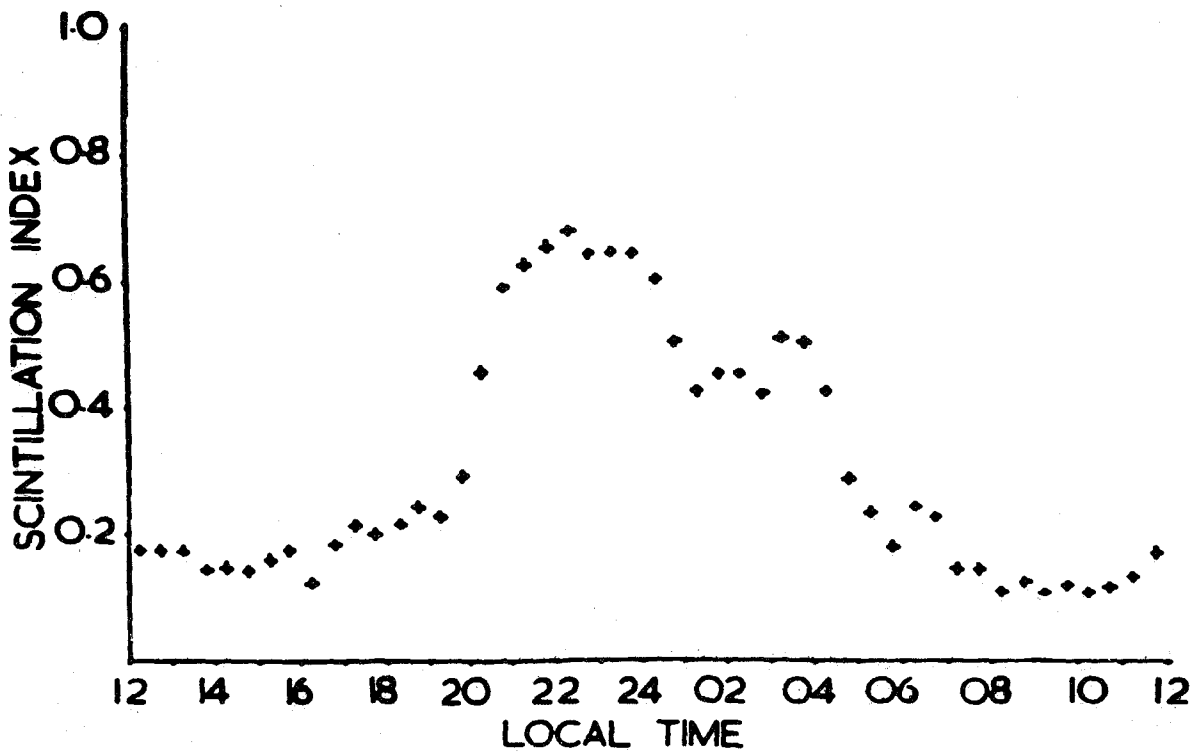
Figure 47c. Average scintillation index derived from 40 MHz
observations at Nairobi during 1966 and 1967.
Scale 0-1.0: 0.5 5 dB peak-to-peak.

decibel fades in the first portion of this period. Addis Ababa showed almost no fades. Dar es Salaam showed some occurrence of fades from 0600-0700 hrs LST.

2. Nighttime: An interpretation of the data shown in Figure 47 is that there is a peak in occurrence above the Addis Ababa station. Both Nairobi and Dar es Salaam records showed increases to the north. Addis Ababa records showed slower scintillations than the other stations.

In the South American area, observations have been made by several groups. One such study involved the analysis of 29 passes of satellite S66 (40 MHz) data taken at Tucuman, Argentina, (geographic latitude 26.9° S, longitude 65.4° W, magnetic latitude -15.4°, magnetic dip -21°). The data were taken from November 1964-February 1965, a period of low sunspot activity. This station, somewhat south of the peak of the anomaly region, showed scintillation occurrence equally to the north and to the south, again indicating the width of the equatorial irregularity region.

During daytime conditions, Rastogi (1982), using Huancayo, Peru, observations of ATS-6 at 40 MHz in 1975, found SI > 0.80 (10 dB) less than 1 percent of the time; SI was between 0.60-0.80 < 3 percent of the time. At 140 MHz in this time period, SI > 0.80 was statistically insignificant.

7.3.3 Statistical occurrence of equatorial scintillations

Reliability of data reduction and the larger data bases available have made measurements at 136, 137, and 140 MHz more useful in determining the occurrence of scintillation than the data observed at 40 MHz. On the magnetic equator (Huancayo, Peru), scintillations at 140 MHz start abruptly as shown in Figure 48 for ATS-6 records. A slow speed recording at the beginning and a fast run record serve to indicate both the clumping and the fading detail. Also included is a tracing of scintillation activity at 360 MHz. Note the higher frequency components in the fading at 140 MHz versus that at 360 MHz (on fast speed portion of records at 0255 hrs UT).

Very long-term, continuous records at Huancayo, Peru, and at Accra, Ghana, are available for the frequency of 136 MHz. While not precisely for the times needed for broadcasting applications, they give useful information of various levels of scintillation activity. The pre-midnight period would have higher occurrence than the post-midnight period, and the early morning hours would have higher occurrence than the afternoon hours.

In Table 19, scintillation occurrence statistics are given for Huancayo, Peru, and Accra, Ghana. Ghana statistics are subdivided into low- and high-
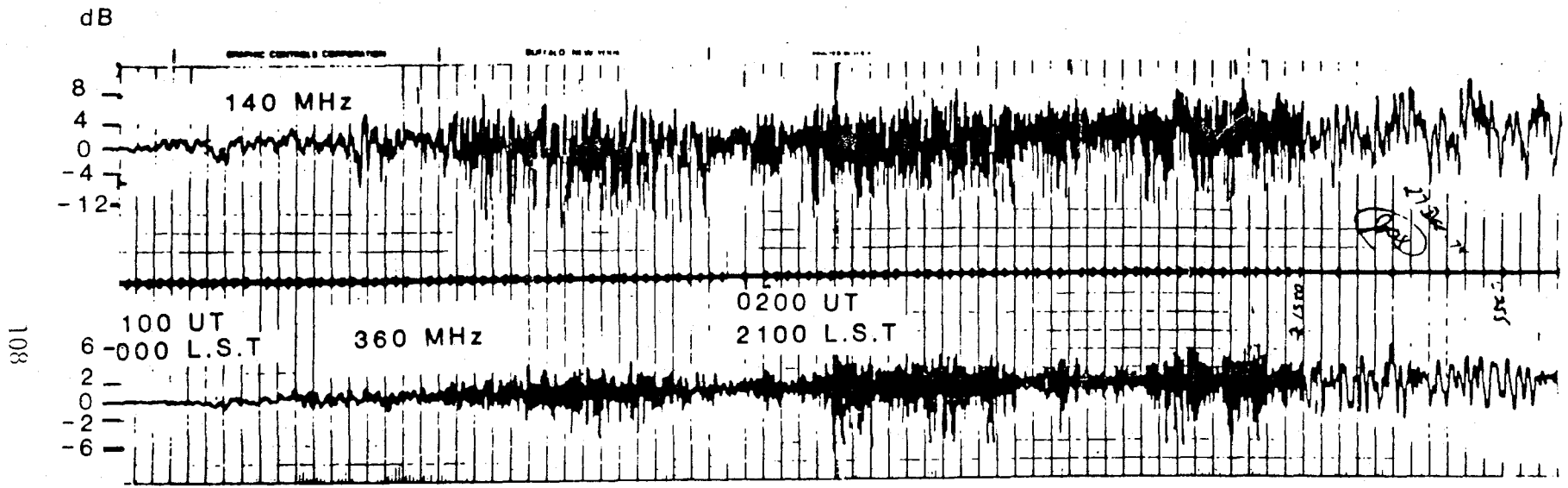
Figure 48.   Observations of scintillation at Huancayo, Peru, from ATS-6 satellite.

planetary magnetic activity (Kp) because there are differences in this region for scintillation activity as a function of the magnetic index, Kp.

Table 19. Peak-to-Peak Fading at 136 MHz

		Peak-to-Peak Fading	NIGHT (1700-0500 hrs LST) Percent Occurrence	DAY (0500-1700 HRS LST) Percent Occurrence
Huancayo		> 6 dB	22	1.3
Peru		> 9 dB	18	.9
Accra	Kp=0-3	> 6 dB	31	1.5
Ghana		> 9 dB	16	.6
	Kp=4-9	> 6 dB	27	1.5
		> 9 dB	12	.6

The evidence from these data is that for the frequencies under consideration there is high occurrence of strong scintillation activity after sunset.

Early morning scintillation may also be present. Further evidence of this is seen in Figure 49, where the percentage of occurrence of scintillations greater than 6 dB peak-to-peak is shown for the high solar activity years of 1979-1980 (DasGupta et al., 1982). Data were taken in Arequipa, Peru, near the magnetic equator. It was found that morning scintillation activity was noted in the December-January period to 0600 hrs LST. For this phase of the solar cycle, one can note that from 2000-2400 hrs LST scintillation was observed to be greater than 6 dB more than 20 percent of the time from August through the end of March. From 1800-2000 hrs LST, scintillations showed a low occurrence.

The morphological behavior of scintillation activity in the equatorial region is well understood. Six years of observations of scintillation activity at 136 MHz yields, for the South American area, the contours shown in Figure 50. Some daytime scintillations are observed in the March-to-May period and in the August-to-October period, but the maximum occurrence is from October to March. Occurrences of low nighttime scintillation activity are to be noted in June and July. The patterns shown for 257 MHz data for the three stations in Figure 51a and 51b are similiar to those in Figure 50. However, the patterns in Figure 51 should be contrasted with those that hold for the Pacific region (Fig. 52) where the low activity months are November-January. Peak levels occur at 1900-2400 hrs LST with lower levels at 1800-1900 hrs LST.
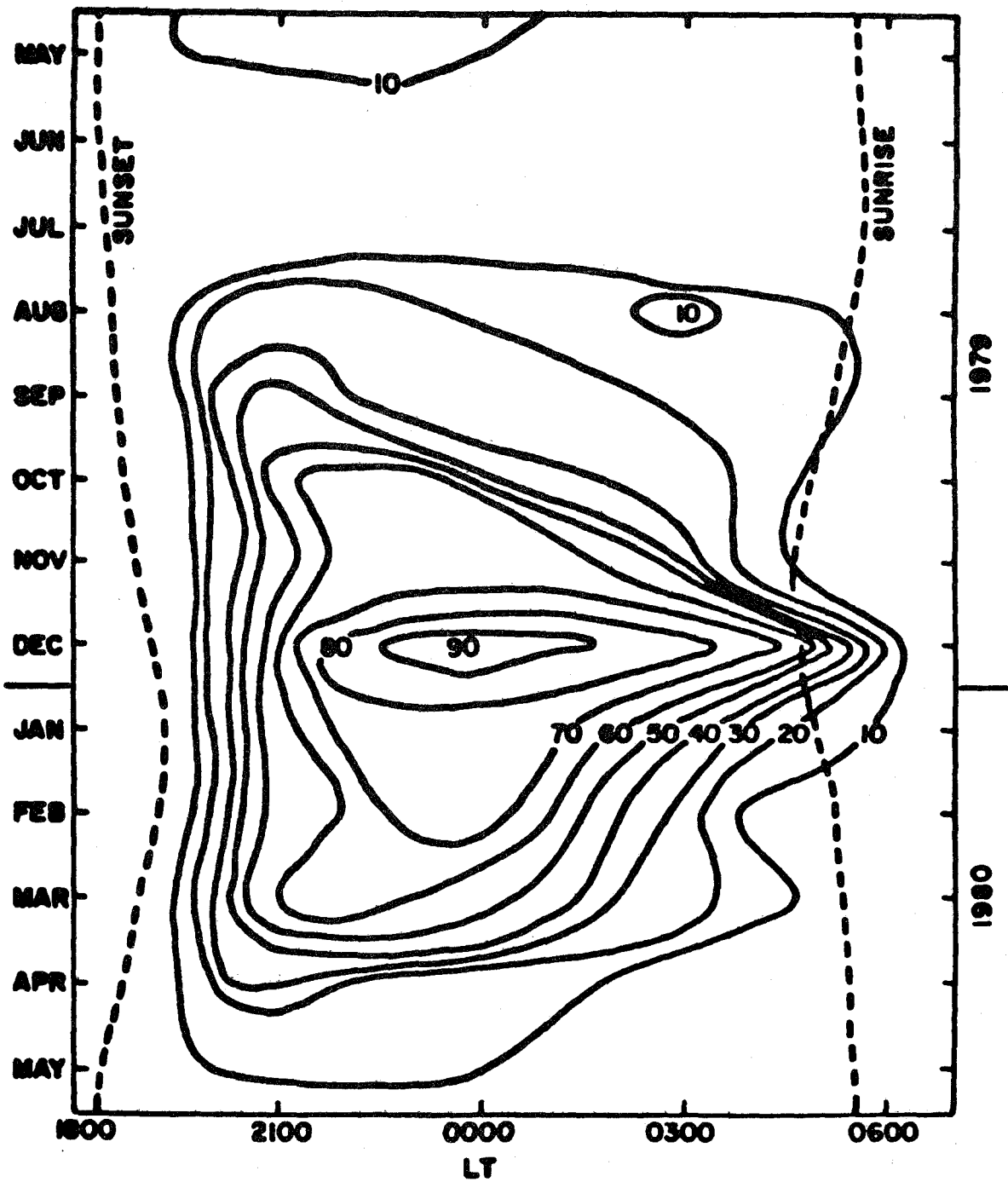
Figure 49. Percentage of occurrence of scintillation >6 dB (137 MHz) at Arequipa, Peru, 1979-1980.
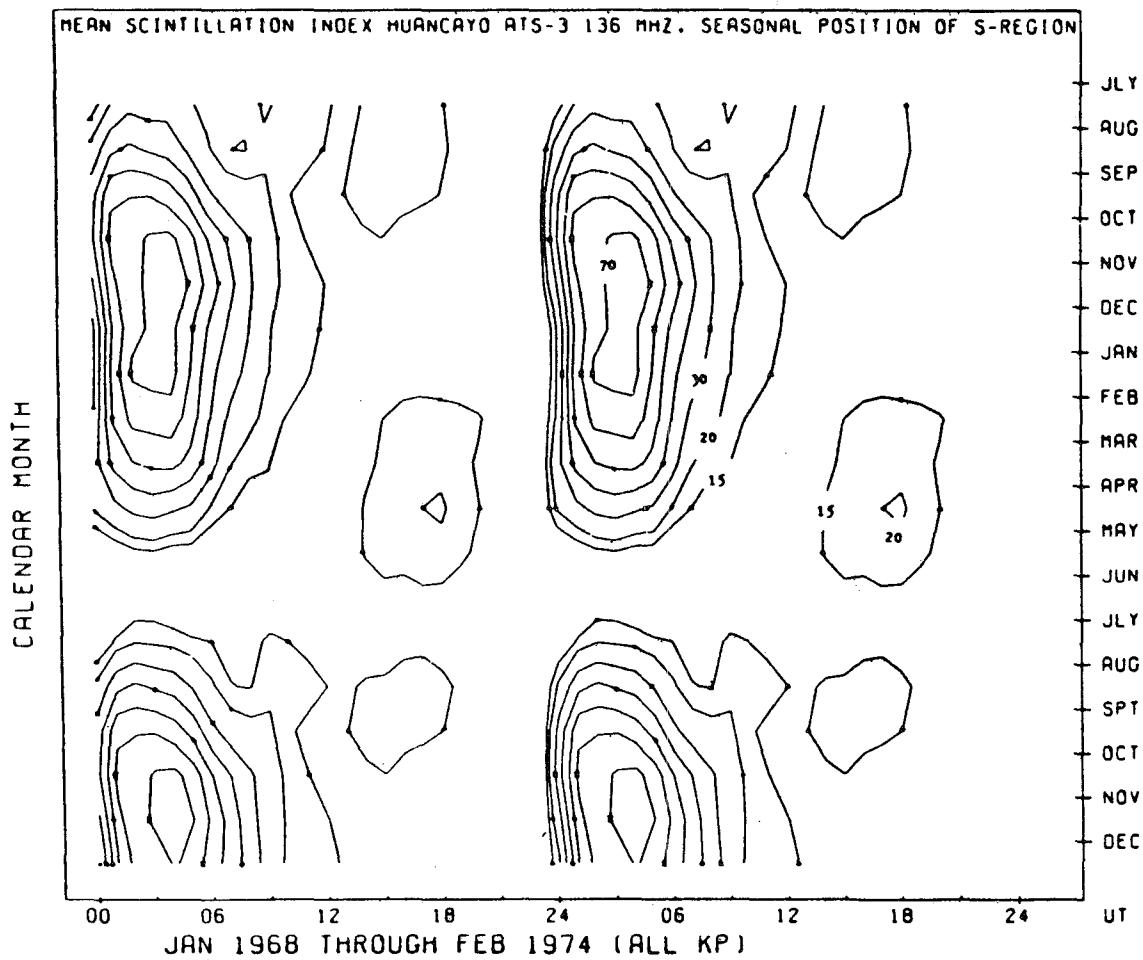
Figure 50. Scintillation contours at 136 MHz for 6-years data from Huancayo, Peru. (Hawkins and Mullen, 1974, SI of 60 ≈ 6 dB).
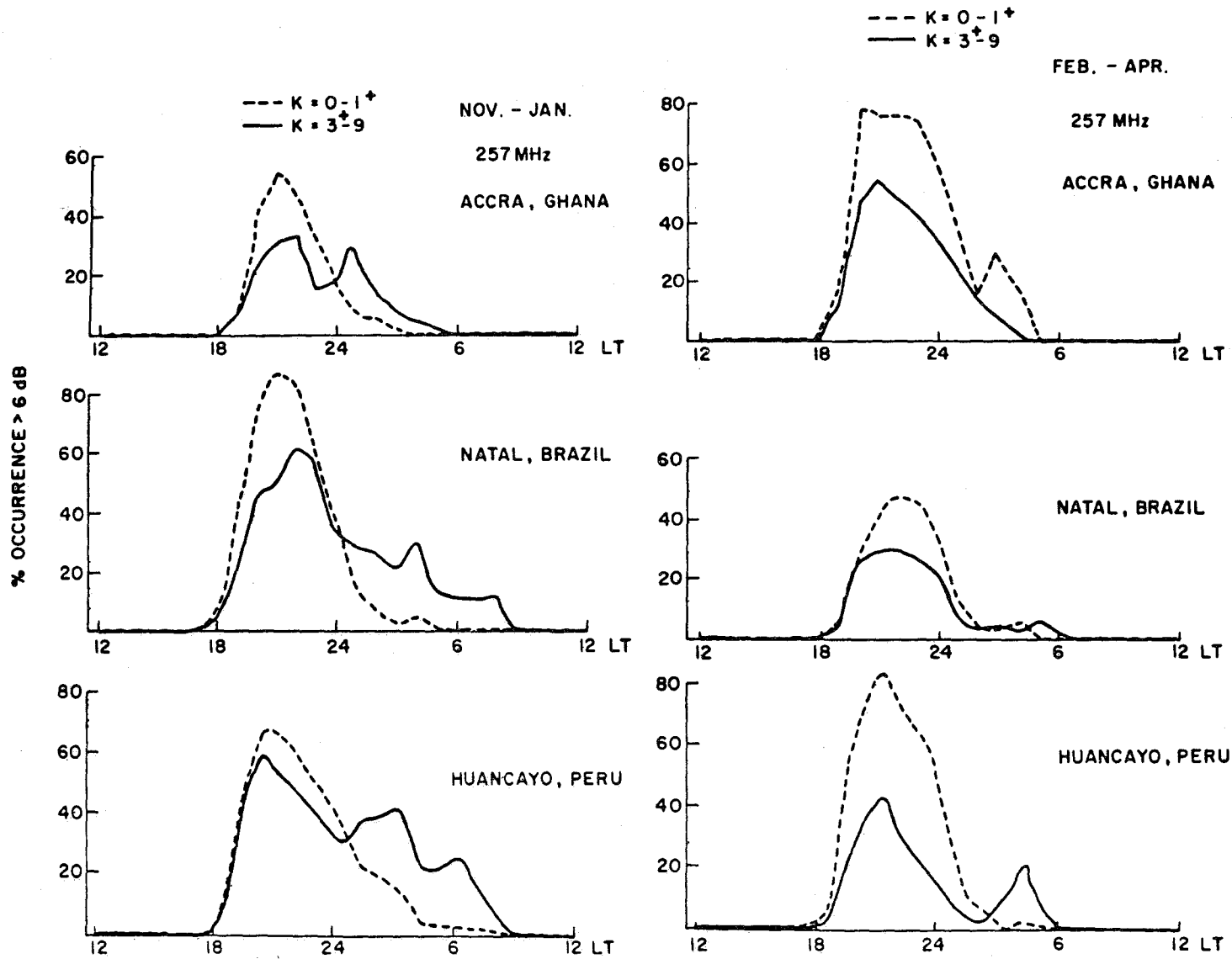
Figure 51a. Variation of the percentage occurrence of scintillation >6 dB at Accra, Natal, and Huancayo, during the November-January and February-April periods observed between 1977 and 1979.
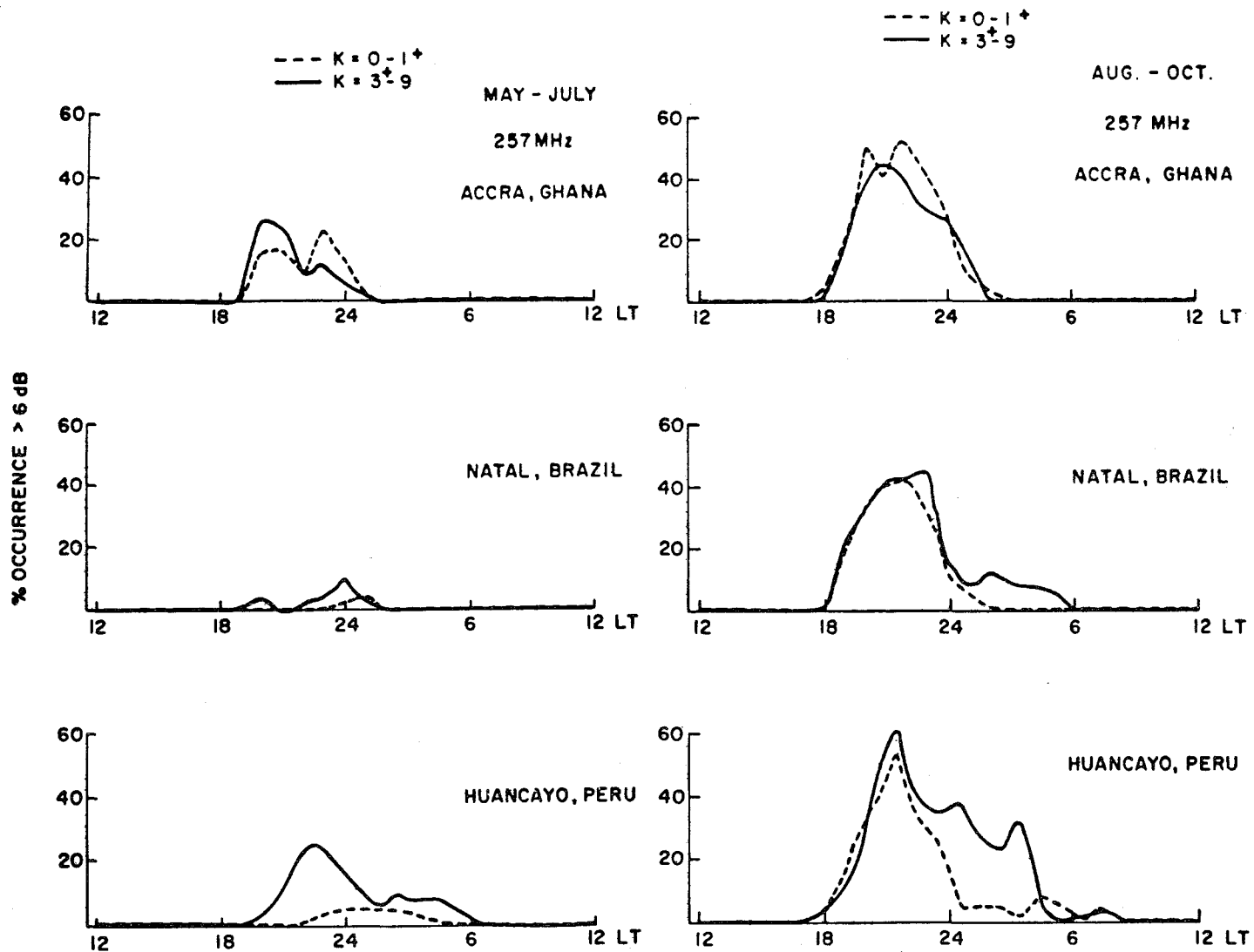
Figure 51b. Variation of the percentage occurrence of scintillation >6 dB at Accra, Natal, and Huancayo, during the May-July and August-October periods observed between 1977 and 1979.
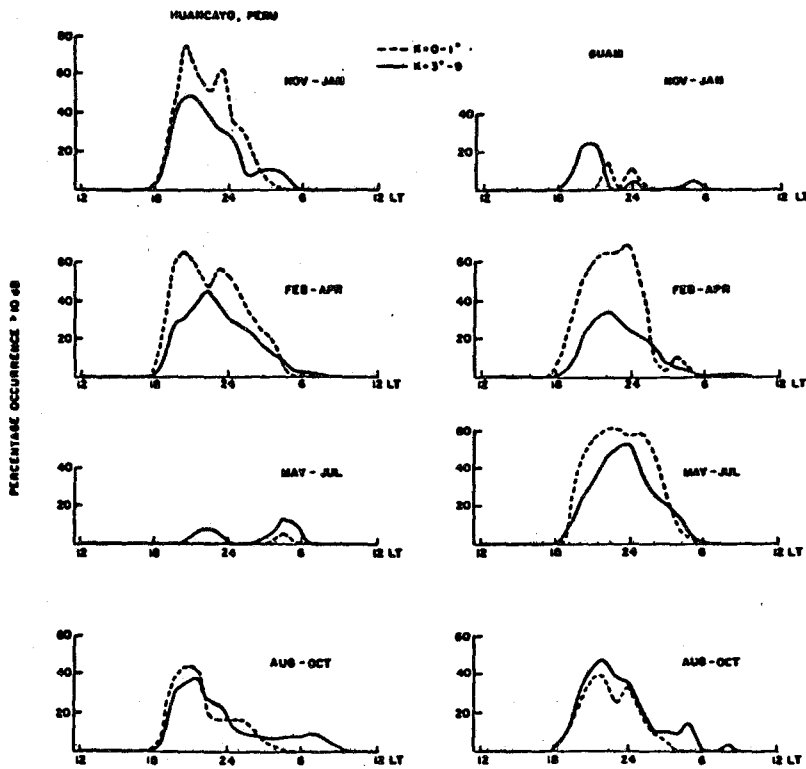
Figure 52. Yearly variation of the percentage occur-
rence of scintillation >10 dB at Huancayo
and Guam for a frequency of 257 MHz.

Poleward of the anomaly regions, scintillation activity is low particularly in years of low sunspot number. Figure 53 (Panama data) indicates that only a very small amount of time is disturbed in this area north of the anomaly region. Similarly, Figure 54 indicates the lower occurrence of scintillation in years of moderate solar activity in Quito, Ecuador, compared to Lima, Peru. In Santiago, Chile, farther from the magnetic equator than Quito, there is less activity than in Quito.

7.3.4 Mitigating equatorial scintillation effects

7.3.4.1 Exploiting the structure of irregularities

In the equatorial region, particularly away from the magnetic equator, there are periods ranging from many minutes to over an hour when irregularities are not present even on a night of intense scintillation activity. The irregularities are of the order of a hundred to several hundred kilometers in the east-west direction, but between them there is almost always a time of very low scintillation activity. Therefore, it may be useful to rebroadcast limited amounts of information continuously in the nighttime periods.

In Figure 55, the coherent radar returns observed in Jicamarca, Peru, show a typical irregularity structure (Basu and Aarons, 1977). The cross section of the irregularities as shown by the backscatter return plus an understanding of the geophysics of irregularities allow an opportunity to minimize the effect of scintillations. The irregularity patch can be pictured as a banana-oriented magnetic north-south direction--its long dimension at times north and south of the magnetic equator. The structures shown in Figure 55 move eastward appearing overhead as strongly scattered signals at 1940 hrs LST. Strongly scattered signals disappear at 2200 hrs LST. Receiving a transionospheric signal through these irregularities, one would see low scintillation levels until 1945 hrs LST and very high levels from 1945 to 2010 hrs LST. Strongly scattered signals would appear between 2030 and 2050 hrs LST. Overhead at Jicamarca, Peru, on the magnetic equator, transionospheric signals in the VHF-UHF range would be affected between 1940 and 2120 hrs LST.

It can be seen in Figure 55 that the irregularities at 700 km show a gap between 2020 and 2040 hrs LST. The lines of force of the earth's magnetic field that are associated with the 700 km point come down to 250 km in the anomaly region. The high-altitude irregularities affect areas away from the equator since the irregularities are channeled along lines of magnetic force. Between
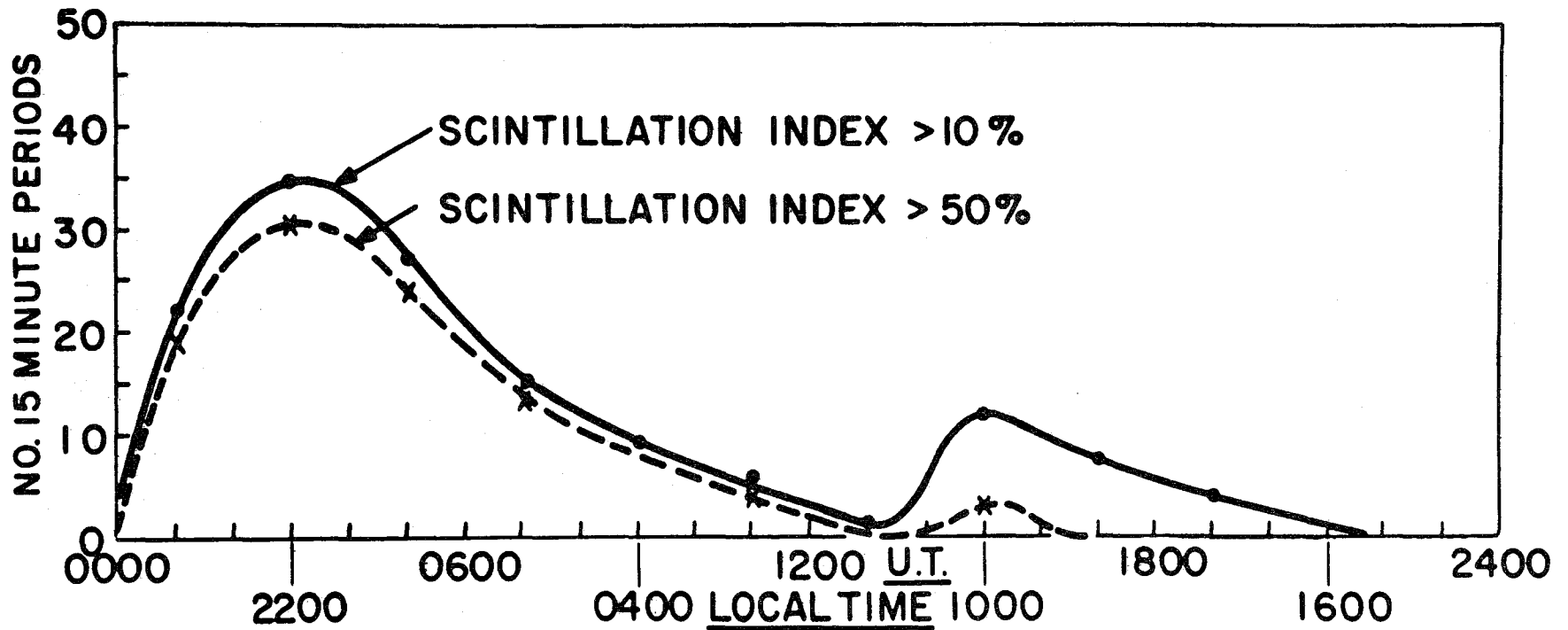
Figure 53.   Diurnal variation of scintillations occurring on ATS-3 signal received at
Panama for a frequency of 137 MHz. Total period of observation is 1000 hours
from July 11 through November 1, 1968.
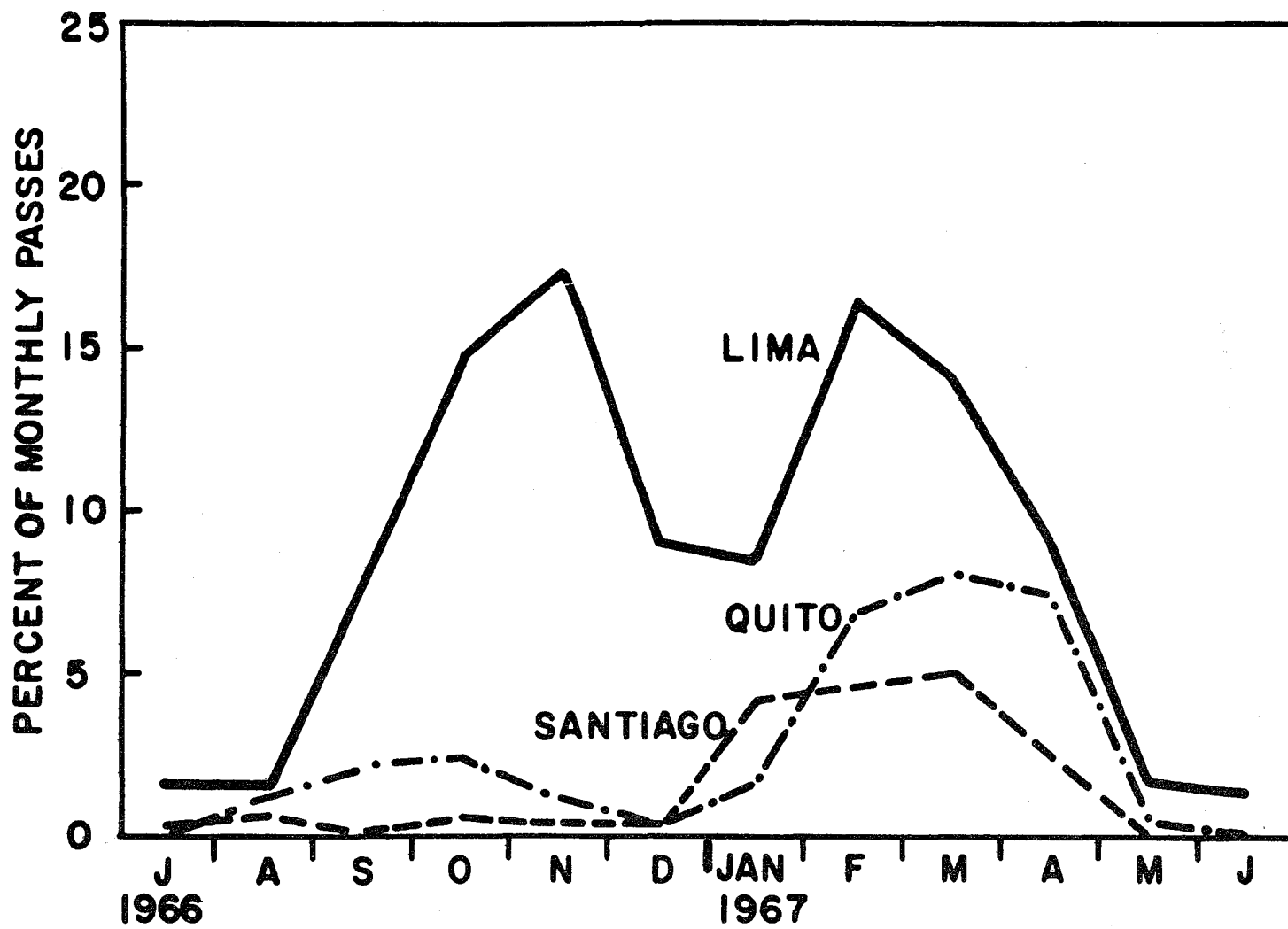
Figure 54.   Scheduled minitrack passes missed by month due to propagation distortion
(Coates and Golden, 1968).

OCTOBER 16-17, 1976   JICAMARCA   50 MHz RADAR BACKSCATTER
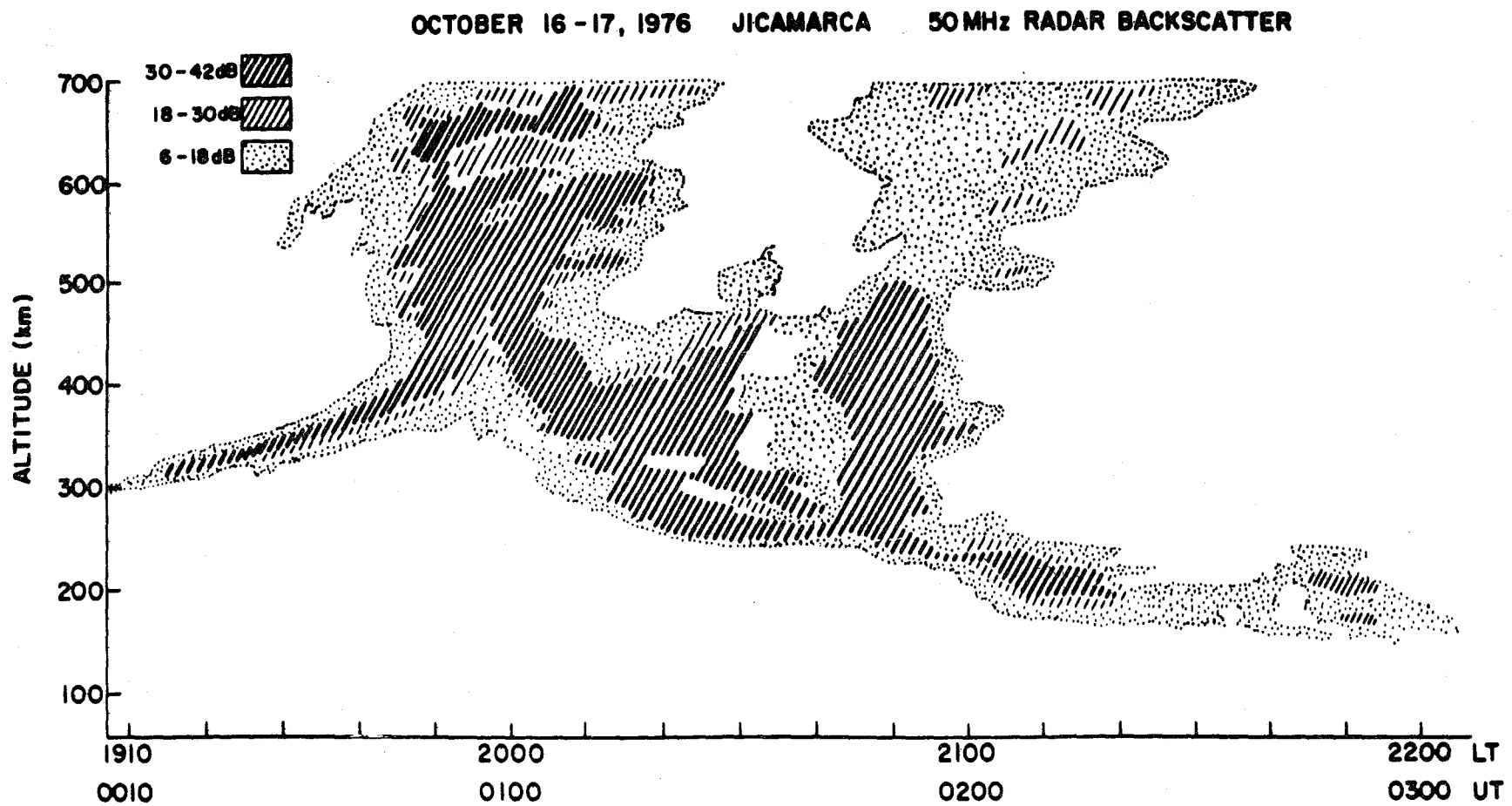
Figure 55.   Coherent radar returns observed at Jicamarca, Peru.

2020 and 2040 hrs LST, therefore, it is possible to have extremely low levels of fading. As an illustration of this, 250 MHz records are shown (Fig. 56) where gaps between the high-intensity scintillations are observable (Goodman and Martin, 1982). Similar observations made at Guam on 250 MHz and given by Paulson (1982) are shown in Figure 57.

Transmission of a repetitive nature in the equatorial region may be effective in mitigating scintillation effects. A knowledge of the morphology of scintillation activity and its peak from one hour after sunset to 2300 hrs LST is of importance. The basic time sequence of the ionospheric irregularities is that the patches form within an hour after sunset, rise into the higher altitudes during formation, and then move eastward. Scintillation effects at the receiving sites will, therefore, vary.

7.3.4.2 Use of multiple frequencies

It is not feasible to overcome the effects of scintillation by use of multiple frequencies transmitted from the same satellite to the same general area. The entire range of frequencies (VHF-UHF) is affected in similar fashion, the higher frequencies somewhat less than the lower frequencies. Frequency diversity will probably not ameliorate scintillation effects on transionospheric signals.

7.3.4.3 Use of multiple satellites

Two synchronous satellites ideally spaced for service to a particular site can be used to minimize both day and night scintillation effects. The gain is somewhat equivalent to having a 2-hour difference between the ionospheric propagation paths. Since the irregularity structure does not act in an orderly way, the effects are not easily determined on any particular day. A set of data has been taken at Huancayo, Peru, with two satellites with paths spaced about 1 hour of local time apart (Bandyopadhyay and Aarons, 1970). Figure 58 illustrates the first appearance of scintillation on a single night. The eastern path should be the first affected by scintillation with the western path affected about 1 hour later. Sometimes the time difference is as expected, sometimes much shorter, sometimes much longer. The disappearance of scintillation activity acts in the same unstructured manner. For low-latitude broadcast service, multiple satellites could produce a gain in scintillation-free time.
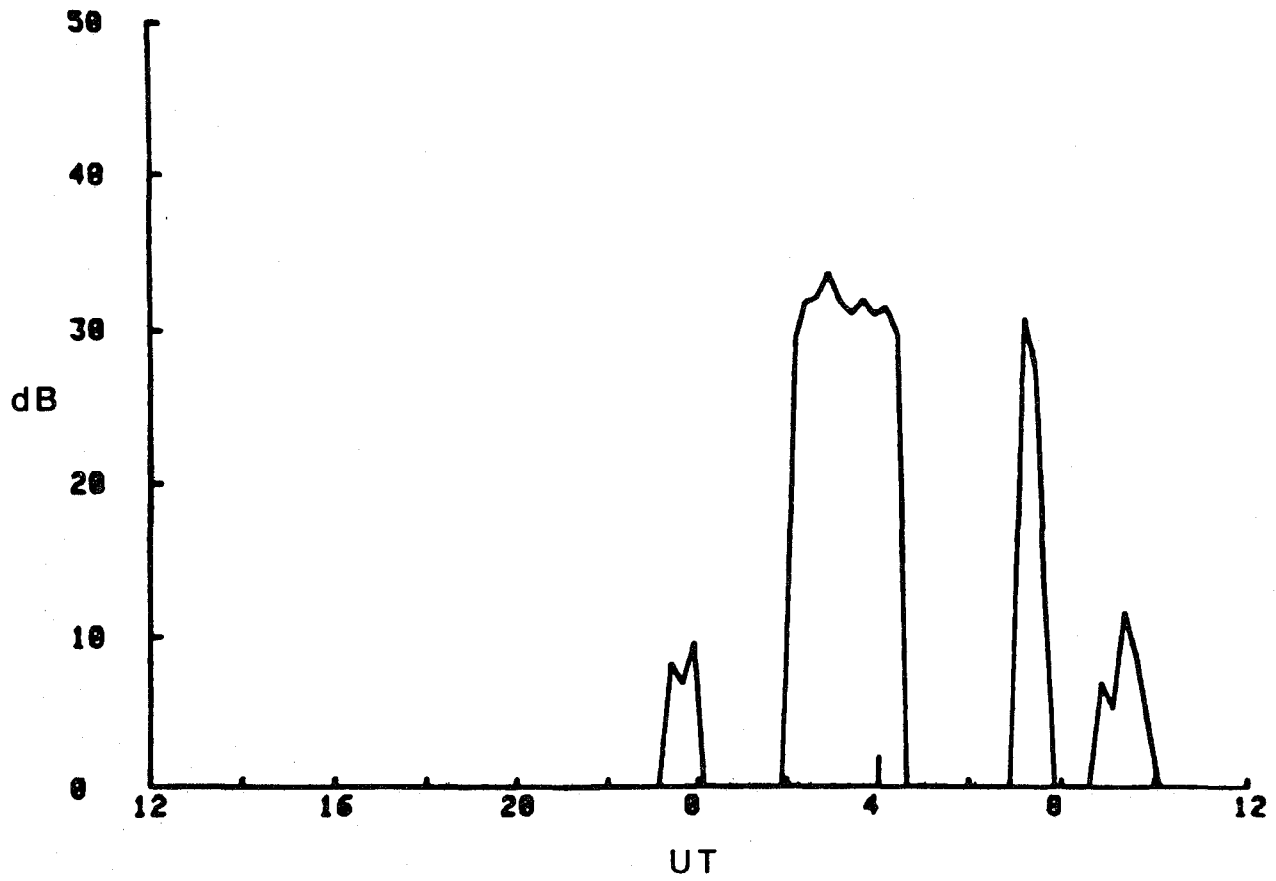
Figure 56.   SSR-1 observed max-min AGC from USNS Hayes, Mag. Lat: -21,
Lat: -38.03, Lon: -57.51 January 28, 1981.

120
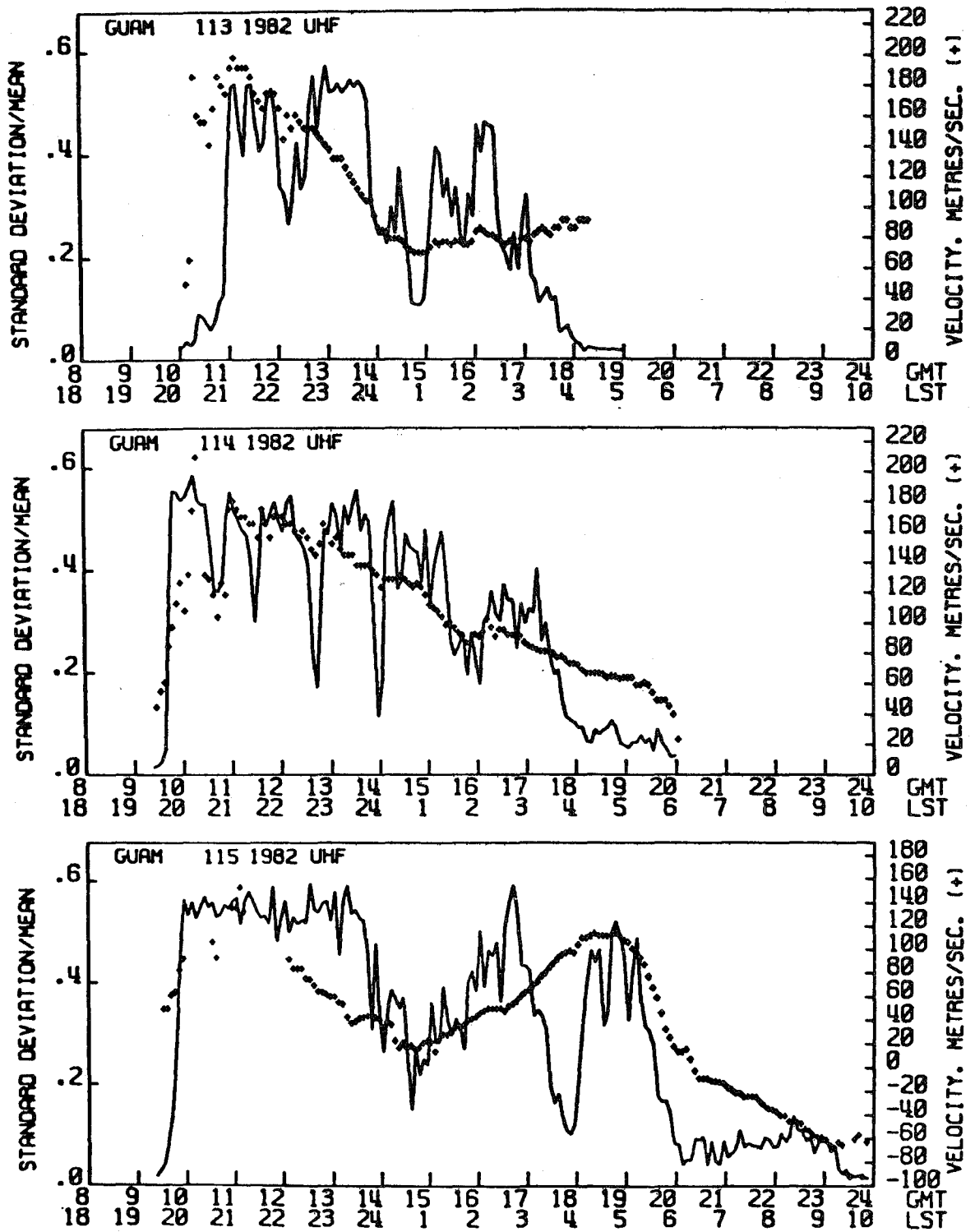
Figure 57.   Scintillation levels at Guam (magnetic equator) at 250 MHz.

121
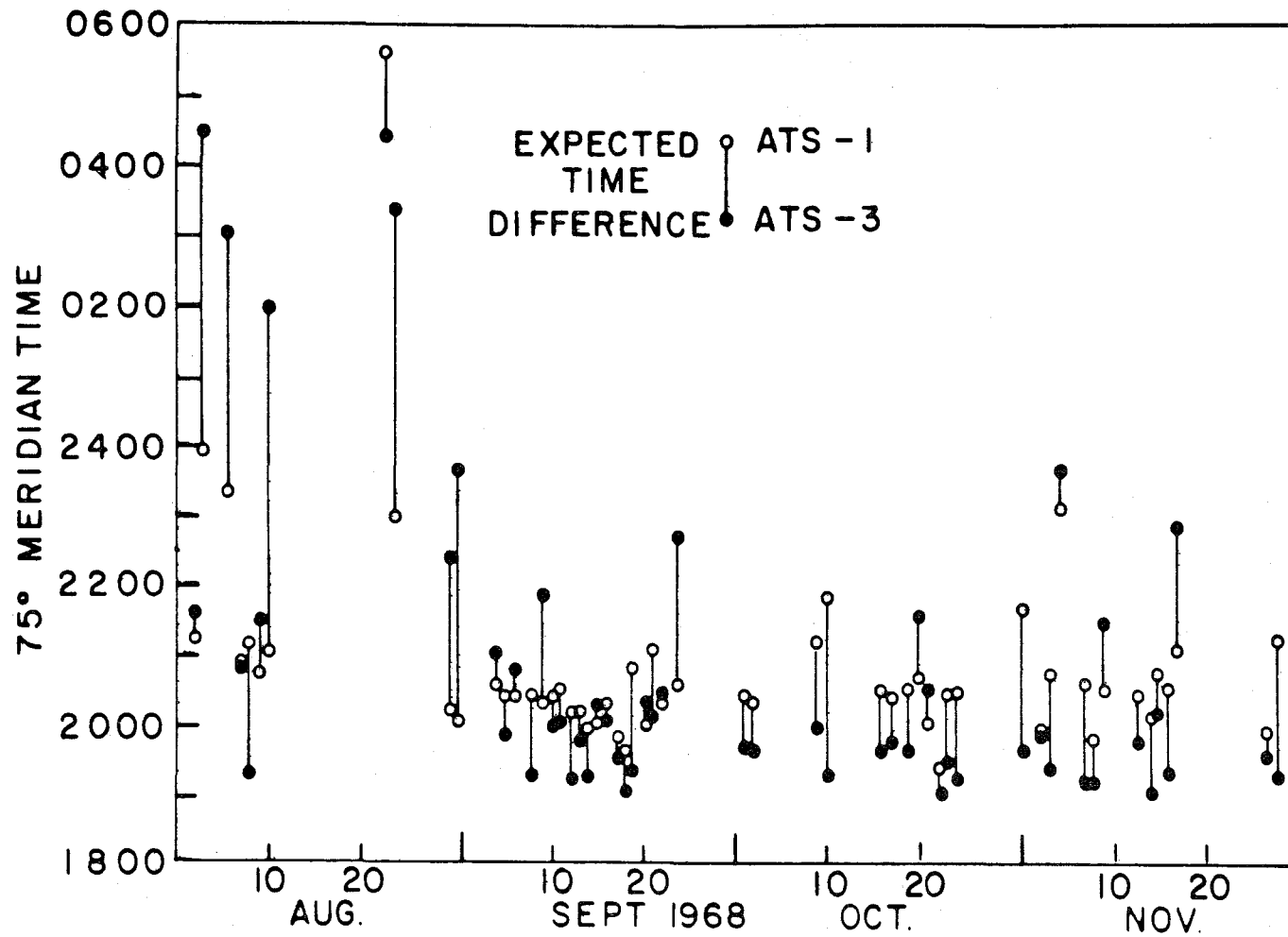
Figure 58. First appearances of high-amplitude scintillation (SI > 60%) in ATS-1 and ATS-3 signals on different nights at Huancayo, Peru. Time difference between the 350 subionospheric longitudes was approximately 1 hour.

7.3.4.4 Use of increased power

It is not reasonable to try to overcome the nighttime (1900-2400 hrs LST) levels of scintillation activity during months of scintillation activity with more power. Fades in the region will be a minimum of 15 dB when irregularities are present. They have reached 50 dB levels at 136 MHz in the worst case (Ascension Island during years of high solar flux).

7.4 Scintillation at Middle Latitudes

The effects of scintillation at the middle-latitude region are not easy to define. At times, equatorial effects impinge; at other times, high-latitude phenomena descend. In a study of 40 MHz scintillation activity at Florence, Italy, scintillation levels as a function of time and latitude were determined. It was found that scintillations increase to the north, and that there were, on occasion, up to 6 dB peak-to-peak scintillations (Cappellini et al., 1966). Figure 59 is a distribution of scintillation values obtained from their observations. Since the irregularities at all latitudes are field aligned in the F layer, there are regions where the receiver observed the satellite along a propagation path, which is along the field line. When this occurs, irregularities will have effects enhanced. If one area is of great importance, the position of the satellite should be such that this alignment should be avoided-- even at middle latitudes.

7.5 Scintillation at High Latitudes

7.5.1 General concepts

The high-latitude region can be divided into three components. The polar latitudes (not covered in the areas graphed in Figure 46) have a different morphology than near the auroral oval and at the subauroral regions. The physical processes that take place in the auroral region are governed by magnetic activity. During strong magnetic activity, the intensity of the ionospheric irregularities increases, the area covered by irregularities spreads both poleward and equatorward, and transmission as high as 100 MHz will be severely disturbed (to Rayleigh limits) in the region covered by the auroral oval. Scintillations will last longer than the magnetic storm. Disturbances at any time of day can last for hours but will maximize during the night hours.

The region separating the quiet, relatively low scintillation middle latitudes and the high latitudes is known as the scintillation boundary. The boundary occurs at a point where the level is of the order of 5 dB peak-to-peak at

123

FLORENCE, ITALY-40 MHz
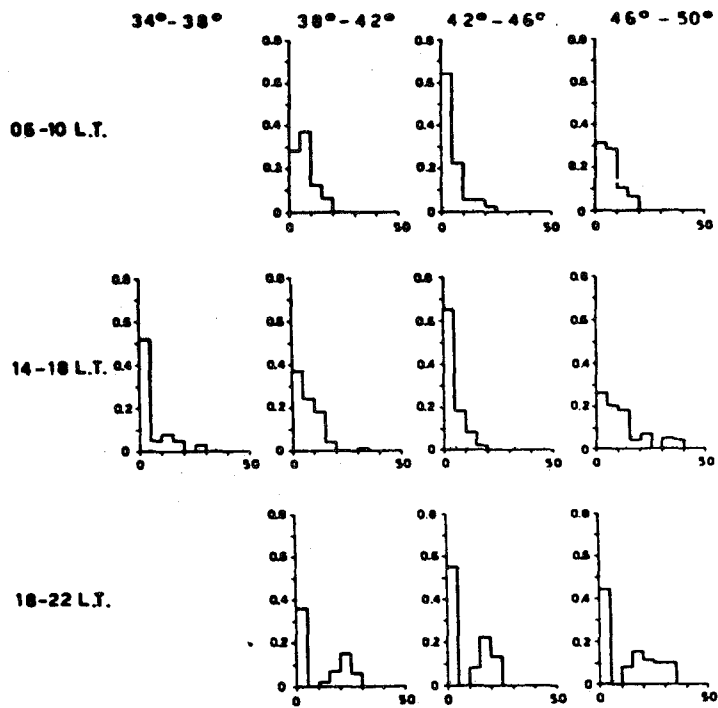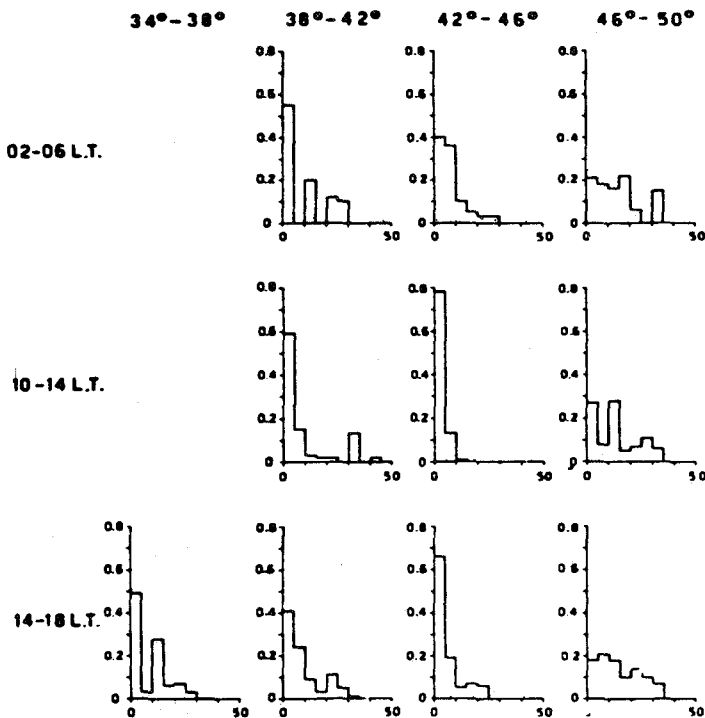
Figure 59. Scintillation observed at Florence, Italy.
Horizontal scale: scintillation index (0-100),
vertical scale: percentage of occurrence (0-1.0),
SI of 50   5 dB peak-to-peak.

40 MHz. The scintillation boundary varies as a function of time (reaching its lowest latitudes at about 2000 hrs LST) and magnetic activity. A map of the boundary of scintillation activity (5 dB peak-to-peak at 40 MHz) is shown in Figure 60. The figure shows that the scintillation boundary moves equatorward with increased magnetic activity.

The sectors shown in Figure 46 that pertain to the high latitudes have been graphed and shaded using corrected geomagnetic latitude values. These were used in order to more accurately represent the magnetic field at high latitudes. For the appropriate sectors given in Figure 46, the boundary positions at 1000 and 2000 hrs LST for moderate magnetic conditions have been shown. We have used in the area maps a nighttime value of 60° corrected geomagnetic latitude (CGL) as the boundary. This is for moderate magnetic conditions (Kp = 3). For use at 30 MHz and 3dB fades, the latitude should be lowered about 3°-5°.

At the high latitudes, the following scintillation effects are noted:

1.   Polar Regions: Extremely high latitudes will have effects similar to those noted at Spitzbergen (78° N 13.6° E) by Frihagen (1968). However, this area is not of importance to broadcasting operations and discussion of these effects is not warranted here.

2.   Auroral Latitudes: For a contrast between middle latitudes (Arecibo, Puerto Rico), subauroral latitudes (Sagamore Hill, Massachusetts), and auroral latitudes (Narssarssuaq, Greenland), 40 MHz data are shown in Figure 61 (Aarons et al., 1968). Two time periods are contrasted to show the mean scintillation levels existing in the area. The mean scintillation index always shows an increase with increasing latitude. The difference in boundary positions or scintillation index with change of frequency (20 and 40 MHz data are shown) as well as differing magnetic conditions is also shown. The corrected geomagnetic latitude of Boston is the same as that at the middle portion of Sector 5, shown in Figure 46. The dip angle of Narssarssuaq, Greenland, is similar to that of Murmansk, USSR, and the northern edge of Norway and Sweden.

7.5.2 Statistical occurrence of high-latitude scintillations derived
        from observations at VHF

From a study of several years' data, statistics of scintillation activity were developed for invariant latitudes of 54° and 60°; the original data base contained over 3 years of observations from Hamilton, Massachusetts, and from Goose Bay, Labrador. Data were taken at 136 MHz with ionospheric intersections
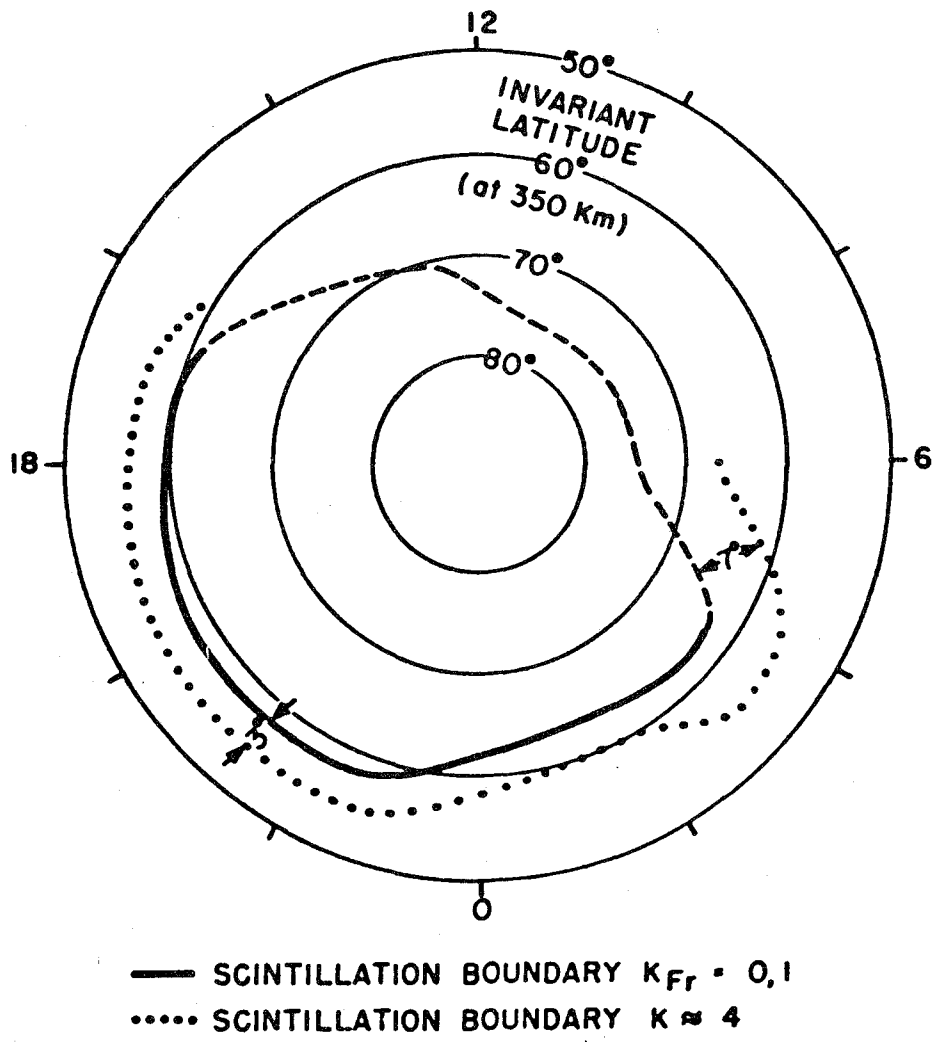
Figure 60. Scintillation boundaries.
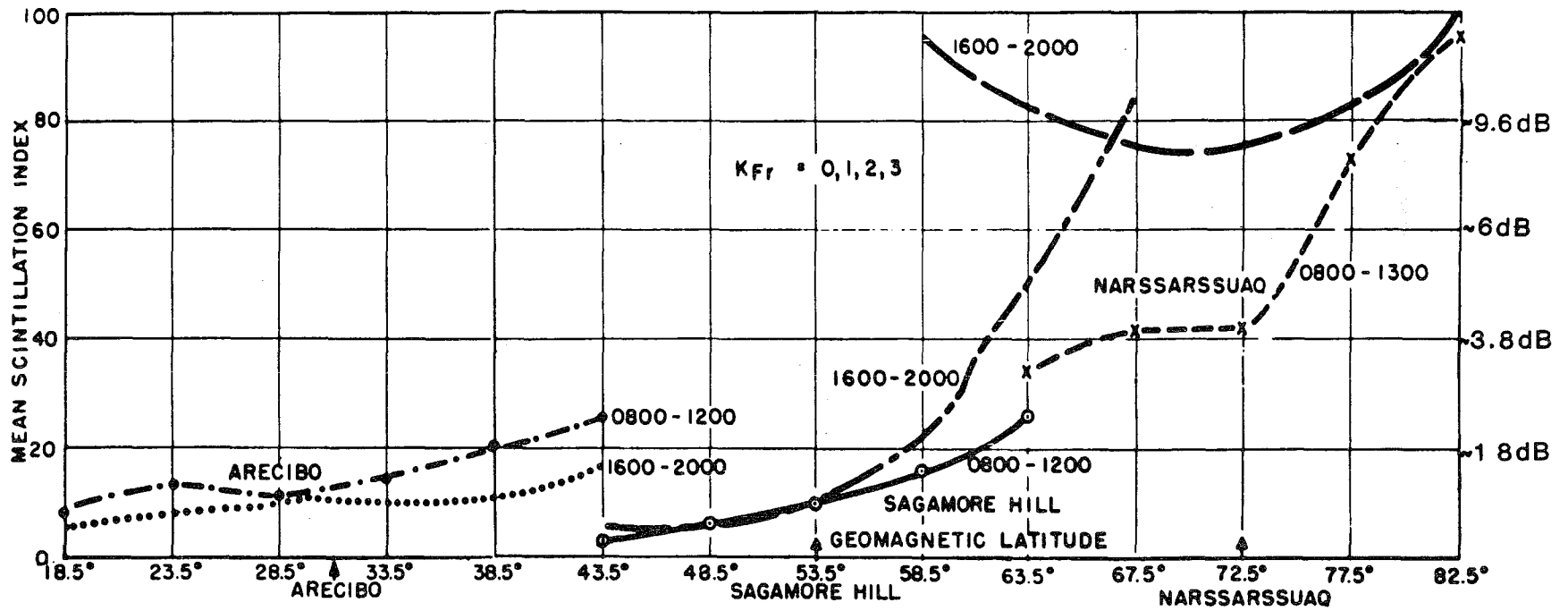
Figure 61.   Scintillations observed at Arecibo, Sagamore Hill, and Narssarssuaq at 40 MHz.

at 350 km altitude at 54° CGL and 60° CGL. It should be noted that we have marked the region above 60° CGL as hatched on the high-latitude maps in Figure 46.

Table 20 shows the occurrence percentage of various fading levels for the two stations for low-magnetic activity (Kp = 1-2) and for moderate activity (Kp = 3-4) for the entire nighttime period.

Table 20. Sagamore Hill, Massachusetts, and Goose Bay, Labrador Observations at 136 MHz

Night Scintillation Occurrence

54° CGL			SI dB	0-6	6-9	9-12	>12
Kp = 1-2	Low SS Activity			95	3	2	0
	High SS Activity			82	7	5	6
Kp = 3-4	Low SS Activity			95	3	2	0
	High SS Activity			73	15	5	7
60° CGL							
Kp = 1-2	Low SS Activity			95	3	1	1
	High SS Activity			63	20	6	11
Kp = 3-4	Low SS Activity			32	19	18	31
	High SS Activity			22	18	20	40

An even larger study encompassing the analysis (by 15-minute segments) of the data from 1968-1972 was made for all the 136 MHz synchronous satellite signals recorded at Sagamore Hill, Massachusetts, and Narssarssuaq, Greenland. In this case, the subionospheric propagation intersections were 54° CGL and 63.5° CGL. Table 21 lists the values at the times of interest to this study.

7.5.3 Mitigating high-latitude scintillation effects

The irregularity structure in auroral latitudes producing scintillation is a function of (1) the diurnal pattern of the auroral oval as it rotates with the sun and (2) the state of the earth's magnetic field. When a magnetic storm commences, and throughout the storm, the entire high-latitude region can produce scintillation.

Localized events, such as substorms, which last for 1 hour to a few hours and which affect a particular longitude, offer a distinct advantage of multiple satellites that are spaced far apart. In addition, multiple satellites can take advantage of the difference in local time of the propagation paths. It should be noted that the geometry of the high-latitude regions is such that the

subionospheric intersections are closer together for synchronous satellites than intersections at equatorial latitudes. However, satellites with Molniya orbits can have separations that will be of advantage. Data exist for evaluation of the advantages, but records have not been analyzed.

Table 21. Percentage of Occurrence of Scintillations of Various Levels as Viewed from Sagamore Hill, Massachusetts, (54° Propagation Latitude) and Narssarssuaq, Greenland, (63.5° Propagation Latitude Intersection)

dB (peak-to-peak)	Kp	2200-0200 hrs LST SAG. HILL		2200-0200 hrs LST NARSS.		0600-1000 hrs LST SAG. HILL		0600-1000 hrs LST NARSS.	
		0-3	4-9	0-3	4-9	0-3	4-9	0-3	4-9
<1.7		70	61	11	1	93	78	52	13
1.7 - 3.6		13	19	16	4	6	17	28	16
3.7 - 5.9		7	7	15	9	.9	3	11	18
6 - 9.4		5	5	17	16	.2	1.3	5	16
9.5 - 12.7		2	3	12	14	.03	.3	2	11
>12.8		3	6	29	56	.001	.2	2	26

7.6 Effect of Scintillation on Receivers

In principle, scintillation fading rates that are low (of the order of seconds or at most hundreds of seconds) should not be of importance to receiver systems using amplitude modulation. It should be possible to separate modulation that is in the tens of hertz to kilohertz from these slow variations. In practice, however, the characteristics of AGC appear to affect the signals. While it is possible to deal with this on specially designed receivers, it is difficult to ascertain effects on equipment presently in use without testing many types and models of receivers.

The effect of scintillations on amplitude modulated signals has not been studied in detail (Crane, 1977). Fluctuations of importance range from .1 seconds to tens of seconds or minutes. Using one of the satellites at 250 MHz (equatorial observations) intelligence was gleaned from speech with a signal-to-noise (S/N) ratio of 15 dB (A. Johnson, personal communication). However, muffled speech has been reported with a need of repetition of two to three times with tests of amplitude modulated signals at the same frequency at Guam (M. Paulson, personal communication); the S/N was 12 dB. It should be emphasized that these experiments were performed near the magnetic equator rather than in the anomaly region--and they were performed at 250 MHz.

129

7.7 Summary

In the equatorial region at night (1900-2400 hrs LST), in the seasons when scintillation activity is high (both near the magnetic equator and in the anomaly region), fades at frequencies from 15 to 100 MHz are extremely large. It does not appear that higher power will ameliorate this problem. However, for the hours of 1800-1900 LST there is a lower occurrence of activity. Also, in the morning hours (0530-0900 LST) fades are not deep at frequencies 40 to 100 MHz. Therefore, it is likely that an operational satellite broadcasting service could be provided using frequencies in the HF range for these intervals.

At high latitudes at night (1800-2400 hrs LST), there is scintillation activity primarily in the auroral region. During magnetic storms in the auroral region when conventional HF circuits are affected, transmissions from a satellite will also be affected. During major magnetic storms, scintillation activity is very high. During magnetic quiet periods in the areas for which satellite broadcasting services are under consideration (<60° CGL), signals could be provided to defeat scintillation in most of the area. During the morning hours, the scintillation boundary has receded poleward so that no areas are affected under quiet or moderate magnetic conditions. During severe magnetic storms, the areas will be affected, however.

8. SUMMARY AND CONCLUSIONS

The results presented in this report indicate that radio waves in the high frequency part of the electromagnetic spectrum can be used to provide broadcasting services from satellites with certain limitations. These limitations arise primarily from the impact of the ionosphere upon radio waves that are propagated through it. It was found convenient in this study to concentrate on selected parameters that are believed to be characteristic of the operation of a direct broadcast satellite service. The parameters chosen were the frequencies that penetrate the ionosphere into a given area (termed the penetration frequency) and the loss of signal strength as the radio wave propagates through the ionosphere (termed ionospheric loss). In addition, the total loss, which is the sum of the free-space loss and the ionospheric loss, has been used to characterize DBS operations under certain conditions.

Because the ionosphere displays variations that have diurnal, seasonal, and solar cycle periods, the DBS parameters are expected to show comparable variations. To account for the variability of the DBS parameters within a month, the

frequency that penetrates the ionosphere 90 percent of the time at a given location and time has been used in most instances to determine the appropriate penetration frequency. This has been accomplished by applying the statistics of the variations of foF2 that are available in HF propagation prediction programs, such as given by Stewart et al. (1983), to the equations governing transionospheric propagation. The ionospheric loss has been determined for those frequencies that will penetrate the ionosphere 90 percent of the time.

The highest penetration frequencies needed to provide coverage to a particular area occur during solar maximum. This is exactly as expected on the basis of the known solar cycle variation of foF2. The values of the 90 percent penetration frequencies show an obvious seasonal dependence. The lowest penetration frequencies are needed during local winter evenings. The highest penetration frequencies are generally needed during the equinoctial periods. The location of the satellite used in DBS operations relative to the intended reception zone exerts a large influence upon the value of the penetration frequency. The lowest values of penetration frequency occur when the satellite is directly above the intended target area. For low-latitude broadcast zones, satellites in geostationary orbits positioned at longitudes near the center of the intended reception zone provide the best geometries. For middle-latitude reception zones, satellites in geostationary orbit require penetration frequencies that can be greater than those allocated to the HF broadcasting services. Use of orbiting satellites (such as an 8-hour orbit) or satellites that hover above a given region will lead to much smaller required penetration frequencies to cover an entire broadcast zone.

In this study, emphasis has been placed upon determining the penetration frequencies needed to provide DBS coverage to an entire broadcast reception zone. It is likely that lower penetration frequencies would result if, instead of considering an entire broadcast zone, a limited target area within a zone was addressed. The results obtained would be critically dependent upon the ionospheric structure characteristic of the target area and the propagation path geometry between the satellite and the target area.

Table 22 gives typical 90 percent penetration frequencies needed to ensure DBS service over the entire year to low-latitude and middle-latitude locations for solar-minimum and solar-maximum conditions and for various orbital configurations. Also given in the table is the ionospheric loss associated with the 90-percent penetration frequency. It is safe to conclude that an upper limit of

Table 22. Overall Summary of Results

Satellite Type, Orbit, Solar Condition, Reception Zone	90 Percent Penetration Frequency (MHz)	90 Percent Ionospheric Loss (dB)	Polarization Margin (dB)
HF/DBS; GSHE; SS Min; Low	16	3	3
HF/DBS; GSHE; SS Max; Low	26	3	3
HF/DBS; GSHE; SS Min; Mid	20	3	3
HF/DBS; GSHE; SS Max; Mid	32	3	3
HF/DBS; GSLE; SS Max; Low	40	2	3
HF/DBS; GSLE; SS Max; Mid	40	2	3
HF/DBS; MOL; SS Max; Mid	10	3	3
HF/DBS; 8Hr; SS Max; Low	18	2	3
VHF/DBS	Any >60	1	3

KEY:
	HF/DBS:	HF Direct Broadcast Satellite
	VHF/DBS:	VHF Direct Broadcast Satellite
	GSHE:	Geostationary Orbit High Evevation Angle
	GSLE:	Geostationary Orbit Low Elevation Angle
	MOL:	Molniya orbit
	8HR:	8-hour orbit
	SS Min:	Solar Minimum Conditions
	SS Max:	Solar Maximum Conditions
	Low:	Low-Latitude Reception Zone
	Mid:	Middle-Latitude Reception Zone

3 dB will account for the ionospheric loss at all frequencies in the HF band that penetrate the ionosphere 90 percent of the time. An additional margin is required to overcome the problems associated with Faraday rotation of the plane of polarization of a linearly polarized signal that is transmitted through the ionosphere. The cost, in terms of decibels, needed to operate a DBS with circularly polarized signals is estimated to be 3 dB. This, too, is listed in Table 22.

Obviously if frequencies in the HF broadcasting service can be used in DBS operations, frequencies in the VHF broadcast bands could be used. The use of VHF signals will reduce the ionospheric loss to less than 1 dB, and the VHF signals will provide the required coverage to any reception zone assuming realistic orbital configurations. The need to transmit circularly polarized signals even at VHF, however, still requires the 3 dB polarization margin.

The effect of sporadic E on the penetration frequencies and on the ionospheric loss was studied. It was concluded that sporadic E would not raise the penetration frequency above that determined by the penetration through the F2 region. Similarly, the occurrence of sporadic E is not expected to add significantly to the ionospheric loss.

Arguments were put forward that the operation of a direct broadcasting satellite service would not interfere with the existing ground-based service any more than the existing ground-based broadcasting services interfere with themselves. These arguments were based on the fact that DBS signals that could be the source of potential interference would not propagate better and would not suffer lower absorption in general than ground-based HF signals. There is little or no evidence that HF (or VHF) signals emitted from high-altitude satellites (located in orbits above 2000 km) are preferentially launched into ionospheric ducts.

Perhaps the major limitation to the operation of an effective direct broadcasting satellite service is the occurrence of ionospheric scintillation. The expected magnitude of the scintillation, and its occurrence in time and space, was reviewed in detail. The operation of a DBS service during the evening broadcasting hours at low-latitude target areas is expected to be adversely impacted over much of the solar cycle. The use of multiple frequencies and multiple satellites will not ameliorate this situation totally.

The discussion provided in the previous section is based on sound physical principles and upon the results of observations of transionospheric propagation phenomena. It is unfortunate, however, that there exists little or no data that

can be directly related to transionospheric HF broadcast planning applications. There is a need to evaluate the effects of ionospheric scintillation on trans-ionospheric HF signals observed at low latitudes. There is also a need to obtain data that demonstrate the conclusions drawn in Section 5--namely, that the operation of a direct broadcast satellite would not give rise to increased interference to the existing HF broadcasting service.

Many of these issues could be addressed and resolved if a satellite experiment could be conducted. Simple multifrequency HF and VHF transmissions from a geostationary satellite could be monitored over vast regions of the globe. Experiments could be devised to allow the integration of available transionospheric propagation data at low latitudes with observations of the effect of ionospheric irregularities on AM or FM transmissions. Measurements of HF signals at locations beyond the line-of-sight to the satellite could prove invaluable in finalizing the likelihood of a DBS operation causing interference to other telecommunication systems. Measurements of the reception of HF signals at low and middle latitudes coupled with local ionospheric observations of foF2 and foEs can be used to extend the results to other orbital configurations (such as a hovering-type satellite). Observations should be such as to give the impulse response and Doppler/time delay characteristics of the satellite-earth path. Because there is a lack of transionospheric HF data, such an experiment would undoubtedly prove to be of interest to a wide variety of telecommunication users, scientists, and engineers.

9. REFERENCES

Aarons, J., J. P. Mullen, H. M. Silverman, and F. Steenstrup (1968), Latitudinal movements in the auroral ionosphere as shown by scintillation measurements, Joint Satellite Studies Group (JSSG) Report, Auroral Observatory, Tromso, Norway, April.

Aarons, J. (1982), Global morphology of ionospheric scintillations, Proc. IEEE 70, pp. 360-378.

Bandyopadhyay, P., and J. Aarons (1970), The equatorial F-layer irregularity extent as observed from Huancayo, Peru, Radio Sci. 5, pp. 931-938.

Barghausen, A. F., J. W. Finney, L. L. Proctor, and L. D. Schultz (1969), Predicting long-term operational parameters of high frequency sky-wave telecommunication systems, ESSA Technical Report, ERL 110-ITS-78 (NTIS Access. No. N70-24144).

Basu, Santimay, and J. Aarons (1977), Equatorial irregularity campaigns, Air Force Geophysics Laboratory TR-77-0264.

Beni, P., F. Bertini, and P. F. Pellegrini (1978), HF transionospheric long range propagation from satellite observed at Florence, Planet. and Space Sci. 26, 1, pp. 37-49.

Bold, G. E. J. (1969), Power distribution near the antipode of a short-wave transmitter, J. Atmos. Terr. Phys. 31, pp. 1391-1411.

Burtnyk, N., C. W. McLeisch, and J. Wolfe (1962), Ionospheric layer tilts at Ottawa, Canada, Can. J. Phys. 40, pp. 1614-1619.

Cappellini, V., P. F. Checcacci, M. T. de Giorgio (1966), October-November 1964 S 66 scintillation results, JSSG Report (AFGL), October.

Coates, R. J., and T. S. Golden (1968), Ionospheric effects of telemetry and tracking signals from orbiting spacecraft, Report No. X-520-68-76, Goddard Space Flight Center, Greenbelt, MD.

CCIR (1982), Report 250-5, Long-distance ionospheric propagation without intermediate ground reflection, Recommendations and Reports of the CCIR, International Telecommunication Union, Geneva.

CCIR (1983), Report of Working Parties 6/12 and 10/5 to Study Groups 6 and 10, International Telecommunication Union, Geneva.

Crane, R. K. (1977), Ionospheric scintillation, Proc. IEEE 65, 180-199.

DasGupta, A., Santimay Basu, J. Aarons, J. A. Klobuchar, Sunanda Basu, and A. Bushby (1982), VHF amplitude scintillations and associated electron content depletions as observed at Arequipa, Peru, Geo. Res. Let. 9, pp. 147-150.

Davies, K. (1965), Ionospheric radio propagation, National Bureau of Standards Monograph 80, (NTIS Acces. No. PB257-342/AS).

Davies, K. (1980), Recent progress in satellite radio beacon studies with particular emphasis on the ATS-6 radio beacon experiment, Space Sci. Rev. 25, pp. 357-430.

Elkins, T. J., K. Toman, and G. Sales (1980), Theoretical and experimental studies of HF ducted propagation, RADC Tech Rpt 80-360, December.

Frihagen, J. (1968), Satellite scintillation at high latitudes and its possible relation to precipitation of soft particles, JSSG, April.

Gerson, N. C., J. G. Hengen, R. M. Pipp, and J. B. Webster (1969), Radio wave propagation to the antipode, Can. J. Phys., pp. 2143-2159.

Goodman, J. C., and A. J. Martin (1982), A summary of propagation studies undertaken by the 1981 expedition of the U.S.N.S. Hayes, NRL Report 4720.

Gurevich, A. G., and E. E. Tsedilina (1979), Ultra long distance propagation of short waves, (Nauka Publishing House, 246, Moscow, U.S.S.R.).

Hawkins, G., and J. Mullen (1974), Daytime equatorial scintillations in VHF trans-ionospheric radio wave propagation from ATS-3 at Huancayo, Peru, 1974 Fall URSI Meeting, Boulder, CO.

Haydon, G. W., J. W. Herbstreit, M. PoKempner, and G. A. Codding (1982), Planning principles and planning methods for the high frequency broadcasting service, U.S. Department of Commerce Report H-82941, pp. D1-D57.

Herman, J. R., J. A. Caruso, and R. G. Stone (1973), Radio astronomy explorer RAE-1, Observations of terrestrial radio noise, Planet. Space. Sci. 21, pp. 443-461.

Horner, F., and R. B. Bent (1969), Measurement of terrestrial radio noise, Proc. Ray. Soc., Ser. A 311, pp. 527-542.

Hortenbach, K. J., and F. Rogler (1979), On the propagation of short waves over very long distances: predictions and observations, Telecomm. J. 46, pp. 320-329.

Kelleher, R. F., and J. Sinclair (1968), Diurnal and latitudinal dependence of scintillations in satellite transmissions, JSSG, April.

Llewellyn, S. K., and R. B. Bent (1973), Documentation and description of the Bent ionospheric model, AFCRL-TR-73-0657 (NTIS Access. No. AD772733).

Maliphant, R. G. (1962), The refractive deviation of radio waves that penetrate the earth's ionosphere, Defence Research Telecommunications Establishment Report No. 1090, Ottawa, Canada.

Maliphant, R. G. (1967), Ionospheric refraction of high-frequency radio waves propagating between the earth and orbiting satellites, Propagation Factors in Space Communications, AGARD Conf. Proc. 3, W. T. Blackband (Ed.), pp. 85-103, (Technivision, Maidenhead, England).

Nakagami, M. (1960), The m-distribution - A general formula of intensity distribution of rapid fading, in Statistical Methods on Radio Propagation, W. G. Hoffman, Ed. New York, Pergamon Press.

Paulson, M. R. (1982), Equatorial scintillations of satellite signals and the drift characteristics of the scintillation, NOSC TN 1138, 16 August 1982.

Phillips, G. I., and P. Knight (1978), Use of the 26-MHz band for satellite broadcasting, E.B.U. Review--Technical Part 170, pp. 173-178.

Rastogi, R. G. (1982), Equatorial radio scintillations of ATS-6 Beacons-- Phase 1: Huancayo 1974-1975, Indian Journal of Radio and Space Physics 11, pp. 159-168.

Ratcliffe, J. A. (1959), The Magneto-ionic Theory and its Applications to the Ionosphere, (Cambridge University Press, Cambridge, England).

Rush, C. M., and T. J. Elkins (1975), An assessment of the magnitude of the F-region absorption on HF radio waves using realistic electron density and collision frequency models, ITU Telecommun. J. 8, pp. 476-488.

Stewart, F. G., L. A. Berry, C. M. Rush, and V. Agy (1983), An air-to-ground HF propagation prediction model for fast multicircuit computation, NTIA Report 83-131 (NTIS Access. No. PB84-145861).

Teters, L. R., J. L. Lloyd, G. W. Haydon, and D. L. Lucas (1983), Estimating the performance of telecommunication systems using the ionospheric transmission channel--ionospheric communications analysis and prediction program user's manual, NTIA Report 83-127 (NTIS Access. No. PB84-111210).

Toman, K. (1979), High-frequency ionospheric ducting -- a review. Radio Sci. $\underline{14}$, pp. 447-453.

Toman, K., and D. C. Miller, (1977), Computation study of long-range high-frequency ionospheric ducting, Radio Sci. $\underline{12}$, pp. 371-374.

Whitney, H. E. (1974), Notes on the relationship of scintillation index to probability distributions and their uses for system design, Report of JSSG Lannion, France, January.

BIBLIOGRAPHIC DATA SHEET

1. PUBLICATION NO. NTIA Report 84-158	2. Gov't Accession No.	3. Recipient's Accession No.

4. TITLE AND SUBTITLE Study of Factors Affecting an HF/VHF Direct Broadcasting Satellite Service	5. Publication Date September 1984
	6. Performing Organization Code NTIA/ITS.S

7. AUTHOR(S) C. Rush, J. Aarons, F. Stewart, J. Klobuchar, P. Doherty, M. PoKempner, and R. Reasoner	9. Project/Task/Work Unit No.
8. PERFORMING ORGANIZATION NAME AND ADDRESS U.S. Department of Commerce National Telecommunications and Information Admin. Institute for Telecommunication Sciences Boulder, CO 80303	
	10. Contract/Grant No.

11. Sponsoring Organization Name and Address	12. Type of Report and Period Covered
	13.

14. SUPPLEMENTARY NOTES

15. ABSTRACT *(A 200-word or less factual summary of most significant information. If document includes a significant bibliography or literature survey, mention it here.)*

The Institute for Telecommunication Sciences has undertaken an assessment of the link margin required for the satisfactory performance of a direct broadcasting satellite service operating in the high frequency (HF) and in the very high frequency (VHF) bands. The assessment involved the determination of a number of issues relating to performance of HF and VHF satellite-based transmission systems. These issues included determining under what conditions a frequency allocated to the broadcasting service can be expected to reach the surface of the earth from a satellite, the loss of signal strength due to passage through the ionosphere, the impact of sporadic E and ionospheric ducting, the effect of scintillation on broadcast performance, the impact of Faraday rotation on system design, and the possibility of a satellite-based broadcasting service interfering with existing ground-based services. In this report, the results of this study are presented.

16. Key Words *(Alphabetical order, separated by semicolons)*

direct broadcasting satellite; Faraday rotation; HF broadcasting satellite; HF propagation; ionospheric loss; ionospheric penetration frequency

17. AVAILABILITY STATEMENT ☒ UNLIMITED. ☐ FOR OFFICIAL DISTRIBUTION.	18. Security Class. *(This report)* Unclassified	20. Number of pages 151
	19. Security Class. *(This page)* Unclassified	21. Price: